GAIT ANALYSIS AND FALL RISK ASSESSMENT WITH WEARABLE INERTIAL SENSORS

by

Can Tunca

B.S., Computer Science and Engineering, Sabancı University, 2010

M.S., Computer Engineering, Boğaziçi University, 2012

Submitted to the Institute for Graduate Studies in
Science and Engineering in partial fulfillment of
the requirements for the degree of
Doctor of Philosophy

Graduate Program in Computer Engineering

Boğaziçi University

2019

GAIT ANALYSIS AND FALL RISK ASSESSMENT WITH WEARABLE INERTIAL SENSORS

APPROVED BY:

Prof. Cem Ersoy (Thesis Supervisor)	.....
Assoc. Prof. Özlem Durmaz İncel	.....
Assoc. Prof. Hatice Köse	.....
Assoc. Prof. Arzucan Özgür	.....
Assoc. Prof. Albert Ali Salah	.....

DATE OF APPROVAL: 04.01.2019

ACKNOWLEDGEMENTS

I would like to sincerely thank my thesis supervisor Cem Ersoy, who has been there with me at every step of this long and life-changing journey, sharing his knowledge, kindness and friendship. I look up to him for every aspect of life and I wish I can be an academician and a mentor exactly like him one day.

I especially thank Gülüstü Salur MD, who guided our research to a problem that really matters. This thesis would be impossible without her vision, knowledge and tremendous efforts. I greatly admire her dedication to make the lives of the patients and the elderly better, and on this note, I would also like to thank our patients and their families for their participation and understanding. I sincerely hope that our work could make at least a tiny bit of difference to improve their lives.

I would like to express my gratitude to my core jury members Albert Ali Salah and Özlem Durmaz İncel for their invaluable contributions over the years, which have made this thesis the way it is today. I would also like to thank my jury members Arzucan Özgür and Hatice Köse for their time, sincere comments and suggestions.

I would like to thank Nezihe Pehlivan for kickstarting the fall risk assessment study and helping me with many aspects of this thesis, and Aynur Güven and Nağme Ak for their efforts in data collection and for making me feel at home at the clinic. I also thank Bert Arnrich for his time and contributions.

I am grateful to all my colleagues who have been benevolent and caring companions. I especially thank Cihat Baktır, who is a great friend and a fellow, with whom I shared many hours of fruitful work and cheerful laughter, Orhan Ermiş, who is like a brother to me, showing me the way of things, and Sinan Işık, who has been there with me through all my accomplishments and important moments. I would also like to thank Atay Özgövde, Serhan Daniş, Alp Kındıroğlu, Çağatay Sönmez, Turgay Pa-

muklu, Burçin Camcı, Barış Yamansavaşçılar, Yiğit Yıldırım, Alper Alimoğlu, Hakan Selvi, Anıl Özmen, Niaz Chalabianloo, Yunus Dönmez and Hande Alemdar.

My gratitudes go to the members of the CMPE family, especially Suzan Üsküdarlı, Tuna Tuğcu, Mehmet Ufuk Çağlayan, Haluk Bingöl, Pınar Yolum Birbil, Ali Taylan Cemgil and Lale Akarun, with whom I shared many joyful and candid moments.

I would like to thank my mother Fatmanur and my father Erdal for their unquestioning support and love throughout my life. Without them, I could never even dream of becoming who I am today. I would also like to thank my uncle Ümit and his wife Ayşegül for encouraging me to pursue an academic career, and my parents-in-law Ece and Cenk İskender for considering me as their own child.

I wholeheartedly thank my loving and caring wife Ceren, who understands and sees me better than anyone else. Without her, this accomplishment would mean absolutely nothing. We now have two PhDs in our home, which gives me tremendous joy.

This thesis has been supported by Turkish State Planning Organization (DPT) under the TAM project, number 2007K120610, and by Scientific and Technical Research Council of Turkey (TÜBİTAK) under BİDEB 2211-E national PhD scholarship.

ABSTRACT

GAIT ANALYSIS AND FALL RISK ASSESSMENT WITH WEARABLE INERTIAL SENSORS

The gold standards for gait analysis are instrumented walkways and camera-based motion capture systems which are highly accurate, but require costly infrastructure and are only available in hospitals and specialized gait clinics. Hence, a mobile and pervasive alternative suitable for non-hospital settings is a clinical necessity. Using wearable inertial sensors for gait analysis has been explored in the literature with promising results; however, the majority of the existing work do not consider realistic conditions where data collection and sensor placement imperfections are imminent. Moreover, some of the typical underlying assumptions are not compatible with pathological gait, decreasing the accuracy. To overcome these challenges, we propose a wearable inertial sensor-based gait analysis system that builds upon the state-of-the-art gait analysis methods. Our system copes with various data collection difficulties and relaxes some of the assumptions invalid for pathological gait. The system is able to extract a rich set of standard gait parameters and produce average stride profile visualizations, easily interpretable by clinicians. To validate the success of our system and highlight its clinical applicability, we collected a gait dataset from more than 60 neurological disorder patients and conducted a feature selection study to identify the key gait parameters in neurological disorders. To demonstrate how the extracted gait parameters can be used for a higher level inference problem, we also introduce an automated fall risk assessment solution, exploiting deep learning methods. The achieved classification accuracies outperform the existing solutions. As a final contribution, we present the design and evaluation of a computing and communication architecture that shows how the fall risk assessment methods can be transformed into a pervasive healthcare service that can handle numerous users concurrently under realistic conditions.

ÖZET

GİYİLEBİLİR HAREKET ALGILAYICILARI İLE YÜRÜME ANALİZİ VE DÜŞME RİSKİ DEĞERLENDİRMESİ

Aletli yürüme bantları ve kameralı hareket yakalama sistemleri yürüme analizi için altın standart olarak kabul edilmektedir, fakat yüksek maliyetlidirler ve yalnızca hastanelerde veya yürüme kliniklerinde bulunurlar. Bu nedenle, hastane dışı kullanıma uygun mobil ve yaygın bir alternatif gereklilik haline gelmiştir. Giyilebilir hareket algılayıcılarının hareket analizi için kullanımının literatürde ümit verici örnekleri olmasına rağmen, çoğu çalışma veri toplama ve algılayıcıların yerleştirilmesi ile ilgili problemleri göz ardı etmektedir. Dahası, tipik varsayımların bazıları patolojik yürüme ile uyum göstermemekte ve hataları artırmaktadır. Bu zorlukları aşmak amacıyla, en güncel yürüme analizi yöntemlerini ileriye taşıyan giyilebilir hareket algılayıcılı bir hareket analizi sistemi öneriyoruz. Sistemimiz birçok veri toplama zorluğu ile baş edebilmekte ve patolojik yürüme koşullarında da çalışabilmektedir. Sistem zengin bir yürüme parametreleri kümesi çıkartabilmekte ve kolayca yorumlanabilen adım profili görselleştirmeleri üretebilmektedir. Sistemimizin başarımını doğrulamak ve klinik kullanıma uygunluğunu vurgulamak için 60'tan fazla nörolojik hastadan yürüme verisi topladık ve nörolojik hastalıklara özgü anahtar yürüme parametrelerini belirlemek adına bir öznitelik seçme çalışması yürüttük. Ayrıca, yürüme parametrelerinin yüksek seviyeli bir çıkarım problemi için uygunluğunu göstermek amacıyla, derin öğrenme yöntemlerinden faydalanan bir otomatik düşme riski değerlendirmesi çözümü önerdik. Elde edilen sınıflandırma başarısı var olan çözümlerden daha üstündür. Bu katkılara ek olarak, düşme riski yöntemlerinin yaygın bir sağlık hizmetine nasıl dönüştürülebileceğini gösteren, bir dizi kullanıcının aynı anda ve gerçekçi ortamlarda kullanabileceği bir hesaplama ve iletişim mimarisinin tasarımını ve değerlendirmesini sunduk.

TABLE OF CONTENTS

ACKNOWLEDGEMENTS iii
ABSTRACT v
ÖZET vi
LIST OF FIGURES x
LIST OF TABLES xiii
LIST OF SYMBOLS xiv
LIST OF ACRONYMS/ABBREVIATIONS xvii
1. INTRODUCTION 1
1.1. Thesis Contributions 3
1.2. Thesis Outline 5
2. BACKGROUND 6
2.1. Human Gait Cycle and Gait Parameters 6
2.2. Challenges of Working with IMUs 10
2.2.1. Error Sources in Inertial Sensors 10
2.2.2. Operational Challenges and Difficulties in Data Collection . . . 12
3. LITERATURE REVIEW 15
3.1. Related Work on Gait Analysis with Inertial Sensors 15
3.2. Related Work on Fall Risk Assessment 22
4. INERTIAL GAIT DATASET 29
4.1. Equipment 29
4.2. Data Collection Procedure 30
4.3. Subjects 32
5. GAIT ANALYSIS WITH INERTIAL SENSORS 36
5.1. Introduction 36
5.2. Methods 38
5.2.1. Problem Definition 39
5.2.2. Zero-Velocity Updates 40
5.2.3. Error-State Tracking Kalman Filter 41

5.2.4. Smoothing . . . 45
5.2.5. Foot Orientation Estimation . . . 47
5.2.6. Foot Ankle Rotation Axis and Rate Estimation . . . 50
5.2.7. IC/FO Events Detection . . . 53
5.2.8. Detection of Turning Steps . . . 55
5.2.9. Extraction of Spatio-Temporal Gait Parameters . . . 55
5.2.10. Average Lateral Stride Profile Visualization . . . 56
5.3. Experiments . . . 58
5.3.1. Comparative Validation with Kinect and Slow Motion Camera . 58
5.3.2. What Can the Gait Parameters Tell Us? . . . 62
5.3.2.1. Healthy Control Subjects . . . 63
5.3.2.2. Neurological Disorder Subjects . . . 65
5.4. Conclusion . . . 71
6. IDENTIFYING IMPORTANT GAIT PARAMETERS FOR NEUROLOGICAL DISORDERS . . . 73
6.1. Introduction . . . 73
6.2. Methods . . . 74
6.2.1. Gait Parameters Pre-processing . . . 75
6.2.2. Predictor Selection . . . 75
6.2.3. Validation of Selected Predictors . . . 79
6.3. Results . . . 79
6.3.1. Multicollinearity Analysis . . . 79
6.3.2. Predictor Selection . . . 82
6.3.3. Validation . . . 84
6.4. Discussion . . . 85
6.5. Conclusion . . . 89
7. FALL RISK ASSESSMENT . . . 90
7.1. Introduction . . . 90
7.2. Methods . . . 91
7.2.1. Data Augmentation . . . 92
7.2.2. Aggregated Gait Parameters . . . 93

7.2.3. Sequential Gait Parameters 94
7.2.4. Machine Learning Classifiers 95
7.2.4.1. Traditional Classifiers 95
7.2.4.2. Long Short-Term Memory Networks 98
7.2.5. Classifier Performance Evaluation 99
7.3. Results & Discussion 100
7.4. Fall Risk Assessment as a Pervasive Healthcare Service 107
7.4.1. Multi-Tier Computing and Communication Architecture 111
7.4.1.1. Fall Risk Assessment Service Architecture Overview . 111
7.4.1.2. SDN Control Plane Components and Northbound Application 112
7.4.2. Performance Evaluation in an Emulation Environment 116
7.4.2.1. Multi-Tier Network Emulation 116
7.4.2.2. Performance Evaluation Results 119
7.5. Conclusion 121
8. CONCLUSION 123
REFERENCES 127

LIST OF FIGURES

Figure 2.1. Healthy human gait cycle. 7

Figure 2.2. Typical drifts observed in integration of data from inertial sensors. 11

Figure 4.1. ExLs3 IMU and its placement on the foot. 30

Figure 4.2. Sensors during a data collection session. 31

Figure 5.1. Inertial sensor-based gait analysis system block diagram. 38

Figure 5.2. Zero-velocity phase detection. 41

Figure 5.3. Kalman filtering and RTS smoothing comparison in lateral view. . 46

Figure 5.4. 3D feet position estimated by Kalman filter and RTS smoother. . 47

Figure 5.5. Example particle filter operation. 49

Figure 5.6. Foot-local coordinate system. 51

Figure 5.7. Extracted ankle axis rotation rate vs. x-axis gyroscope data of a correctly positioned sensor. 52

Figure 5.8. Detected FO & IC events. 54

Figure 5.9. Turn angles for individual steps and detected substantial turns. . . 55

Figure 5.10. Example average stride profile fit over individual stride profiles. . . 57

Figure 5.11. Comparison of average stride profiles of healthy and PD subjects. 57

Figure 5.12. Correlation and Bland-Altman plots for stride length validation. . 61

Figure 5.13. Correlation and Bland-Altman plots for swing time validation. . . 62

Figure 5.14. Feet elevation (clearance) asymmetry. 68

Figure 5.15. Even footfall indicated by lower secondary peaks. 69

Figure 5.16. Stride profile of a PD patient in medication ON/OFF states. . . . 71

Figure 5.17. Change of stance and swing time ratios due to fatigue. 72

Figure 6.1. Pairwise Pearson correlation matrix for gait predictors. 80

Figure 6.2. Box plots for gait predictors. 83

Figure 6.3. Random forest predictor importance estimates. 84

Figure 6.4. ROC curves for validating selected predictors. 86

Figure 6.5. 3D visualization of selected parameters (SVM with linear kernel). 88

Figure 6.6. 3D visualization of selected parameters (SVM with RBF kernel). . 89

Figure 7.1. Data processing pipeline for fall risk assessment. 92

Figure 7.2. Schematic representation of an LSTM module. 98

Figure 7.3. Confusion matrices for fall risk classifiers. 103

Figure 7.4. ROC curves for fall risk classifiers. 104

Figure 7.5. Box plots for fall risk classifier fold accuracies. 105

Figure 7.6. Multi-tier fall risk assessment service architecture. 111

Figure 7.7. Emulation topology of multi-tier architecture. 117

Figure 7.8. Performance comparison of multi-tier approaches. 120

Figure 7.9. Contribution of network and execution conditions in overall delay. 121

LIST OF TABLES

Table 2.1. Spatio-temporal gait parameters. 8

Table 3.1. Related work on gait analysis with inertial sensors. 18

Table 3.2. Related work on fall risk assessment with inertial sensors. 25

Table 4.1. Neurological disorder subjects. 32

Table 5.1. Gait parameters extracted from control subjects. 64

Table 5.2. Gait parameters extracted from neurological disorder subjects. . . 66

Table 6.1. Aggregated gait parameter names and definitions. 76

Table 6.2. Multicollinearity analysis with variance inflation factors. 81

Table 6.3. Descriptive statistics of predictors and ANOVA results. 82

Table 6.4. Gait predictors selected by feature selection methods. 85

Table 7.1. Aggregated gait parameters. 94

Table 7.2. Fall risk classifier performance results. 101

Table 7.3. Subject-wise classification analysis of fall risk classifiers. 102

Table 7.4. Number of users in emulation scenario locations. 118

LIST OF SYMBOLS

$\mathbf{0}$	Zero matrix
$\boldsymbol{a}_t$	Gravity excluded acceleration of IMU at time t
$\boldsymbol{B}_t$	Skew symmetric matrix form of $\boldsymbol{\omega}_t$ at time t
c_i	Shorthand representation for $\cos \delta\hat{\phi}_t^i$
$\boldsymbol{f}_t$	Accelerometer measurement at time t
f_t^x	X-component of accelerometer measurement at time t
f_t^y	Y-component of accelerometer measurement at time t
f_t^z	Z-component of accelerometer measurement at time t
$\boldsymbol{F}_t$	Error-state update matrix at time t
$\boldsymbol{g}$	Vector of gravitational acceleration of Earth
$\boldsymbol{G}_t$	Smoother gain at time t
$\boldsymbol{H}$	Error-state correction filtering matrix
$\boldsymbol{I}$	Identity matrix
$\boldsymbol{K_t}$	Kalman gain at time t
$\boldsymbol{p}$	Projection of $\boldsymbol{v}$ onto $\boldsymbol{v_a}$
$p_s(t)$	Probability of selecting edge server s at time t
$\boldsymbol{P}_{t\|t}$	Corrected error-state covariance matrix at time t
$\boldsymbol{P}_{t\|t-1}$	Predicted error-state covariance matrix at time t
$\boldsymbol{q}$	Delta rotation quaternion
$\boldsymbol{q_a}$	Quaternion representing rotation around ankle axis
$\boldsymbol{r}_t$	Attitude of IMU in quaternion representation at time t
$\boldsymbol{R}_t$	Attitude rotation matrix of IMU at time t
$\hat{\boldsymbol{R}}_t$	Corrected attitude rotation matrix of IMU at time t
$\hat{\boldsymbol{R}}_{t\|t-1}$	Predicted attitude rotation matrix of IMU at time t
s_i	Shorthand representation for $\sin \delta\hat{\phi}_t^i$
$\boldsymbol{s}_t$	Displacement of IMU at time t
$\hat{\boldsymbol{s}}_t$	Corrected displacement of IMU at time t
$\hat{\boldsymbol{s}}_{t\|t-1}$	Predicted displacement of IMU at time t

$\boldsymbol{S}_t$	Skew-symmetric matrix form of vector $\boldsymbol{R}_t\boldsymbol{f}_t$ at time t
$\boldsymbol{v}$	Vector component of delta rotation quaternion
$\boldsymbol{v_a}$	Ankle rotation axis vector
$\boldsymbol{v_f}$	Anterior-posterior foot axis vector
$\boldsymbol{v_g}$	Gravity direction axis vector
v_t	Speed estimated by error-state Kalman filter at time t
$\boldsymbol{v}_t$	Velocity of IMU at time t
$\hat{\boldsymbol{v}}_t$	Corrected velocity of IMU at time t
$\hat{\boldsymbol{v}}_{t\|t-1}$	Predicted velocity of IMU at time t
w	Scalar component of delta rotation quaternion
x_e	Particle x-position propagation noise
x_t^i	X-coordinate of i-th particle's position at time t
$\boldsymbol{x}_t$	State of IMU at time t
$\hat{\boldsymbol{x}}_t$	Corrected state of IMU at time t
$\hat{\boldsymbol{x}}_{t\|t-1}$	Predicted state of IMU at time t
X_L	Average left component of a gait parameter
X_R	Average right component of a gait parameter
y_e	Particle y-position propagation noise
y_t^i	Y-coordinate of i-th particle's position at time t
$\boldsymbol{z}_t^i$	State of particle i at time t
$\alpha_s(t)$	CPU load of edge server s at time t
$\delta\hat{\boldsymbol{\phi}}_t$	Error in rotation estimated by Kalman filter at time t
$\delta\hat{\phi}_t^x$	Error in rotation around x axis at time t
$\delta\hat{\phi}_t^y$	Error in rotation around y axis at time t
$\delta\hat{\phi}_t^z$	Error in rotation around z axis at time t
$\delta\hat{\boldsymbol{s}}_t$	Error in displacement estimated by Kalman filter at time t
δt	Duration between successive sensor measurements
$\delta\hat{\boldsymbol{v}}_t$	Error in velocity estimated by Kalman filter at time t
$\delta\hat{\boldsymbol{x}}_t$	Mean error-state estimate at time t
$\delta\hat{\boldsymbol{x}}_{t\|n}$	Smoothed error-state estimate at time t based on time n

$\Delta\alpha_t$	Yaw change estimated by error-state Kalman filter at time t
$\boldsymbol{\Delta r}_t$	Delta rotation quaternion at time t
$\boldsymbol{\omega}_t$	Gyroscope measurement at time t
ω_t^x	X-component of gyroscope measurement at time t
ω_t^y	Y-component of gyroscope measurement at time t
ω_t^z	Z-component of gyroscope measurement at time t
$\hat{\boldsymbol{\Phi}}_t$	Rotation matrix form of $\delta\hat{\boldsymbol{\phi}}_t$ at time t
ρ	Pearson correlation coefficient
σ	Relative rotation of IMU in δt duration
$\boldsymbol{\Sigma}_v$	Correction noise covariance matrix
$\boldsymbol{\Sigma}_w$	Prediction noise covariance matrix
θ_e	Particle orientation propagation noise
θ_t^i	Orientation of particle i at time t

LIST OF ACRONYMS/ABBREVIATIONS

3D	Three Dimensional
AD	Alzheimer's Disease
ANOVA	Analysis of Variance
API	Application Programming Interface
AUC	Area Under the Curve
CNN	Convolutional Neural Network
CPU	Central Processing Unit
CV	Coefficient of Variation
DLB	Dementia with Lewy Bodies
dps	degrees per second
DT	Decision Tree
FO	Foot-Off
FTD	Frontotemporal Dementia
GB	Gigabyte
Gbps	Gigabits Per Second
HMM	Hidden Markov Model
IC	Initial Contact
ICC	Intraclass Correlation Coefficient
IMU	Inertial Measurement Unit
IoT	Internet of Things
IP	Internet Protocol
ISP	Internet Service Provider
KF	Kalman Filter
kNN	K-Nearest Neighbors
LASSO	Least Absolute Shrinkage and Selection Operator
LOA	Limits of Agreement
LR	Logistic Regression
LSTM	Long Short-Term Memory

MAC	Medium Access Control
Mbps	Megabits Per Second
MCI	Mild Cognitive Disorder
MLP	Multilayer Perceptron
NB	Naive Bayes
NN	Neural Network
NPH	Normal Pressure Hydrocephalus
PD	Parkinson's Disease
PF	Particle Filter
PVSD	Progressive Visuospatial Deficit
RF	Random Forest
RMSE	Root Mean Square Error
RNN	Recurrent Neural Network
RTS	Rauch-Tung-Striebel
SDN	Software-Defined Networking
SI	Symmetry Index
SVM	Support Vector Machine
TCP	Transmission Control Protocol
VaD	Vascular Dementia
VaMCI	Vascular Mild Cognitive Disorder
VIF	Variance Inflation Factor
WAN	Wide Area Network

1. INTRODUCTION

Gait abnormalities are common in geriatric populations, getting more frequent and severe with increasing age. The prevalence of gait abnormalities increases from 10% to more than 60%, as people age from their sixties to eighties [1]. Gait pathologies are crucial indicators of the state and the progression of disorders that have motor symptoms. Therefore, gait analysis is essential for clinicians, both for diagnostic and treatment purposes, as the medication effects and the disease progression can be monitored through gait-related symptoms. Gait analysis is especially important for neurological disorders, which require constant monitoring and treatment adjustments. Unlike temporary, treatable or static orthopedic diseases, some neurological disorders are associated with disabling, progressive gait disorders, and increased risk of falls for the remainder of the patient's life. The symptoms may exhibit fluctuations and variable responses to treatment options, which need to be tailored to the patients' changing needs in the real life settings. Many neurological conditions are life-long and managing the gait-related symptoms can have a significant role in increasing the quality of life.

The occurrence and severity of gait abnormalities vary significantly from patient to patient due to possibly multiple underlying problems that are hard to be detected solely by clinical observation. Hence, any additional system that can quantify gait characteristics is beneficial to aid the clinicians confirm their observations and diagnoses. Moreover, gait assessment is essential in predicting and preventing falls which can result in significant morbidity and mortality. To be able to quantify the treatment effects is also an important aspect of clinical efforts, which must be adapted to operate on limited observation and data, since outpatient visits are usually infrequent and short. Moreover, some gait parameters such as feet stance durations, that are on the order of tenths of a second, might be hard to assess by only visual inspection.

Instrumented walkways and camera-based motion capture systems are considered as the gold standard in gait analysis in terms of accuracy. However, both of these

systems are suitable for only hospitals or specialized environments like gait analysis clinics, due to their size, high cost and the need for trained professionals to operate them. These characteristics render these systems rare and inaccessible to a substantial portion of the patients. Therefore, pervasive and objective gait assessment systems that can be deployed easily in non-hospital settings (such as homes or small private clinics) have a significant advantage. Such a system may also complement the gold standard, as an easily accessible and frequently usable counterpart.

The recent developments in wearable sensors made them promising candidates for monitoring motor symptoms and assessing gait dysfunctions [2]. Especially inertial sensors packaged into inertial measurement units (IMUs) are successful in tracking motor activities. Advances in the hardware and the algorithms used in conjunction with these sensors have boosted their applicability in estimating spatio-temporal gait parameters, while the decreases in their costs and sizes have made them more pervasive and attractive than ever. Attachable to almost any body part via straps, they have become viable, non-obtrusive alternatives for analyzing gait. An IMU typically consists of accelerometer, gyroscope and magnetometer sensors combined into a single device. Enhanced with wireless communication capabilities, multiple IMUs can gather real-time, synchronized data from multiple parts of the body that are active in gait. However, processing the data to estimate the three-dimensional position evolution of the attached limb is still challenging due to the error characteristics of the underlying inertial sensors, which are explained in detail in Chapter 2.

The data collection procedures associated with inertial sensors also pose significant difficulties, including variations in sensor placements and data collection durations, and subjects failing to exactly follow the given instructions. The algorithms requiring calibration periods may fail in the case of data collection problems during these periods, leading to the disposal of otherwise valid data. Moreover, pathological gait conditions (e.g. foot dragging) violating the base assumptions of the algorithms may render them inadequate to evaluate the gait of some subjects. These challenges present research opportunities to achieve a better and more robust gait analysis solution.

The output of a successful gait analysis system can be used for a higher level inference objective such as automated fall risk assessment. Prediction of falls can enable preventive measures to be taken to avoid injuries, which hinder the self-independence of the elderly population. Falls also incur indirect costs to the society in the form of hospitalization costs, increased need for caregiver support and facilities. Empowering the clinicians with automated methods to assess the fall susceptibility of their patients is crucial to enable precise and timely treatment and medication adjustments.

Fall risk assessment is essentially a classification problem to distinguish high risk subjects from low risk subjects, making machine learning methods suitable candidates. Features extracted from the inertial sensor data or gait parameters measured by a gait analysis system may be used as the input of a machine learning model that infers fall risk. Identifying the high fall risk cases among a population with gait disorders is challenging, since not all gait abnormalities may indicate an increased risk of falls. Thus, achieving an automated classifier with high accuracy is difficult, and the literature is still keen for such a solution. Deep learning methods, which have recently gained immense popularity, may have the potential to provide the desired accuracies.

1.1. Thesis Contributions

In this thesis, we focus on wearable inertial sensors to formulate a pervasive and robust gait analysis approach. The output of the proposed system is further utilized for an automated fall risk assessment solution. To facilitate and test these two key contributions, we collected an inertial gait dataset from neurological disorder patients with various gait pathologies. The gait problems specifically observed in neurological disorders are also analyzed using the extracted gait parameters, which puts this thesis into context and demonstrates how our proposal can be clinically beneficial. The contributions and the novelties of this thesis are detailed as follows:

- We collected gait data from more than 60 neurological disorder subjects wearing inertial sensors, amounting to a dataset of more than 120 subjects, including the

healthy control subjects. The neurological conditions include Parkinson's disease, dementia and normal pressure hydrocephalus, which have high prevalence among the elderly [3].

- We proposed a wearable inertial sensor-based gait analysis system that can extract a rich set of spatio-temporal gait parameters. The system is completely mobile, requiring only two wireless foot-strapped IMUs, hence is usable in a non-hospital setting without the need for infrastructure. The algorithms do not require a calibration period, and are adaptive to minor sensor placement errors. They can also operate under extreme pathological gait conditions such as foot dragging. In addition to the numeric gait parameters, we also propose a stride profile visualization method to enable fast clinical interpretations. The system is validated against a depth and slow motion camera-based reference system.
- We conducted a feature selection study aiming to determine the important gait parameters that quantify common gait abnormalities in neurological disorders. The primary objectives of this study are to put the proposed gait analysis system into a clinical context and to further validate the predictive power of the extracted parameters. The explored feature selection methods and the resulting reduced parameter set can be beneficial for future gait analysis studies focusing on neurological disorders.
- We proposed an automated fall risk assessment solution that operates on the output of our gait analysis system. We explored the viability of deep learning methods, specifically long short-term memory (LSTM) neural networks, and compared their classification performance with more traditional machine learning methods. The novelty of our approach is to use sequences of gait parameters as input, rather than feeding the raw data directly into the neural network as widely adopted in deep learning studies of other domains. Consequently, we achieved a high degree of accuracy, showing that the domain knowledge inherent in the gait parameters are invaluable and can result in a significant accuracy improvement when combined with a sophisticated machine learning model.
- We examined the applicability of the proposed fall risk assessment solution as a pervasive healthcare service, and consequently proposed a multi-tier computing

and communication architecture that exploits the edge computing and software-defined networking (SDN) paradigms. The proposed architecture is not specific to the fall risk assessment use case and can be employed for a variety of similar healthcare services, with the objective of serving numerous patients and clinicians efficiently. We evaluated its performance in terms of service delays in an emulation environment, using our fall risk assessment system and real data.

1.2. Thesis Outline

The thesis is organized as follows: A background on human gait characteristics and the typical challenges associated with inertial sensors are presented in Chapter 2. In Chapter 3, we present an overview of the related literature and the state-of-the-art solutions for inertial sensor-based gait analysis and fall risk assessment. The actual contributions of the thesis are presented in Chapters 4-7.

In Chapter 4, we present the details of the inertial gait dataset we collected as part of this thesis. The utilized sensor equipment, data collection procedures and the demographic and clinical information on the subjects are explained. In Chapter 5, the proposed wearable inertial sensor-based gait analysis system is described, along with the numerical validation results and example clinical discussions. This contribution is at the heart of this thesis, as the subsequent chapters are built upon it. Chapter 6 presents the feature selection study conducted to identify the key gait parameters for neurological disorders. In Chapter 7, we describe the proposed automated fall risk assessment solution and present its accuracy evaluation on our gait dataset. The multi-tier computing and communication architecture that transforms this solution into a pervasive healthcare service is also detailed in this chapter.

The thesis is concluded with Chapter 8, with an overall discussion of the contributions and their impacts on the state-of-the-art.

2. BACKGROUND

In this chapter, we provide the readership with a brief overview of human gait characteristics and the standard gait parameters that are commonly used by the medical community for detecting different factors leading to pathological (abnormal) gait. We also give examples from the typical gait-related symptoms of some neurological disorders to put them into context. Moreover, we discuss the challenges of working with wearable inertial sensors with the aim of accurate gait analysis, both in terms of the error characteristics of the underlying hardware, and the difficulties in deployment and data collection. These challenges serve as the rationale behind the aims of this thesis, explicitly, to come up with a robust gait analysis solution usable in non-hospital settings, that is minimally affected by the typical errors associated with inertial sensors, either arising from the human factor or the hardware.

2.1. Human Gait Cycle and Gait Parameters

A single gait cycle is defined as the period between any two successive repetitive gait events [4]. The primary events and phases in the gait cycle are presented in Figure 2.1. It consists of two major phases, namely stance and swing phases. The stance phase begins with initial contact (IC), that marks the beginning of the load transfer to the ground-contacting foot. The stance phase ends with foot-off (FO), which marks the complete lifting of the load. Swing phase starts with FO and ends with IC, which is the phase where the actual foot motion occurs. In healthy gait, the stance phase constitutes approximately 60% of the whole gait cycle, and the swing phase constitutes the remaining 40% [5].

Close-ups on the gait events of the right foot are also presented as zoom-in circles in Figure 2.1. The IC and FO events are alternatively named as heel-strike and toe-off, respectively. However, these alternative terms are only valid for healthy gait. In pathological gait, the first contacting point of the foot may not be the heel (especially

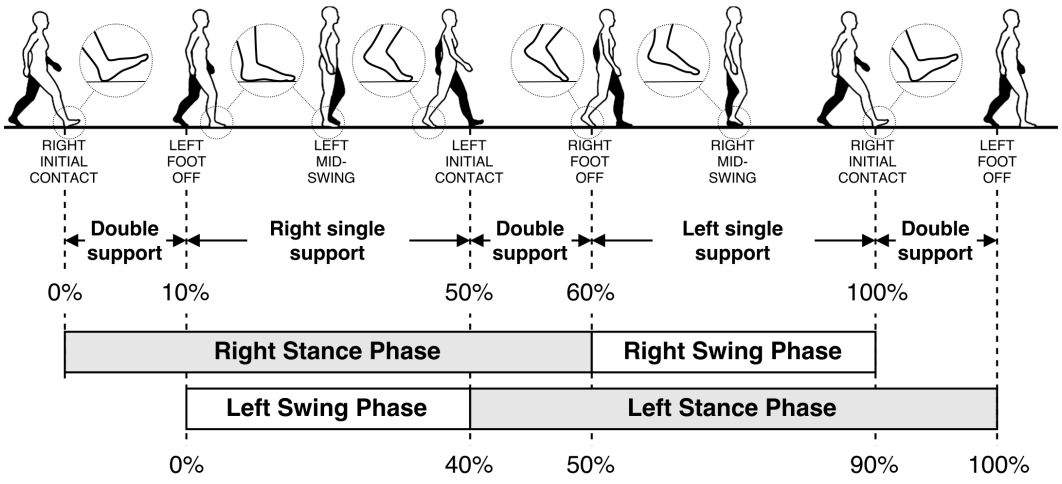


Figure 2.1. Healthy human gait cycle.

in Parkinsonian shuffling gait where the foot strikes the ground all at once). Similarly, toe may not be the last lifted part of the foot in some rare cases. Hence the terms IC and FO are more accurate. Moreover, there may be cases where the subject's feet do not leave the ground at all (i.e. foot dragging). In this case, the FO event is defined as the instant when the forward motion starts and opposingly the IC event is when the forward motion stops [4].

An insightful case of pathological gait is observed in Parkinson's disease (PD). Even though this thesis is not solely focused on PD, a considerable portion of our neurological disorder subjects suffer from it. Moreover, PD shares many gait symptoms with other neurological disorders, rendering it important for understanding common gait abnormalities [6]. Typical gait in PD is shuffling gait, historically so called "marche a petits pas", with slow and small steps [7]. PD usually starts on one side of the body, resulting in asymmetry. As the disease progresses, the feet may become magnetic, hard to lift off the floor, and in some cases there is freezing of gait, i.e. a brief, episodic interruption of forward progression. Comorbidities like vascular brain diseases may result in additional gait problems due to paresis (muscular weakness) and imbalance. Sensory problems like poor eye sight, polyneuropathies that interfere with sensation may also disrupt balance [8]. Conditions like spinal stenosis or normal pressure hydrocephalus may cause problems confined to the lower extremities [6]. It is important to detect different components of gait problems when making a diagnosis and performing subse-

Table 2.1. Spatio-temporal gait parameters.

Gait Parameter	**Definition**
Stride length	Distance between two successive placements of the same foot.
Step length	Distance by which a foot moves in front of the other foot. The sum of two successive step lengths corresponds to stride length.
Walking base	Side to side distance between the motion lines of the two feet.
Cadence	Number of steps taken per minute, i.e. gait frequency.
Cycle time	Duration of a single stride. Cycle time is inverse proportional to cadence and hence can be used as an alternative to it.
Stance time	Duration of stance phase, starting with IC and ending with FO of the same foot.
Swing time	Duration of swing phase, starting with FO and ending with IC of the same foot. The sum of stance and swing times of a single stride defines its cycle time.
Stance ratio	Ratio of stance time over the cycle time.
Speed	Gait speed, defined by stride length / cycle time.
Clearance	Elevation of the foot during the swing phase. This parameter can be diversified as minimum and maximum foot clearance.
Turning rate	Rate of direction change of a foot. Positive values are normally observed during turning steps.

quent patient follow-ups. The identified gait abnormalities can also guide personalized treatment and medication strategies.

Extracting a variety of spatio-temporal gait parameters helps us isolate and identify the components of pathological gait. Standard spatio-temporal gait parameters that have clinical significance are listed in Table 2.1. The temporal parameters deal with the time aspect, while the spatial parameters deal with the space aspect of gait. For instance, stance time and swing time are temporal parameters that represent the duration of the stance and swing phases, respectively. On the other hand, stride length is a purely spatial parameter, representing the distance covered by a single stride of the

same foot. Some parameters, like speed, are influenced by both the temporal and the spatial properties of gait, hence the term *spatio-temporal* is commonly used to cover all of the listed gait parameters.

The listed parameters can all be computed individually for each stride, although some parameters are more meaningful when averaged over a substantial walking period. For instance, speed of a single stride is not as informative as the average walking speed. However, since averages can be easily computed in the presence of stride-wise data, a successful gait analysis implementation should aim to compute these parameters in a stride-wise manner. Moreover, having data for each individual stride is useful to determine the overall temporal changes and variations in gait, which are especially informative for the typical gait-related symptoms of neurological disorders. Another important aspect of gait is left-right asymmetries, which can be deduced from separate stride-wise data of two feet. Both temporal variations and left-right asymmetries, that are post-computed using stride-wise data, are used extensively in Chapter 6, where the common gait abnormalities in neurological disorders are analyzed.

It should also be noted that, some parameters listed in Table 2.1 are derivable from a combination of other parameters. For instance, cycle time is also defined as the sum of stance and swing times in a single cycle. As another example, stride time and cadence can be converted to each other using the equation, $\text{cycle time (sec.)} = 120/\text{cadence (steps/min.)}$. So, the gait parameters can further be divided into core parameters and derived parameters. The core parameters are step length, walking base, stance time, swing time, clearance and turning rate. All other parameters can be derived in the existence of these parameters. Surely, if a core parameter is absent, another parameter can be considered as a core parameter; for instance, stride length becomes the only core spatial parameter in the absence of step length, since it is underivable without it.

The proposed gait analysis system, presented in Chapter 5, is able to estimate all but two of the listed parameters: step length and walking base. Estimating step length

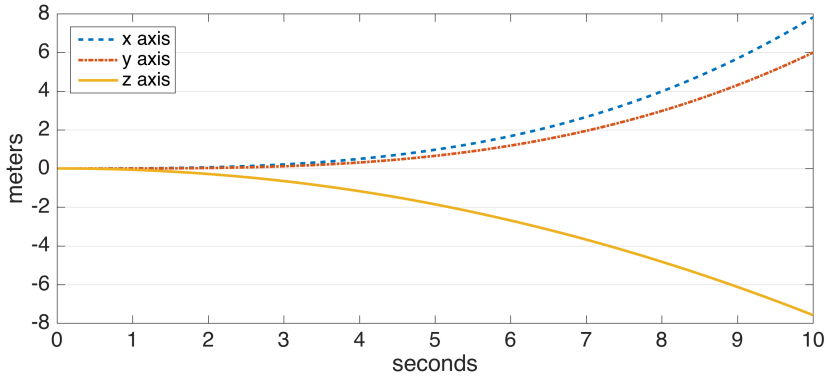
may appear trivial at the first glance; however, the definition presented in Table 2.1 requires the spatial synchronization between two feet, i.e. knowledge of relative displacement and orientation between two feet at all times. The proposed system tracks the position change of the feet separately with respect to their initial positions, thus a positional drift is imminent. Hence the current state of our system does not guarantee spatial synchronization. Walking base also requires spatial synchronization. There are proposals in the literature that employ additional equipment to achieve this synchronization (such as a small camera mounted on a foot to detect the other foot when they are adjacent [9]); however, we chose not to employ additional sensors in this study since they would possibly hinder the non-obtrusiveness of the system.

2.2. Challenges of Working with IMUs

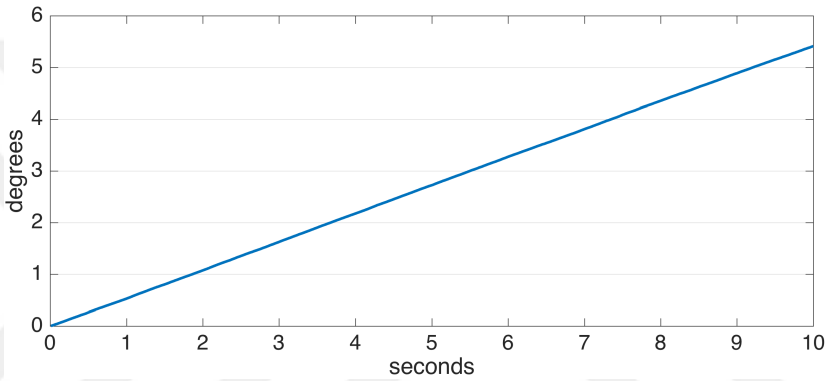
Even though the evolution of technology has improved the underlying sensors in a typical IMU over the recent years, there are still challenges that need to be faced. Some of these challenges can be overcome by the state of the art proposals in the literature, while some of them are not yet addressed or solved. Moreover, some of the solutions in the literature assume controlled data collection environments (error-less system setup and deployment) and perfectly executed data collection procedures, which are rarely achievable even in a professional-aided clinical setting. This issue gets even more challenging in non-hospital settings that we ultimately target in this study.

2.2.1. Error Sources in Inertial Sensors

IMUs consist of accelerometers, gyroscopes and magnetometers. In theory, acceleration measured by the accelerometer can be integrated twice to acquire the relative change in position. Similarly, the angular velocity measured by a gyroscope can be integrated to compute the relative orientation (attitude) change. However, in practice, these sensors are susceptible to noise and other small errors, which cause significant drift when the raw measurements are integrated. It should be noted that, accelerometers or inclinometers could also be used to directly determine the orientation (more



(a)



(b)

Figure 2.2. Typical drifts observed in integration of data from (a) accelerometer, (b) gyroscope.

accurately, the direction of gravity relative to the device) without the need for integration; however, external accelerations applied to these sensors may confuse the detection of the gravity vector. Hence, when determining 3D-orientation, usually data from multiple sensors are fused.

The drift errors due to integration are demonstrated in Figure 2.2. The data is collected from a perfectly stationary IMU. The gyroscope and accelerometer drift result in a linearly growing error in angle and a position error growing proportional to t^2, respectively. Especially the position error, which rises to the order of meters in a few seconds, and to the order of hundreds of meters in a minute, makes it practically impossible to use solely double integration for position estimation. Hence there is a need for additional domain knowledge to estimate and eliminate drift periodically. Fortunately, human steps are of periodic and frequent nature.

The state-of-the-art to cope with the accelerometer and gyroscope drifts involve the combination of a technique referred to as the zero-velocity update, which exploits the periodic nature of human gait, and a Kalman filter to track and correct the correlations of the state errors [9,10]. These techniques are also encountered in the pedestrian navigation literature, where high position accuracy is the primary concern. Brief explanations of zero-velocity updates and Kalman filtering are provided in Sections 5.2.2 and 5.2.3, respectively. In the proposed gait analysis system, we also employ these techniques, but we support them with novel additional methodology to establish a robust system that is minimally affected by unintentional faults in deployment and data collection, such as sensor placement imperfections, loose time synchronization between multiple sensors and errors regarding the application of data collection procedures (e.g., insufficient calibration period). In the next section, these typical data collection-related errors are investigated in detail. The methods presented in Chapter 5 also consider pathological gait, and does not rely on assumptions of normal gait.

2.2.2. Operational Challenges and Difficulties in Data Collection

Typical sensor placement locations for lower-body gait analysis include feet, shanks, thighs and trunk; each with distinct advantages and disadvantages. A complete system with multiple sensors in each of these locations may provide the most information, but with each sensor, the obtrusiveness increases. Considering the objective of extracting as many spatio-temporal gait parameters as possible without diminishing mobility and convenience, placing only two sensors on the feet stand out as a viable tradeoff between obtrusiveness and completeness, since it allows us to employ zero-velocity updates to achieve high spatial accuracy, which in turn can be converted into a rich set of gait parameters. The advantages of foot-mounted inertial sensors are further elaborated in Section 3, with a detailed survey of the related literature. The details of our data collection setup is found in Chapter 4.

The inertial sensors may typically be collocated with the feet via straps or insoles. Insoles offer a more stable sensor placement, but their costs are typically higher. It

goes even further up with the need to have different sizes readily available for different shoe sizes. Moreover, insoles are only usable with certain types of shoes, and they are not suitable for shoeless (bare-foot or with socks) usage. On the other hand, length-adjustable straps (typically velcro) do not have these restrictions at the expense of decreased sensor stability. Because of this and the unrestricted deployment options, defining and enforcing a standard way of strapping the sensor on the foot is impossible; the specific location and the orientation of the sensor may change from session to session and patient to patient. Therefore, assuming a specific sensor orientation relative to the foot (e.g., a specific IMU axis aligned with either the medial-lateral or the anterior-posterior) is highly unrealistic. It should also be noted that, the controlled environments where the validation experiments are conducted are not existent in the field. Moreover, a successful system should be easily usable by a non-professional, who may make mistakes during the data collection procedure, such as placing the IMU backwards. Such mistakes should not render valuable data unusable.

Human errors may sometimes be even inevitable, especially in time-constrained cases where the time allocated for data collection is limited and repetitions to remedy errors are not possible. Clinicians can spend only a limited amount of time for each patient, which may simply prevent perfect data collection. The same also goes for the patients, who may not want to spend hours until the perfect data is finally achieved. In short, we must make use of the data we get, no matter the errors.

Other data collection errors include the initiation of the sensors after the subject starts walking. Many existing studies rely on a calibration period where the subject is expected to perform a specific movement pattern (either standing still or walking on a straight line), for correct operation afterwards. Such a period may not be available due to either human error (e.g., the data collecting personnel may forget about the calibration period altogether, or the subject may start walking immediately without waiting for a cue), or hardware problems leading to data loss (e.g., wireless communication issues at the start of a session that renders calibration data unusable). These examples are from the very problems that our research group encountered in the re-

cent few years. Therefore, the methods proposed in this thesis are designed to operate without the need for a calibration procedure.

Hardware related problems may also lead to time-synchronization issues between multiple IMUs. Most commercial IMUs use timestamps to label the data; but this rarely alleviates the problem, since usually in gait applications, a synchronization on the order of milliseconds is required, which is very difficult to achieve even from the beginning. The internal clocks of the sensors may easily fall out of sync due to battery issues, and a perfect synchronization rarely lasts a few days. Our methodology does not rely on time-synchronization, as different feet are tracked separately, and the parameters are aggregated in the parameter extraction phase rather than in the raw data analysis. Battery life is also an important concern for systems targeting continuous gait monitoring. Although efficient power-aware motor activity monitoring body sensor network architectures have been proposed [11], it still remains a challenge. Of course, these hardware problems are mitigated each day by new technological improvements, and may no longer be of question in the future. But, human errors will certainly remain to be a reality, and unfortunately some of these errors are simply unavoidable. As also dissected in Chapter 3, only a small portion of the related literature stress this reality. One of the primary aims of this thesis is to fill this gap by proposing a robust gait analysis system that is minimally affected by such errors and makes minimal assumptions on the correct application of the data collection procedure.

3. LITERATURE REVIEW

The two umbrella contributions of this thesis are a wearable inertial sensor-based gait analysis system and an automated fall risk assessment solution which is a natural extension of the former. In this chapter, we present an overview of the existing literature on these topics, outlining the state-of-the-art and highlighting the strengths and weaknesses of the existing work. The gait analysis and the fall risk assessment studies are discussed respectively in the upcoming two sections.

3.1. Related Work on Gait Analysis with Inertial Sensors

In this section, we present a review of the gait analysis studies that are relevant to this thesis, not only in terms of the objectives, but also the sensor placement and the employed methodology. We also highlight the advantages and drawbacks of these methods with respect to the current state of our system.

Estimating the temporal gait parameters requires the detection of IC and FO events, which separate the stance and swing phases. A widely adopted method for IC/FO detection is peak detection on the raw acceleration or gyroscope (angular velocity) signals. IMUs placed on either the top of the feet [10, 12–14] or on the ankles/shanks [15, 16] are used for this purpose. Peak detection can be further complemented with additional features such as the derivative of the acceleration signal, which may be fed into a hidden Markov model (HMM) to detect the underlying states of a stride more accurately [17]. Another alternative placement is the trunk at the expense of decreased accuracy, which can be improved with the more advanced methodology of wavelet-based time and frequency analysis [18]. These methods achieve a reasonable timing accuracy; however, the majority of the studies make the assumption of normal gait and foot fall. The peaks required to detect IC events are only observed if there is a pronounced heel strike. Only a few studies consider the possibility of pathological gait (even foot fall) [12]. The IC/FO detection method proposed in this thesis aims to

produce accurate results even in this case.

In [19], the authors conducted a comparative performance evaluation study on various existing temporal gait event detection methods, and also evaluated various sensor placements. They concluded that peak detection-based methods utilizing foot-mounted sensors outperform the other approaches and sensor placements. This finding supports our choice of foot-mounted sensors for the gait analysis methodology proposed in this thesis, presented in Chapter 5.

Some studies employ force sensors integrated to a shoe [20] or an insole [21] to increase the timing accuracy and address the challenges of pathological gait. Even though these approaches produce superior detection performance at the expense of additional hardware, they are more costly compared to the inertial sensor-only solutions and have decreased convenience for the patients due to the need to wear specific shoes and insoles (which should be made available in different sizes for different patients, also contributing to the increased cost).

Extracting spatial parameters such as stride length is a more challenging problem due to the technical challenges associated with inertial sensors (see Chapter 2). A well-explored method for stride length estimation is to construct a geometric human locomotion model using the joint angles estimated via the IMUs [15, 22–24]. The absolute 3D-orientation of the IMUs can be accurately computed via the fusion of acceleration and gyroscope data, which can then be converted into joint angles using the orientation differences between adjacent sensors [25]. This approach also enables the virtual reconstruction of the skeletal motion of the lower body. However, the spatial accuracy of this method is generally low, since the orientation errors even as low as a few degrees correspond to several centimeters in the constructed geometric model, and the errors in adjacent joints produce a cascading effect when determining the displacement of the feet. Another drawback of this method is the need to measure the exact lengths of the lower body segments of the subjects, which adds to the complexity of the pre-test preparations.

Another approach to determine spatial parameters is the double integration of the acceleration signal to measure the displacement [16, 20, 26]. To cope with the drift errors accumulating due to integration, the integration window should be reset periodically. Even small errors in the reset timing lead to large displacement errors. A viable approach to determine the reset times is to detect feet zero-velocity phases [13, 27–29], which is only applicable for foot-placed IMUs. However, zero-velocity updates only prevent the drift errors to grow beyond acceptable levels and do not attempt to minimize the already accumulated error. A better approach is to use Kalman filtering aided with zero-velocity updates to track the errors and correct them retrospectively [9, 10], which leads to high spatial accuracy. Another method to determine the stride length is to use a single trunk-placed sensor and utilize double integration along the vertical gravity aligned vector, which is then converted into horizontal displacement using the inverted pendulum model [18]. The advantage of this method is using only a single IMU, however the spatial accuracy of this approach is lower.

Another important spatial gait parameter is foot clearance, especially considering its influence on fall risk [5]. However, it is neglected in many existing gait analysis studies, as there are only a few studies that focus on estimating foot clearance [30, 31]. The approach is similar to stride length estimation, as zero-velocity corrected double integration of the acceleration signal is used to estimate the displacement in the vertical domain. We did not encounter any study that employs Kalman filtering to mitigate the already-accumulated displacement errors, which exposes a shortcoming of the existing literature and a potential to enhance the clearance estimation accuracies.

Other gait analysis studies of interest include [32–34], which are quite different compared to the other studies reviewed in this chapter, as they do not aim to extract standard gait parameters. However, they are worth attention since they aim to extract balance and symmetry related upper-body features from the raw data of sensors placed on the trunk. In our proposal, we do not employ these approaches, but they are important contributions which may extend the current capabilities of our gait analysis system in the future, at the expense of an additional sensor.

The details of the prominent studies overviewed in this chapter are presented in Table 3.1. The aims of the studies along with the corresponding methodology (highlighted in parentheses), the number and placement of the sensors, the number of test subjects, and the strengths and weaknesses of the studies are included.

Table 3.1. Related work on gait analysis with inertial sensors.

Ref.	**Aim (*Methodology*)**	**Sensors**	**Subjects**	**Strengths (Novelty)**	**Weaknesses**
[25]	Body joint angles estimation (*3D-orientation differences between sensors*).	Force sensors; IMUs: 2 on ankles, 2 on knees, 1 on trunk	1 healthy	Multiple sensors enabling accurate joint angles information.	Only proof of concept (single subject). No gait parameters extracted. Relatively higher cost.
[26]	Calibration procedure for sensor misplacement, stride length estimation (*double integration*).	2 IMUs on ankles	8 healthy	Considers sensor placement errors and proposes a procedure to mitigate them.	Low spatial accuracy due to double integration. Only healthy subjects.
[22]	Drift removal in gyroscope signals. Estimation of cycle time, stride length, step length, cadence (*geometric human locomotion model*).	IMUs: 1 on pelvis, 2 on thighs, 2 on shanks, 2 on feet	5 healthy	Rich set of parameters. Drift removal to increase accuracy.	Only healthy subjects, not targeted towards gait abnormalities. Obtrusive due to number of sensors.
[12]	IC/FO detection (*peak detection*).	IMUs: 2 on shanks, 2 on feet	13 spinal cord injury, 12 healthy	Considers pathological gait. Experiments with real patients.	Obtrusive: Sensors wired to PDA; sensors on shank attached to skin via tape. No spatial parameters.
[15]	IC/FO detection (*peak detection*), stride length estimation (*geometric human locomotion model*).	IMUs: 2 on forearms, 2 on shanks, 2 on thighs	10 PD, 10 healthy	Rich set of spatio-temporal parameters. Real patients.	Low accuracy in spatial parameters. Obtrusive due to number of sensors.
[16]	Analyzing changes prior to freezing of gait. IC/FO detection (*peak detection*), stride length estimation (*double integration*).	2 IMUs on ankles	5 PD	Rich set of spatio-temporal parameters. Real patients.	Low accuracy in spatial parameters. Limited number of subjects. No control group.
[17]	IC/FO detection (*peak detection complemented with HMM*).	1 IMU alternated placements	1 healthy	A solution adaptive to a variety of placements.	Not targeted for pathological gait. Only one healthy subject.
[23]	Estimation of cycle time and stride length (*geometric human locomotion model*).	IMUs: 2 on shanks, 2 on thighs	6 PD, 7 healthy	Real patients.	Low accuracy in spatial parameters. Stance/swing times are not extracted (only cycle time).

Table 3.1. Related work on gait analysis with inertial sensors (cont.).

Ref.	**Aim (*Methodology*)**	**Sensors**	**Subjects**	**Strengths (Novelty)**	**Weaknesses**
[24]	Estimation of stride length and stride velocity (*geometric human locomotion model*).	2 IMUs on shanks	10 PD, 36 hip replacement, 7 coxarthrosis; 18 healthy	High number of real patients with multiple different conditions affecting gait.	Dataset from previous studies. Limited temporal parameters (only stride velocity).
[20]	IC/FO detection (*force sensors*), stride length estimation (*double integration*).	Force sensors; 2 IMUs shoe integrated	5 PD, 10 healthy	Different modalities integrated in a shoe. Real patients.	Low spatial accuracy due to double integration. Relatively higher cost.
[21]	Classification of movement patterns, estimation of stance/swing times (*naive Bayes classifier*).	Force sensors and an IMU integrated in an insole	5 healthy	Ability to detect different types of steps including lateral and backward walking.	Only healthy subjects, not targeted towards gait abnormalities. Relatively higher cost.
[32]	Detection of heel strikes (*peak detection*), asymmetry indices from raw acceleration intensity (*spectral analysis*).	1 IMU on trunk	15 healthy	Asymmetry indicators computed from raw data.	Only healthy subjects. No standard spatio-temporal parameters extracted.
[14]	IC/FO detection (*peak detection*), balance detection (*raw acceleration signal processing*).	IMUs: 2 on feet, 1 on waist	21 AD, 50 healthy	Balance features that indicate the intensity of lateral sway.	IC/FO detection methodology is not novel. No spatial parameters extracted.
[33]	Regularity and symmetry indices (*Fourier analysis on raw acceleration signals*).	1 IMU on waist	64 PD, 32 healthy	High number of real patients.	Methods are not clearly explained.
[18]	IC/FO detection (w*avelet analysis*), stride length estimation (*inverted pendulum model with double integration*).	1 IMU on trunk	30 PD, 30 healthy	High number of real patients.	Low accuracy in spatial parameters.
[13]	IC/FO detection (*peak detection*), stride length estimation (*double integration aided with zero-velocity updates*).	2 IMUs on feet	10 healthy	Increased spatial accuracy due to zero-velocity updates (compared to only double integration).	Obtrusive system: The sensors are wired to a control node. Only healthy subjects.
[28]	Stride length estimation (*double integration with zero-velocity updates*), gait on level-ground, ramp, or stairs classification (*threshold-based algorithm*)	2 IMUs on feet	8 healthy	High spatial accuracy. Gait surface classification.	Not targeted for pathological gait. Few subjects.

Table 3.1. Related work on gait analysis with inertial sensors (cont.).

Ref.	**Aim (*Methodology*)**	**Sensors**	**Subjects**	**Strengths (Novelty)**	**Weaknesses**
[29]	IC/FO detection (*peak detection*), stride length estimation (*double integration with zero-velocity updates*)	2 IMUs on feet	20 healthy	High spatial accuracy. Also discusses gait asymmetries in extracted parameters.	Not targeted for pathological gait.
[9]	3D feet position estimation (*KF with zero-velocity updates*), spatial feet sync. (*camera-based detection*)	2 IMUs on feet, 1 camera on single foot	1 healthy	High spatial accuracy and spatial synchronization.	No standard parameters. Not targeted for pathological gait. Only one subject.
[10]	IC/FO detection (*peak detection*), stride length estimation (*KF with zero-velocity updates*).	2 IMUs on feet	16 PD (ON state)	High spatial accuracy due to Kalman filtering methodology. Real patients.	IC/FO detection not suitable for pathological gait. Patients are in ON state. No control group.
[30]	Clearance estimation (*double integration with zero-velocity updates*)	2 IMUs on feet	12 healthy	One of the few studies focusing on clearance.	Low heel clearance accuracy (mean error: 4.1 cm). Not targeted for pathological gait.
[31]	Clearance estimation (*double integration with zero-velocity updates*)	2 IMUs on feet	20 healthy	One of the few studies focusing on clearance. Higher accuracy compared to [30].	Not targeted for pathological gait.

For further reading, comprehensive surveys on gait analysis with inertial sensors include [2, 35–37]. The existing literature suggest that even though the extraction of spatio-temporal gait parameters are in the focus of many studies, a complete system, that uses efficient methodology such as zero-velocity update aided Kalman filters-smoothers to extract a wide range of spatio-temporal parameters (including spatial parameters in the elevation domain, such as clearance) is still not present. Many studies focus on a single group of parameters (either only spatial or temporal parameters), failing to provide a comprehensive system. Moreover, the majority of the proposals are suitable for healthy gait patterns and their applicability to pathological gait are questionable. It should be noted that, this is not due to the targeted standard gait parameters as they are able to capture many gait abnormalities. For instance, a patient with advanced PD may have magnetic feet, which would increase the stance times (due to the difficulty to lift the feet off the ground). This would lead to a stance ratio

higher than the typical value of 60%. A system that makes the assumption of healthy gait may still be able to compute a parameter in case of pathological gait, but the accuracy of the computed value would be very low. Our proposal aims to achieve a high accuracy, even in pathological cases.

Another weakness observed in many studies is the lack of validation studies with a sufficient number of real patients. A final observation is that, even though all of the studies dissected in this section have clinical significance, the technical contributions and clinical discussions rarely come together, hence the applicability of the output of existing systems for clinical purposes is not clear. We aim to fill this gap by providing real examples of what our system can detect, by combining them with the interpretation of a neurologist (see Section 5.3.2). We also present a systematic predictor importance analysis study in Chapter 6, which aims to identify common gait pathologies observed in neurological disorders.

We also observed that, none of the reviewed studies make a conscious effort to mitigate potential errors related to sensor placements or data collection procedures. The majority of the existing work assume tightly controlled data collection environments with sensors carefully attached to the target limb by a professional. Some studies even require a calibration period, the lack of which would lead to the disposal of otherwise valid data. During our own data collection efforts, we realized that such ideal conditions are rarely achievable and some factors cannot be tightly controlled. Therefore, in this thesis, we aim to formulate a robust gait analysis solution that does not require a calibration procedure and is minimally affected by sensor placement errors.

Comparing the Kalman filtering-based methods to other methods in the literature, it is evident from the evaluation results that the former is superior in terms of spatial accuracy. Hence, we opted to go with this approach to accurately track the 3D position of the feet. However, the extraction of the spatio-temporal parameters is a whole different problem that requires additional methodology that efficiently combines the spatial and temporal elements of gait. Therefore, we aim to extend the

capabilities of the existing methodology to estimate a substantial portion of the typical spatio-temporal parameters presented in Section 2.1. The details of the proposed gait analysis system can be found in Chapter 5.

3.2. Related Work on Fall Risk Assessment

In this section, we present the related work on fall risk assessment with wearable inertial sensors. We have reviewed over 90 papers in the literature to sift out the high-quality studies that have some relevance to this thesis. The relevance criteria include the usability in a non-hospital setting, i.e. not relying on costly non-portable infrastructure like instrumented walkways or motion capture systems. Apart from a few, the majority of the studies that conform to this condition utilize inertial sensors, similar to our study. Another criteria is the active inclusion of gait features or parameters that are extracted from the sensor data. Some studies rely mostly on functional test scores as input, requiring clinical personnel and effort, and use sensor data only as a complement. Such studies are also not included in this section. It should be noted that, this does not mean all studies that use functional tests in some way are eliminated, since functional tests are still a viable approach for determining the ground truth for fall risk and the validation of the proposals.

There are many alternative interpretations of the ground truth for fall risk. The most accurate approach is to consider prospective falls, i.e. the falls that occur in a predetermined time interval after the data is collected. However, this approach is not always possible due to time limitations and the lack of patient follow-up reports. Therefore, there are fewer prospective studies in the literature [38–44], and the majority of the studies use retrospective falls, i.e. the recent fall history, as the ground truth. In this thesis, we also employ the retrospective approach. Other alternatives include any combination of fall history, functional test scores and questionnaires. Functional tests provide finer levels of fall risk (not just two levels as in high and low risk), but tend to be subjective since they are usually conducted and interpreted by a clinician.

In terms of the input, the studies either employ gait features extracted from the raw gyroscope or acceleration data, or higher level spatio-temporal gait parameters. The typical gait features include the mean, variance and energy of the windowed inertial data; spectral components such as dominant frequency and harmonic ratio [45]; and autocorrelation, gait regularity or stability indices [46]. Higher level parameters are usually computed with more sophisticated methods and can capture the implicit risk-related factors in the low-level features [47]. Also, gait parameters are more easily interpretable than features. Even though these properties render gait parameters more valuable, the raw features can still have some nuances that are unintentionally filtered by the parameter extraction process. Of course, there are studies which get the best of the two worlds by combining both [38, 41, 44, 48].

The go-to methods of the medical community for fall risk assessment include logistic regression (LR) [38, 43, 46, 49], and statistical significance assessment tests such as t-test and ANOVA (analysis of variance) [39, 45, 48, 50–52]. These methods can determine the discriminative power of the individual features, and have the important advantage of transparency, i.e. the individual contributions of the features in the decision-making are visible. However, they are less powerful than machine learning models in terms of classification accuracies in many cases. Moreover, turning the results of the statistical tests into automated classifiers is not trivial and involves threshold-based approaches prone to error and classification bias.

More advanced machine learning models are less frequently employed in this domain, although decision trees (DT) are used relatively frequently [40,41,53]. Other employed methods include support vector machine (SVM), neural networks (NN), specifically multilayer perceptrons (MLP), naive Bayes classifier (NB), random forest (RF), k-nearest neighbors (kNN) and regularized discriminant model classifier [44, 53–56]. These methods produce readily applicable automated classifiers and usually exhibit superior classification performance. Moreover, compared to the statistical significance tests that analyze features individually, some machine learning models are capable of determining multivariate discriminants taking into account multiple features. They can

also produce non-linear decision boundaries, potentially leading to superior accuracy.

A study worth extra attention is presented in [57]. The authors employ deep learning methods, namely long short-term memory (LSTM) and convolutional neural networks (CNN), on the raw acceleration data to infer fall risk. They explore various neural network architectures and also utilize multi-task learning (with gender and age recognition as the auxiliary tasks) to achieve a classifier with an area under the curve (AUC) value of 0.75. To the best of our knowledge, this is the only fall risk assessment study that employs deep learning methods, at the time of writing this thesis. Even though the reported classification accuracy is low, this study showcases the potential of deep learning for the problem of fall risk assessment. The fall risk assessment method proposed in this thesis (Chapter 7) also attempts to utilize deep learning methods, specifically LSTM networks, in order to come up with an accurate fall risk classifier.

Other studies worthy of mention include [42, 58], which use posturography in addition to gait analysis. Posturography is the study of posture and balance, and is executed via functional tests that involve the subjects standing on a special foam surface and trying to maintain balance. The standing surface is typically complemented with a force platform that measures the pressure exerted by the feet. Inertial sensors may be used during these tests to extract balance-related features, which may increase the fall risk assessment accuracy [59]. Even though posturography is not in the scope of this thesis, they have merit and can be used as complementary methods to improve the accuracy of the gait analysis-based fall risk assessment approach, if needed.

The details of the most relevant and outstanding studies are listed in Table 3.2. The aims and the respective methods, the employed sensor equipment and the number of subjects are included in the table. The strengths and weaknesses of the individual studies are also highlighted, including their ground truth measures.

Table 3.2. Related work on fall risk assessment with inertial sensors.

Ref.	**Aim (*Methodology*)**	**Sensors**	**Subjects**	**Strengths (Novelty)**	**Weaknesses**
[54]	Extract gait features (*from raw data*), feature selection (*forward wrapper selection*), classification into high/low risk (*RBFN, SVM, kNN, NB*)	10 Accelerometers on various body locations	20 various (15 high risk, 5 low risk)	High classification accuracy (95%). Uses machine learning methodology.	Limited number of healthy subjects. Very obtrusive (the sensors are wired and taped on the skin).
[53]	Extract gait features (*from raw data*), feature selection (*only forward*), classification into high/low risk (*kNN, NB, NN, SVM, RF, DT, LR*)	1 IMU on trunk; 1 force platform	296 various (51 high risk, 245 low risk)	High number of subjects. Uses machine learning. High/low ground truth determined by functional tests. High accuracy (DT: 88.2%).	Not targeted towards neurological disorders. Requires a force platform.
[51]	Extract temporal gait parameters (*methods from other studies*), assess significance of parameters in terms of fall risk (*various statistical tests*)	1 IMU on trunk	107 PD patients (40 fallers, 47 non-fallers)	Long term data collection (3-days) for each subject. Focused on PD. High number of subjects.	Only non-specific temporal parameters (e.g., % of time spent walking, # of steps). No automated classifier.
[49]	Extract temporal gait parameters (*methods from another study*), classification into fallers/non-fallers based on history (*LR*)	2 IMUs on shanks	349 various (207 fallers, 142 non-fallers)	High number of subjects.	Not targeted towards neurological disorders. Low accuracy (76.8%). Only temporal parameters.
[38]	Extract gait features (*from raw data*), classification into fallers/non-fallers (*LR*)	1 Accelerometer on trunk	169 various (60 fallers, 109 non-fallers)	6-months prospective study. 8 consecutive days of data collection. High number of subjects.	Not targeted towards neurological disorders.
[50]	Extract gait features during timed-up-and-go test (*from raw data*), assess significance of features (*t-test*)	1 Smartphone in pocket	18 various (5 high risk, 13 low risk)	High/low risk status determined by a combination of POMA and TUG functional tests (not only fall history).	Lacks an automated classifier. Low number of subjects. Not targeted towards neurological disorders.
[39]	Extract gait parameters (*instrumented walkway*) and gait features (*from raw data*), assess the significance of parameters (*t-test*)	2 IMUs on feet, 1 instrumented walkway (GAITRite)	97 various - all women (54 fallers, 43 non-fallers)	12-months prospective study. High number of subjects.	Only one feature from IMU data (fractal scaling index). IMUs are wired to a data-logger (obtrusive). Low accuracy (67%).

Table 3.2. Related work on fall risk assessment with inertial sensors (cont.).

Ref.	**Aim (*Methodology*)**	**Sensors**	**Subjects**	**Strengths (Novelty)**	**Weaknesses**
[40]	Extract gait features (*from raw data, stride-wise*), classification into fallers/non-fallers (*DT*)	1 IMU on unspecified location	40 Dementia (20 fallers, 20 non-fallers)	2, 4, 8 months prospective study. Considers each gait cycle data as a separate instance (larger dataset).	Low sensitivity in long-term classification (33.6%). Cycle-wise instances cannot represent intra-subject variability.
[52]	Extract temporal gait features (*from raw data*), assess significance of features in terms of fall history (*ANOVA*)	1 Accelerometer on trunk	53 various (20 fallers, 33 non-fallers)	One of the first studies to employ an IMU.	Only three temporal gait features (stride frequency, symmetry and regularity), spatial parameters are not extracted via the IMU.
[55]	Extract angular rate features during posturography (*from raw data*), classification into Tinetti scores 1 and 3 (*NN*)	1 Accelerometer on trunk	260 various (130 fallers, 130 non-fallers)	High accuracy (97%). High number of subjects.	Target variable is Tinetti score which is a subjective measure for fall risk and is directly related to balance.
[60]	Extract temporal and spectral gait features during functional tests (*from raw data*), regression to infer number of falls (*Linear Regression*)	1 Accelerometer on trunk	68 various (22 fallers, 46 non-fallers)	High number of features (126) combining acceleration and functional test features. Multiple classes (# of falls).	No spatial parameters considered. Not targeted towards neurological disorders.
[41]	Extract gait features and parameters (*Methods from other studies*), classification into fallers/non-fallers (*DT, LR*)	1 Accelerometer on trunk	46 various (19 fallers, 27 non-fallers)	12-months prospective study.	Low sensitivity (58%) - Though it increases to 74% in case physical activity scores (collected through 12-months) are included.
[48]	Extract gait features, regularity, asymmetry indices (*methods from other studies*), assess significance of features in terms of fall risk (*ANOVA, t-test, ICC, LR*)	1 Accelerometer on trunk	121 various (40 high risk elderly, 41 low risk elderly, 40 low risk young)	Fall risk assessed as a combination of fall history, TUG and Tinetti tests. High number of patients.	Lacks an automated classifier. Not targeted towards neurological disorders.
[43]	Extract spectral gait features, harmonic ratio (*from raw data*), assess significance of features in terms of prospective falls (*t-test, LR*)	2 Accelerometers on lower and upper trunk	73 various (16 fallers, 57 non-fallers)	12-months prospective study.	Lacks an automated classifier. Not targeted towards neurological disorders. Only one gait feature per sensor axes (harmonic ratio).

Table 3.2. Related work on fall risk assessment with inertial sensors (cont.).

Ref.	**Aim (*Methodology*)**	**Sensors**	**Subjects**	**Strengths (Novelty)**	**Weaknesses**
[61]	Extract gait parameters (*methods from other studies*), assess significance of the parameters in terms of Tinetti score (*ANOVA*)	1 Accelerometer on trunk	100 various (50 high risk, 50 low risk)	High number of subjects. Includes both temporal and spatial gait parameters.	Fall risk ground truth only based on Tinetti test. Lacks an automated classifier.
[45]	Extract spectral gait features (*from raw data*), assess significance of features (*various statistical tests*)	1 IMU on trunk	131 various (42 fallers, 89 non-fallers)	High number of subjects.	No automated classifier.
[56]	Extract gait features (*from raw data*), classification into fallers/non-fallers (*regularized discriminant classifier*)	2 IMUs on shanks	22 various (11 fallers, 11 non-fallers)	Explores combination of inertial data and clinical data.	Low number of subjects. Low accuracy (72.7%).
[46]	Extract gait stability measure (*from raw data*), classification into fallers/non-fallers (*LR*)	1 Accelerometer on trunk	71 various (32 fallers, 39 non-fallers)	High number of subjects. Compact gait stability measure.	Dataset from earlier study [62]. Low accuracy (AUC: 0.75).
[44]	Extract gait features and parameters (*methods from other studies*), feature selection (*ReliefF*), classification into fallers/non-fallers (*NB, MLP, SVM*)	Accelerometers: 1 on head, 1 on pelvis, 2 on shanks	75 various (28 fallers, 47 non-fallers)	High number of subjects. Prospective study.	Low accuracy (65%).
[63]	Extract gait features (*from raw data*), classification into fallers/non-fallers (*RF*)	1 Accelerometer on pelvis	67 women (19 fallers, 48 non-fallers)	Uses machine learning. Feature importance analysis with RF.	Low accuracy (73.7%).
[57]	Classification into fallers/non-fallers (*LSTM with raw data as input*)	1 Accelerometer on trunk	296 various (101 fallers, 195 non-fallers)	Uses deep learning. High number of subjects. Prospective study.	Low accuracy (AUC: 0.75%).

For further reading, surveys on fall risk assessment studies that use wearable inertial sensors can be found in [47, 64, 65]. The trend of machine learning seems to gain attraction in this topic as well, which is fitting, given the nature of the problem that deems an automated classifier. However, the reported classification accuracies are still usually low, which is not surprising considering the challenge of the problem. Fall

risk assessment is generally more meaningful when targeted towards people who already have gait disorders, since identifying the specific abnormalities leading to fall risk is more valuable and may help clinicians to instill additional treatment measures for those who have a higher risk of falls. This makes the classification problem more difficult, as it requires more than simple recognition of the existence of abnormalities. Machine learning models certainly have potential, however it still remains untapped as apparent from the low accuracies. Hence the literature is still hungry for a high-accuracy solution. We attempt to fill this gap by formulating a solution that combines machine learning methods and the output of our gait analysis system, which is infused with the domain knowledge that have the potential to boost the classification accuracy. We specifically employ LSTM neural networks and use the spatio-temporal gait parameter sequences as input. We also compare its performance to more traditional machine learning methods to demonstrate its superiority. The details of the proposed fall risk assessment methods are presented in Chapter 7.

Our dataset of neurological disorder patients provide a realistic and challenging use case. Assessing fall risk in neurological disorders is especially important, since many neurological disorders lead to gait abnormalities that may eventually lead to falls [65]. This specific use case also increases our study's value.

Automated fall risk assessment is a good example of a pervasive healthcare application that requires a ubiquitous service architecture. Imagine a nursing home setting in which numerous residents can be monitored in real time by an inertial sensor-based fall risk assessment solution. To enable such a use case and address the associated challenges, we explore the applicability of our methods as a pervasive healthcare service, and propose a multi-tier computing and communication architecture that utilize edge computing and software-defined networking paradigms. The details of the architecture are presented in Section 7.4.

4. INERTIAL GAIT DATASET

In this chapter, the details of the gait dataset we collected as part of this thesis are given. First, we present the properties of the utilized sensors and their placement on the human body along with accompanying technical considerations. Then, we explain our data collection procedure. Finally, we present the clinical and demographic information on the test subjects, along with our inclusion and exclusion criteria.

4.1. Equipment

As the inertial sensory equipment, we used EXEL ExLs3 IMUs [66]. As many commercial IMUs currently available in the market, they are low-cost, light, small and battery operated, which allow them to fit well within the considerations of a pervasive and unobtrusive gait analysis solution. Each unit is comprised of an accelerometer, a gyroscope and a magnetometer sensor, which produce tri-axial measurements aligned with the unit's body coordinate frame. The IMU supports a sampling rate of up to 200 Hz for all sensors. The accelerometer supports a full-scale acceleration range configurable between ± 2 and ± 16 g. The gyroscope supports a full-scale angular velocity range configurable between ± 250 and ± 2000 dps (degrees per second). For the data collection, we configured the IMUs to the sampling rate of 100 Hz, the acceleration range of ± 8 g and the angular velocity range of ± 1000 dps. These range settings are determined with the consideration of the intensity of typical human motion, while not sacrificing too much measurement sensitivity.

ExLs3 IMUs have wireless communication capabilities via Bluetooth 2.1, which allow them to transmit the data to a Bluetooth-capable computer, in real time. They additionally have a local flash storage of 1 GB, so the data can also be stored on the device for later acquiry and analysis. We used either of the data acquisition modes throughout our data collection efforts, depending on the conditions. The battery life varies between 3-5 hours depending on the configuration.



(a) (b) (c)

Figure 4.1. (a) ExLs3 IMU, (b) strapped to shoe, (c) strapped on socks.

The IMUs are strapped on top (dorsum) of a subject's both feet via adjustable elastic velcro straps with IMU housing pockets. The ExLs3 IMU and the straps are shown in Figure 4.1. The feet are chosen as the sensor placement location due to their superior spatial accuracy potential, as supported by the related studies presented in Chapter 3. Using two sensors for the left and right feet also allows us to capture asymmetries, at the expense of slightly increased complexity compared to the single-sensor solutions. Alternative sensory equipment solutions for feet include insoles or shoes integrated with IMUs. We chose to employ straps over insoles and shoes due to their lower cost, higher convenience and ease of placement, at the expense of decreased sensor placement stability. Insoles and shoes require different sizes and hence multiple devices to be made readily available for different subjects, substantially increasing the cost. Straps do not have this disadvantage, as they are usable on any type and size of shoes, and are even suitable for bare-foot usage, which is especially important for patients having difficulty wearing shoes. We aim to alleviate the stability issues associated with straps via the proposed gait analysis methodology presented in Chapter 5.

4.2. Data Collection Procedure

An important highlight of this thesis is that data collection is difficult, and data not perfectly fitting a predefined procedure should not be easily discarded. Achieving perfect data is impossible, as we learned the hard way during our initial data collection efforts. These difficulties certainly motivated us to seek gait analysis methods adaptive to imperfect data collection conditions, hence nudging us towards a solution appropriate

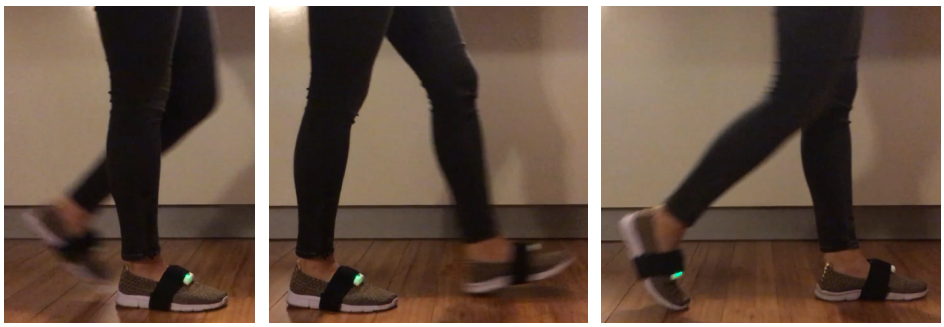


Figure 4.2. Sensors during a data collection session.

for the conditions of real life, as also required by pervasive healthcare applications that deem robust and error-resistant solutions.

A data collection session for a subject involves walking back and forth along a straight path with an approximate length of 8 meters, at least three times. A typical scenario is walking along a corridor and turning back each time the end of the corridor is reached. However, the procedure is not bound to corridors, as it can also be executed in open spaces. The data collection were carried out in various locations including campus, office, house and private clinic environments. The subjects are instructed to walk at their own habitual pace. The sensors during a data collection session are depicted in Figure 4.2.

Our data collection procedure has less strict requirements compared to the majority of the related work, in accordance with our pervasiveness considerations. The proposed gait analysis system can operate with data containing back, side and turning steps, hence we do not discard data if a subject does not exactly follow the suggested walking instructions. However, having absolutely no forward steps in a single session would hinder the operation of some of the gait analysis system modules. Moreover, each walking session should have sufficient number of steps (i.e., typically more than 10 steps), for the gait parameters aggregated over multiple strides to be meaningful, though such parameters can still be computed from shorter data. Naturally, longer data would yield more conclusive analysis reports, but short data does not pose any technical challenges on our gait analysis methodology.

We also do not enforce a specific foot-sensor alignment. The IMU should be strapped roughly on top of the foot, but its orientation and placement can be arbitrary. This is especially important when data collection is carried out by a non-professional, since exact alignments are easy to confuse. Moreover, our gait analysis system does not require any calibration period or a synchronization procedure whatsoever, hence the data collection may be initiated even after the subject has started walking.

4.3. Subjects

We collected gait data from a total of 74 neurological disorder patients. The inclusion criteria were the existence of a neurological condition that exhibits gait related symptoms and the subject being able to walk unassisted for a span of at least ten steps. Among these subjects, we excluded the subjects with comorbid orthopedic conditions that may affect gait, serving as our primary exclusion criteria. Ultimately, we have 60 neurological disorder subjects that meet these criteria, whose data are used in the analyses presented in Chapters 5, 6 and 7. The complete list of these subjects are presented in Table 4.1. The list includes their age, height, gender, neurological condition(s), history of falls within a year prior to the data collection, and their usage of a walking aid (e.g., cane, walker) in daily life. The neurological conditions include, but are not limited to, Parkinson's disease (PD), vascular dementia (VaD), frontotemporal dementia (FTD), dementia with lewy bodies (DLB), normal pressure hydrocephalus (NPH), progressive visuospatial deficit (PVSD), vascular mild cognitive disorder (VaMCI) and Alzheimer's disease (AD). The neurological disorder subjects (33 females, 27 males) have an average age of 76.2 ± 10.2 (range: 51–91), and an average height of 1.63 ± 0.08 meters (range: 1.48–1.80).

Table 4.1. Neurological disorder subjects.

ID	Gender	Age	Height	Condition	Fall History	Walking Aid
1	M	72	1.74	VaMCI, DLB	No	No
2	M	85	1.65	DLB	No	No
3	F	73	1.62	PD	Yes	No

Table 4.1. Neurological disorder subjects (cont.).

ID	Gender	Age	Height	Condition	Fall History	Walking Aid
4	F	82	1.58	PD	No	Yes
5	M	80	1.76	VaD, DLB	Yes	No
6	F	85	1.65	NPH	Yes	No
7	F	81	1.60	PD	Yes	No
8	F	80	1.60	VaD, DLB, PD	Yes	No
9	M	82	1.65	VaD	No	No
10	F	52	1.56	PD	No	No
11	F	90	1.60	PD	Yes	No
12	M	83	1.59	PD	No	No
13	M	84	1.69	VaD, PD	No	Yes
14	F	82	1.50	DLB	Yes	No
15	F	56	1.58	FTD	No	No
16	F	79	1.57	NPH	Yes	No
17	M	74	1.70	Frontal Gait Apraxia	No	No
18	M	68	1.73	Progressive Dysarthria	No	No
19	M	65	1.68	Alcoholic Dementia	No	Yes
20	F	71	1.70	Narcolepsy	Yes	No
21	F	51	1.52	Cerebellar Ataxia	Yes	No
22	M	72	1.73	FTD	No	No
23	F	75	1.62	Narcolepsy	No	No
24	F	74	1.56	FTD, Epilepsy	Yes	No
25	F	73	1.58	PD	No	No
26	M	75	1.72	PD	No	No
27	M	78	1.76	VaD, AD	No	No
28	F	77	1.58	NPH	Yes	No
29	F	85	1.48	VaMCI	Yes	Yes
30	F	85	1.51	Mixed Dementia	Yes	Yes
31	F	85	1.60	DLB	Yes	No
32	M	84	1.60	VaD	Yes	No

Table 4.1. Neurological disorder subjects (cont.).

ID	Gender	Age	Height	Condition	Fall History	Walking Aid
33	F	70	1.60	PD	No	No
34	M	78	1.65	DLB	No	No
35	F	89	1.62	VaMCI	No	No
36	F	74	1.56	PVSD	No	No
37	M	82	1.80	Mixed	No	No
38	F	75	1.60	DLB	No	No
39	M	79	1.65	Parkinsonism	Yes	No
40	M	82	1.65	Mixed Dementia	No	No
41	F	91	1.50	AD	No	No
42	M	90	1.75	Mixed Dementia	No	Yes
43	F	80	1.65	PD	Yes	No
44	F	75	1.60	NPH, Vascular Disease	No	No
45	M	61	1.67	NPH, Parkinsonism	No	No
46	M	87	1.76	Vascular Disease	No	No
47	F	86	1.52	PD	Yes	Yes
48	F	70	1.60	Vascular Disease	No	No
49	F	77	1.60	NPH	Yes	Yes
50	F	82	1.63	PD	Yes	No
51	M	83	1.75	PD	Yes	No
52	M	82	1.60	NPH	No	Yes
53	F	88	1.56	Mixed Dementia	No	No
54	M	90	1.58	PD	No	Yes
55	M	68	1.75	VaMCI	Yes	No
56	F	53	1.60	Polyneuropathy	No	No
57	M	59	1.68	Cerebellar Syndrome	No	No
58	M	75	1.60	Mixed	No	Yes
59	F	59	1.59	Hemiparesis	No	No
60	M	74	1.78	Hemiparesis	No	No
61	F	51	1.65	PD	Unknown	No

It should be noted that there is an extra patient listed with identifier 61 in Table 4.1. This patient is not included in the analyses due to her unknown fall history. However, her data is used for demonstrative purposes in Section 5.3.2, since we were able to collect data from medication ON and OFF periods separately, which showcases our system's ability to detect medication effects, i.e. intra-subject changes.

We also collected data from 60 healthy subjects (32 females, 28 males), which serves as a control group. These subjects do not have any neurological or orthopedic condition that may affect their gait, as confirmed by the neurologist. The control subjects have an average age of 66.9 ± 8.1 (range: 50–84) and an average height of 1.65 ± 0.08 meters (range: 1.50–1.80).

This study and the data collection efforts were conducted in accordance with the Declaration of Helsinki, and the protocol was approved by the Ethics Committee of Bogazici University Institutional Review Board for Research with Human Subjects (identification code 2015/56). All subjects gave their informed consent for inclusion.

5. GAIT ANALYSIS WITH INERTIAL SENSORS

In this chapter, we present the details of the proposed wearable inertial sensor-based gait analysis system. We aim to achieve a robust gait analysis solution adaptive to sensor placement imperfections and pathological gait conditions. The methods, validation results and clinical discussions presented in this chapter are published in [67].

5.1. Introduction

It is shown that, measurement accuracy achievable by inertial sensors is comparable to the gold standard gait analysis tools (e.g., instrumented walkways) [68–71]. Unlike gold standard methods which are bound to special settings like hospitals and gait clinics, wearable inertial sensors are low-cost, portable and usable in out-of-hospital settings. Hence, they are good alternatives to support pervasive healthcare applications. Especially for lower-body gait analysis with foot-located IMUs (either via straps or insoles), which have several advantages compared to other sensor placements as discussed in Chapter 3, an accurate spatial tracking methodology that utilizes zero-velocity updates combined with Kalman filtering to cope with positional drift errors has been proposed and tested [9, 10]. However, the existing work still have some shortcomings. The ultimate aim of a gait analysis system is to extract a variety of standardized gait parameters to be easily interpreted by a clinician. However, a system solely consisting of wearable sensors, without the aid of infrastructural system elements, rarely achieve completeness in terms of gait parameters. The literature still lacks a complete system, solely consisting of mobile sensors, that can be easily used by non-professionals in non-hospital settings. Another shortcoming is that the applicability of many existing proposals is questionable under pathological gait conditions, and they usually require perfect sensor placement and data collection conditions.

As a step towards this goal, in this chapter, we present an infrastructure-less system based on the above-mentioned established methods, that is extended with novel

methodology to improve the operation of the system in non-hospital settings where data collection and sensor placement errors are possible. Specifically, we propose a medial-lateral foot angular change detection method that is able to operate regardless of the sensor placement on the foot, which is in turn used in an initial-contact (IC) and foot-off (FO) events detection algorithm that is adaptive to pathological gait. Our system has minimal requirements on the data collection procedures and setup, and is able to extract a rich set of spatio-temporal gait parameters that also include parameters about foot clearance and turning steps, which are disregarded in many existing studies. The contributions and highlights of the proposed system can be summarized as follows:

- The proposed system is completely mobile, requiring only two IMUs and a data-processing notebook, and is usable in non-hospital settings, without the need for infrastructure.
- We propose a robust initial contact/foot-off (IC/FO) detection method that is able to operate under imperfect foot-relative sensor placement and orientation conditions. This method is also adaptive to pathological gait (i.e., foot dragging, the absence of the heel strike or left-right asymmetries), where the typical temporal phases of gait may not be observed.
- The system is able to detect and operate with side, back and turning steps, in contrast to solely walking straight, thanks to a novel particle filter-based foot orientation estimation algorithm.
- A rich set of standard spatio-temporal gait parameters are extracted, which can easily be interpreted by a clinician without the need of professional support. The extracted parameters include stride length, cadence, cycle time, stance time, swing time, stance ratio, speed, maximum/minimum clearance and turning rate.
- In addition to numeric parameters, a novel lateral stride profile visualization method is proposed, to give instant insight on spatial gait characteristics.

To evaluate the success of our approach, we conducted a validation study on a disjoint dataset of 22 subjects, using a reference system consisting of a depth camera (Microsoft Kinect v2) and a slow motion camera. Apart from the numerical validation,

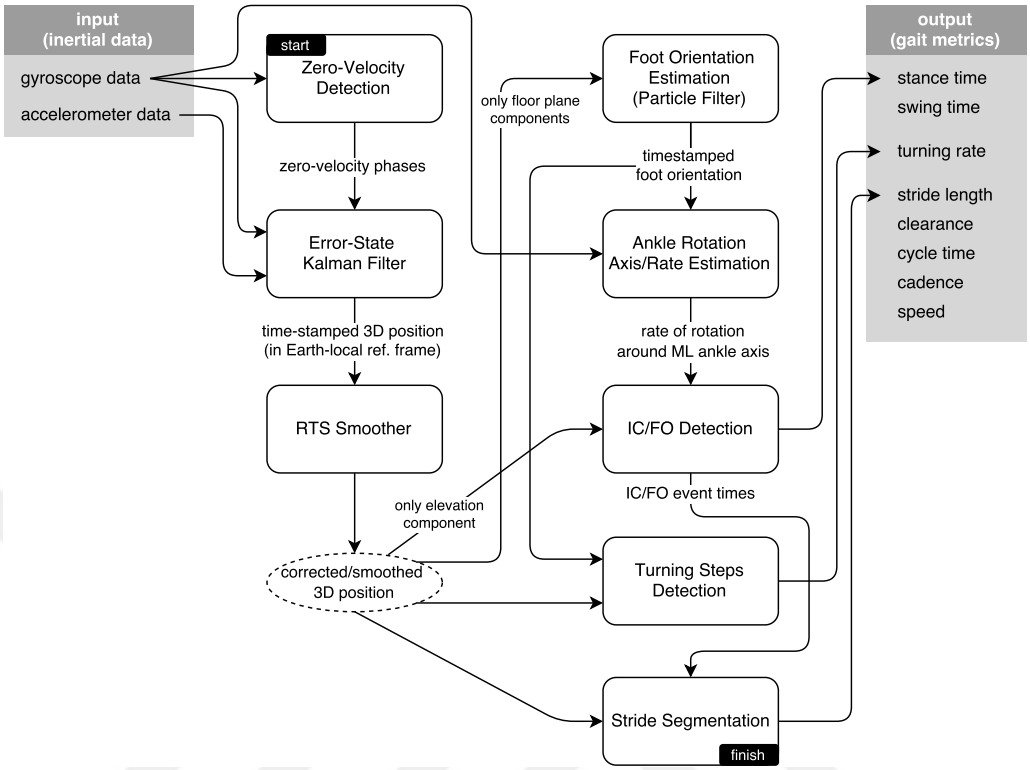


Figure 5.1. Inertial sensor-based gait analysis system block diagram.

we also extracted gait parameters from several subjects in our dataset (see Chapter 4), and compared the findings with the interpretations of a neurologist, along with visualizations, to show how the output of the system can be used for clinical purposes.

5.2. Methods

The interaction of the system modules are presented in Figure 5.1. In this section, we present the methodology driving these modules, in an approximately sequential order. First, we present brief information on the zero-velocity updates and Kalman filtering techniques to extract the three-dimensional (3D) position of the feet; then we explain the smoothing approach to further mitigate the position errors during foot swing phases. Foot orientation and foot ankle rotation axis/rate estimation methods serve to mitigate the effects of sensor misplacement on the subsequent IC/FO detection algorithm, while producing additional output to be used in detecting and processing turning steps. Finally, we discuss how we extract the spatio-temporal parameters and how the output is visualized as average lateral stride profiles.

The Kalman filtering and zero-velocity update methodology are based on the existing literature [9, 10]; however, the smoothing approach to back-correct the mid-swing errors, the particle filter-based foot orientation estimation method that serves to mitigate the sensor misplacement errors, the turning steps detection algorithm and the average lateral stride profile visualization method are novel. We are also able to extract parameters related to feet elevation, i.e. feet minimum/maximum clearance, which are rarely encountered in the reviewed studies. Our IC/FO detection algorithm is based on the observations in [10] and [72], but we extend them significantly to come up with a novel algorithm that can also operate in cases of pathological gait.

5.2.1. Problem Definition

The inertial sensor produces 3-dimensional acceleration and angular velocity (rotation rate) measurements

$$\boldsymbol{f}_t = (f_t^x, f_t^y, f_t^z) \tag{5.1}$$

$$\boldsymbol{\omega}_t = (\omega_t^x, \omega_t^y, \omega_t^z) \tag{5.2}$$

where $\boldsymbol{f}_t$ and $\boldsymbol{\omega}_t$ are the accelerometer and gyroscope output, respectively. The state of the inertial sensor at time t, and coincidentally the foot it is strapped to, can be defined in terms of its attitude (3D orientation), velocity and displacement

$$\boldsymbol{x}_t = (\boldsymbol{R}_t, \boldsymbol{v}_t, \boldsymbol{s}_t) \tag{5.3}$$

where $\boldsymbol{R}_t$ is the rotation matrix defining the attitude of the sensor with respect to the local Earth reference frame, and $\boldsymbol{v}_t$ and $\boldsymbol{s}_t$ are 3-dimensional vectors specifying its velocity and displacement, respectively. The attitude $\boldsymbol{R}_t$ can be estimated with the rectangular integration scheme

$$\boldsymbol{R}_t = \boldsymbol{R}_{t-1}\left(\boldsymbol{I} + \frac{\sin\sigma}{\sigma}\boldsymbol{B}_t + \frac{1-\cos\sigma}{\sigma^2}\boldsymbol{B}_t^2\right) \tag{5.4}$$

where $\boldsymbol{I}$ is the identity matrix, $\sigma = |\boldsymbol{\omega}_t \delta t|$, and $\boldsymbol{B}_t$ is the skew-symmetric matrix form of the vector $\boldsymbol{\omega}_t$. The velocity and displacement can then be computed by

$$\boldsymbol{a}_t = \boldsymbol{R}_t \boldsymbol{f}_t + \boldsymbol{g} \tag{5.5}$$

$$\boldsymbol{v}_t = \boldsymbol{v}_{t-1} + \delta t \cdot \boldsymbol{a}_t \tag{5.6}$$

$$\boldsymbol{s}_t = \boldsymbol{s}_{t-1} + \delta t \cdot \boldsymbol{v}_t \tag{5.7}$$

where $\boldsymbol{g} = (0, 0, -9.807)^\top$ is the gravitational acceleration vector, $\boldsymbol{a}_t$ is the acceleration measurement projected to the local Earth reference frame with gravity excluded, and δt is the time passed since the previous measurement, i.e., the duration between time instances $t-1$ and t.

In theory, assuming a known starting point and given a stream of acceleration and angular velocity readings, these equations are sufficient to indefinitely estimate and track the state of the sensor. However, this is not practically possible due to the error sources and the consequential drift, as discussed in Section 2.2.1. Hence, we use the zero-velocity updating technique to periodically correct the drift in the state elements.

5.2.2. Zero-Velocity Updates

To cope with the position and orientation drift, a periodic correction (ground truth) of the state elements is required. Fortunately, the human gait is highly periodic and the foot remains stationary for a short period within each recurring stance phase. In this period (i.e. the zero-velocity phase), the foot is in total contact with the ground and has near-zero velocity. Foot-mounted inertial sensors allow us to detect these phases, which can be used to correct the velocity component in the state vector.

Furthermore, if we assume that the walking subject does not change elevation/floors, we can also assume that the z component of the displacement (i.e. elevation with respect to the ground) is zero during zero-velocity phases.

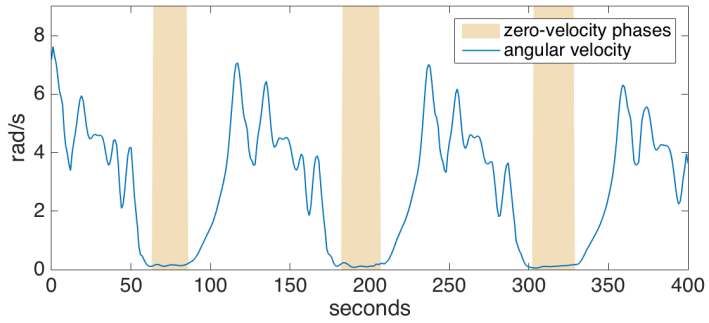


Figure 5.2. Zero-velocity phase detection.

To detect the zero-velocity phases, we check if the magnitude of the angular velocity drops below a certain threshold. To cope with the noise and outliers in the data, we employ a grace period, during which the angular velocity magnitude should be under the specified threshold before we can safely assume that the foot has gone into the zero-velocity phase. An example is shown in Figure 5.2. Acceleration thresholding can be additionally employed in order to improve the confidence of the zero-velocity phase detector, however we determined that the gyroscope readings are much more reliable than accelerometer readings and such an extra mechanism barely increases the accuracy [73]. Indeed, we rarely encountered a problem with zero-velocity updates during the experiments, even for pathological gait data (e.g., foot dragging or the absence of heel strike), as also supported by the other studies utilizing the same method [9, 10].

Once the zero-velocity phases are detected, we can apply the zero-v and zero-z updates by directly modifying the corresponding state vector components. Even though this naive approach results in a significant improvement, it is not optimal, since it does not consider the correlations between the state elements, e.g., the velocity also influences the displacement, hence zero-v updates can be used to correct the displacement too. Next, we describe the better Kalman filtering approach.

5.2.3. Error-State Tracking Kalman Filter

Kalman filters are Bayesian filters that are able to accurately track correlations between the state elements with known update equations and error models. It is possible to formulate a Kalman filter that tracks the total state of the inertial sensor, incor-

porating the tracking equations presented in Section 5.2.1; however, the non-linearity of the equations requires the use of a linearized filter which has greater computational and implementation complexity. Instead we utilize an error-state tracking Kalman filter, which only tracks the probability distributions of the errors building up for the different state elements, which are used to optimally correct the state during zero-velocity phases [10].

The Kalman filter consists of two stages: *prediction* and *correction*. The prediction stage is executed each time a new set of acceleration and angular velocity measurements is received, and the covariance of the state component errors, i.e. the error-state covariance matrix, is updated according to the measurements by

$$\boldsymbol{P}_{t|t-1} = \boldsymbol{F}_t \boldsymbol{P}_{t-1|t-1} \boldsymbol{F}_t^{\mathsf{T}} + \boldsymbol{\Sigma}_w \tag{5.8}$$

where $\boldsymbol{F}_t$ is the error-state update matrix, $\boldsymbol{P}_{t-1|t-1}$ is the previously corrected error-state covariance matrix estimate at time $t-1$, and $\boldsymbol{\Sigma}_w$ is the process noise covariance modeling the accelerometer and gyroscope errors. We assume that the errors in gyroscope and accelerometer readings are Gaussian. The error variances are empirically determined to include the noise and scaling errors. The error-state update matrix, which propagates the error-state given the sensor measurements, is defined as

$$\boldsymbol{F}_t = \begin{pmatrix} \boldsymbol{I} & \mathbf{0} & \mathbf{0} \\ \delta t \boldsymbol{S}_t & \boldsymbol{I} & \mathbf{0} \\ \mathbf{0} & \delta t \boldsymbol{I} & \boldsymbol{I} \end{pmatrix} \tag{5.9}$$

where $\boldsymbol{S}_t$ is the skew-symmetric matrix form of the vector $\boldsymbol{R}_t \boldsymbol{f}_t$, $\boldsymbol{I}$ is the 3×3 identity matrix, and $\mathbf{0}$ is the 3×3 zero matrix.

The standard Kalman filter prediction stage equations also include the mean error-state update equation; however, the initial error-state mean estimate $\delta\hat{\boldsymbol{x}}_0$ is $\mathbf{0}$, hence its propagation through time always results in a zero mean estimate, i.e., the mean error-state estimate at time t is always zero ($\delta\hat{\boldsymbol{x}}_t = \mathbf{0}$). Therefore, tracking only

the error-state covariance is sufficient.

Parallel to the prediction stage, the tracking equations presented in Section 5.2.1 are executed as normal, since we do not have correcting information yet. The estimated state as a result of the tracking equations is represented by

$$\hat{\boldsymbol{x}}_{t|t-1} = (\hat{\boldsymbol{R}}_{t|t-1}, \hat{\boldsymbol{v}}_{t|t-1}, \hat{\boldsymbol{s}}_{t|t-1}). \tag{5.10}$$

The correction stage is where the actual zero-v and zero-z updates (i.e., the zero-updates) are performed, which is executed each time a zero-velocity phase is detected. The corrected error-state $\delta\hat{\boldsymbol{x}}_t$ and its corrected covariance $\boldsymbol{P}_{t|t}$ are calculated by

$$\boldsymbol{K_t} = \boldsymbol{P}_{t|t-1}\boldsymbol{H}^\mathsf{T}\left(\boldsymbol{H}\boldsymbol{P}_{t|t-1}\boldsymbol{H}^\mathsf{T} + \boldsymbol{\Sigma}_v\right)^{-1} \tag{5.11}$$

$$\delta\hat{\boldsymbol{x}}_t = \boldsymbol{K}_t\left(\boldsymbol{0} - \boldsymbol{H}\hat{\boldsymbol{x}}_{t|t-1}\right) \tag{5.12}$$

$$\boldsymbol{P}_{t|t} = \boldsymbol{P}_{t|t-1} - \boldsymbol{K}_t\boldsymbol{H}\boldsymbol{P}_{t|t-1} \tag{5.13}$$

where $\boldsymbol{0}$ is a 4-dimensional vector of all zeros (denoting the actual zero-updates), $\hat{\boldsymbol{x}}_{t|t-1}$ is the predicted state calculated by the navigation equations before any zero-updates, $\boldsymbol{H}$ is the 4×9 matrix with ones and zeros that filters the predicted state so that it contains only the elements that are corrected (velocity and z-component of displacement), and $\boldsymbol{\Sigma}_v$ is the error covariance matrix describing the small amount of uncertainty in the zero-updates. The error-state estimate, which denotes the difference between the predicted and corrected state of the sensor, is defined by

$$\delta\hat{\boldsymbol{x}}_t = (\delta\hat{\boldsymbol{\phi}}_t, \delta\hat{\boldsymbol{v}}_t, \delta\hat{\boldsymbol{s}}_t) \tag{5.14}$$

where $\delta\hat{\boldsymbol{\phi}}_t$, $\delta\hat{\boldsymbol{v}}_t$ and $\delta\hat{\boldsymbol{s}}_t$ are the errors in rotation, velocity and displacement, respectively. The elements of the error-state estimate vector $\delta\hat{\boldsymbol{x}}_t$ are then used to correct the

predicted state via the equations

$$\hat{\boldsymbol{R}}_t = \hat{\boldsymbol{\Phi}}_t \hat{\boldsymbol{R}}_{t|t-1} \tag{5.15}$$

$$\hat{\boldsymbol{v}}_t = \hat{\boldsymbol{v}}_{t|t-1} + \delta\hat{\boldsymbol{v}}_t \tag{5.16}$$

$$\hat{\boldsymbol{s}}_t = \hat{\boldsymbol{s}}_{t|t-1} + \delta\hat{\boldsymbol{s}}_t \tag{5.17}$$

where $\hat{\boldsymbol{\Phi}}_t$ is the rotation matrix form of the rotation error vector $\delta\hat{\boldsymbol{\phi}}_t = (\delta\hat{\phi}_t^x, \delta\hat{\phi}_t^y, \delta\hat{\phi}_t^z)$, which can be computed via the exact form

$$\hat{\boldsymbol{\Phi}}_t = \begin{pmatrix} c_y c_z & c_y s_z & -s_y \\ s_x s_y c_z - c_x s_z & s_x s_y s_z + c_x c_z & s_x c_y \\ c_x s_y c_z + s_x s_z & c_x s_y s_z - s_x c_z & c_x c_y \end{pmatrix} \tag{5.18}$$

where $s_i = \sin\delta\hat{\phi}_t^i$ and $c_i = \cos\delta\hat{\phi}_t^i$. The computation cost of the exact form may be undesirably high for a real-time application running on a device with limited computational capabilities (e.g., a smartphone); hence, at the expense of accuracy, one can use the small angle approximation

$$\hat{\boldsymbol{\Phi}}_t \approx \hat{\boldsymbol{\Phi}}_t^{approx} = \begin{pmatrix} 1 & \delta\hat{\phi}_t^z & -\delta\hat{\phi}_t^y \\ -\delta\hat{\phi}_t^z & 1 & \delta\hat{\phi}_t^x \\ \delta\hat{\phi}_t^y & -\delta\hat{\phi}_t^x & 1 \end{pmatrix}. \tag{5.19}$$

A potential problem of the small angle approximation is that $\hat{\boldsymbol{\Phi}}_t^{approx}$ may no longer be a rotation matrix, i.e., its transpose may no longer be equal to its inverse, so the subsequent $\hat{\boldsymbol{R}}_t$ estimates may also decay over time. A standard way to convert it to a rotation matrix is to use the well-known Cayley transform

$$\hat{\boldsymbol{\Phi}}_t \approx \hat{\boldsymbol{\Phi}}_t^{cayley} = \left(\boldsymbol{I} + \frac{\hat{\boldsymbol{\Phi}}_t^{approx} - \boldsymbol{I}}{2}\right)\left(\boldsymbol{I} - \frac{\hat{\boldsymbol{\Phi}}_t^{approx} - \boldsymbol{I}}{2}\right)^{-1}. \tag{5.20}$$

After the error-state $\delta\hat{\boldsymbol{x}}_t$ is used to correct the sensor state, it is immediately reset to zero, and the Kalman filter operations resume with the subsequent measurements.

5.2.4. Smoothing

The error-state tracking Kalman filter can produce accurate state estimations immediately after the zero-updates, while the estimation accuracy continues to degrade as the errors accumulate, until the next zero-updates. This is sufficient for a navigation application interested only in the absolute position, however for the aims of this study, the evolution of the 3D position through each stride (even when the foot is in motion) is also important, especially since we are also interested in extracting mid-swing parameters such as clearance.

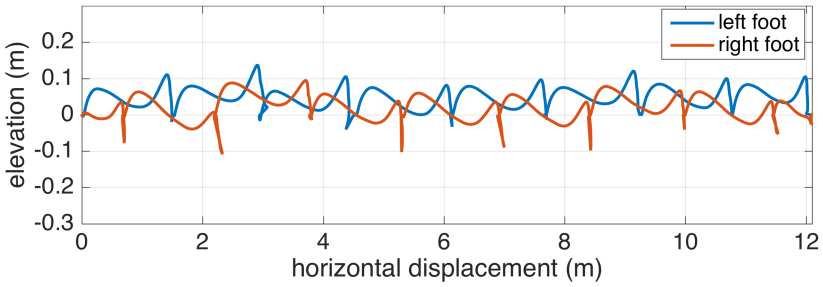
To achieve this objective, we employ the Rauch-Tung-Striebel (RTS) smoother, which additionally performs a backward pass on the estimated state. The smoother is initiated each time zero-updates are encountered. The newly received correction information is propagated backwards to eliminate the accumulated errors, until the previous correction (previous zero-velocity phase) is reached. The backward recursion initiated at such time n, when a zero-velocity phase is detected, is executed by

$$\boldsymbol{G}_t = \boldsymbol{P}_{t|t}\boldsymbol{F}_{t+1}^{\mathsf{T}}\boldsymbol{P}_{t+1|t}^{-1} \tag{5.21}$$

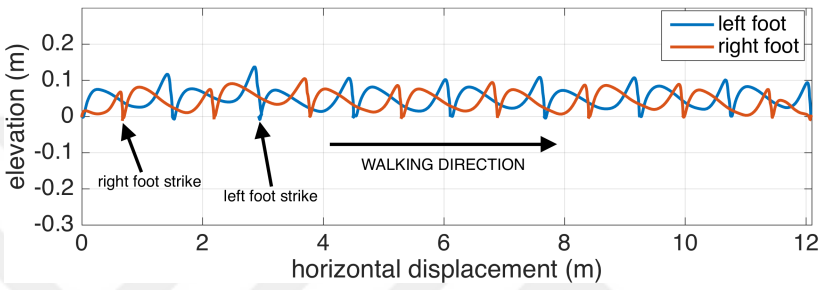
$$\delta\hat{\boldsymbol{x}}_{t|n} = \boldsymbol{G}_t\delta\hat{\boldsymbol{x}}_{t+1|n} \tag{5.22}$$

where $\delta\hat{\boldsymbol{x}}_{t|n}$ is the smoothed mean error-state estimate at time t, which is then used to compute the smoothed sensor state $\hat{\boldsymbol{x}}_{t|n}$ using equations 5.15-5.17.

The smoothing procedure introduces a total delay of a single stride duration to the system operation. Such a delay does not impair the near real-time property of the system, since a typical step is never longer than a few seconds, and even under one second in most cases.



(a)



(b)

Figure 5.3. Lateral view of a walking subject, (a) Only Kalman filtering, (b) Kalman filtering with RTS smoothing.

The benefits of the RTS smoother is demonstrated in Figure 5.3, where it is compared with only Kalman filtering. The figure shows the feet position change of a subject walking to the right, when looking through the medial-lateral axis (i.e., looking from the side). The Kalman filter is able to accurately correct the position in each zero-velocity phase following the foot strikes, but the foot position during the swing phases are subject to increasing position errors until a zero-velocity phase is reached (as observed in mid-swing positions that go below 0, which is floor-level). The backward passes executed after each zero-velocity period can accurately correct mid-swing errors.

Consequently, the Kalman filtering and RTS smoothing approach is able to produce 3D feet displacement estimates as demonstrated in Figure 5.4. A visual inspection reveals that the displacement curves conform to the expected visual gait patterns. The numerical error evaluation of the spatial gait parameters (e.g., stride length) extracted from the resulting displacement estimates is presented in Section 5.3.1, which indirectly demonstrates the spatial accuracy of our approach.

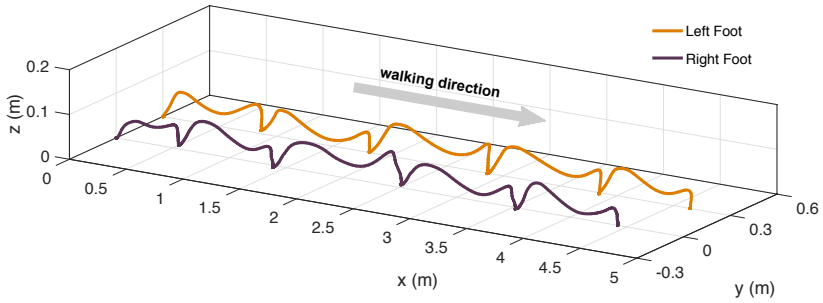


Figure 5.4. 3D feet position estimated by Kalman filter and RTS smoother.

5.2.5. Foot Orientation Estimation

A naive foot orientation estimation approach may be to directly compute it from the foot position change on the ground-tangential plane. This may yield accurate results if the subject is walking straight all the time, but in reality there are turning, side and even backward steps that would confuse this approach. Though, it is not very unrealistic to assume that people walk straight and forwards most of the time and the forward steps usually cover more ground than side and back steps.

Based on this assumption, the problem of foot orientation estimation can be formulated as a problem of continuous parameter estimation, which should employ corrections with confidence proportional to the displacement (since steps with higher displacement are more likely to be forward steps). An option would be to use another Kalman filter for this purpose; however, Kalman filters require a linear state transition model, and in this case it is non-linear since the relationship between displacement and heading is non-linear. An extended Kalman filter, which is the linearized version of the Kalman filter, would be a viable option; however, particle filters proved to be a better choice since as the error distribution of the foot orientation estimation grows, its shape deviates significantly from a Gaussian distribution, and particle filters are a good option to model such non-Gaussian error distributions. This is one of the reasons why particle filters are so popular in the robot navigation literature, especially in odometry-based robot heading estimation studies, which bare many similarities to the problem at hand [74].

Before going into the formulation of the filter, it is important to remind that the error-state Kalman filter and the RTS smoother system is able to output accurate 3D position relative to the starting point, velocity and orientation change in the local frame of reference. Hence we can deduce the speed in the ground-tangential plane and the yaw change about the axis of direction of gravity, and use these information as input to the particle filter. What the Kalman filter does not know is the orientation of the foot relative to the computed positional change, which the particle filter is aimed to estimate.

The particle filter (PF) tracks the probability distribution of the underlying state by a cloud of numerous particles, subject to the same state transition and error models. The i-th particle's state at time t is defined by

$$\boldsymbol{z}_t^i = (x_t^i, y_t^i, \theta_t^i) \tag{5.23}$$

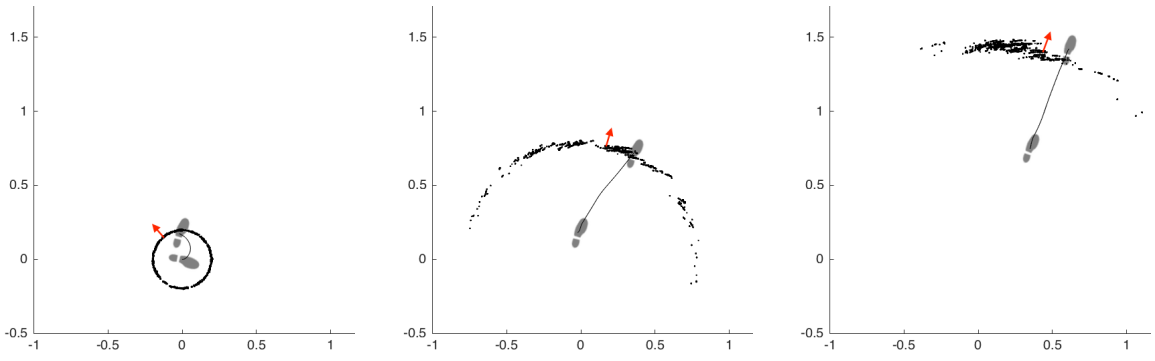
where x_t^i and y_t^i denote the position of the particle on the ground-tangential plane (imagine looking top-down on a walking person's foot), and θ_t^i is the orientation of the particle. The particle propagation step updates the state of a particle by sampling the motion model distribution $\Pr(\boldsymbol{z_t}|\boldsymbol{z_{t-1}}, v_t, \Delta\alpha_t)$, where v_t and $\Delta\alpha_t$ are the speed and the yaw change estimated by the error-state Kalman filter, respectively. The state of a particle is propagated by the equations

$$\theta_t = \theta_{t-1} + \Delta\alpha_t + \theta_e \tag{5.24}$$

$$x_t = x_{t-1} + v_t \cdot \delta t \cdot \cos(\theta_t) + x_e \tag{5.25}$$

$$y_t = y_{t-1} + v_t \cdot \delta t \cdot \sin(\theta_t) + y_e \tag{5.26}$$

where θ_e, x_e and y_e are small noises acting on different components of the state vector, drawn from a zero-centered Gaussian distribution. These noises are required to prevent particle depletion, which is the problem of particles concentrating on similar states due to the frequent resampling of the same particles, and consequently premature convergence, which causes the filter's belief estimate to converge on a single local



(a) (b) (c)

Figure 5.5. Example particle filter operation (footprints: true foot orientation, red arrows: estimation of PF).

optimum due to the decreased variety of particle states. The particle weights are then computed to be proportional to the output of a zero-mean Gaussian probability distribution function with the distance of the particle position to the position computed by the error-state Kalman filter used as input. The standard deviation of this Gaussian distribution is selected to be large (specifically 2 meters in this study), to allow the particle weights to remain considerably large until they are too far behind a significant displacement (to make use of the base assumptions). The particles are then resampled according to these weights.

At the end of each segmented step, the aggregate foot orientation is computed by taking the weighted average of the particles' orientations. It is then propagated backwards through the stride by using the inverted $\Delta\alpha_t$ values, so that we can get a good continuous foot orientation estimate for the whole stride duration.

A demonstrative example of the particle filter operation is presented in Figure 5.5. The subfigures represent three consecutive steps of the left foot, from left to right. The other foot is omitted for visual simplicity. The particles are denoted by black dots and the aggregate foot orientation estimation of the filter is denoted by red arrows. The footprints show the true orientation of the foot. The first step is a side step with a turn of approximately 90 degrees. We selected this challenging case to demonstrate the capabilities of the filter better. The filter estimation after the first step is not

accurate, but as the subject starts walking straight, the filter quickly converges on the true orientation.

It should be noted that, this method aims to estimate the orientations of the two feet separately relative to the underlying displacement computed by the error-state tracking Kalman filter. Therefore, it computes the orientation changes relative to an arbitrary starting condition, as dictated by the underlying displacement data, and not the absolute orientation. The initial orientation state could be input to the system to allow this, if needed. Another alternative would be to utilize the magnetometer in the IMU to determine the absolute initial orientation of the sensor, although magnetometers are also subject to errors due to the magnetic interference in the environment. In this study, we employ neither of these approaches since the stride-wise relative orientation changes are sufficient for the purposes of this study, i.e. to be able to detect side and back steps in addition to forward steps, to estimate the correct rate of rotation along the estimated ankle rotation axis (which is input to the IC/FO algorithm), and to estimate the relative turning rate.

A drawback of this approach is that it neglects the toe out angle, defined as the natural outward alignment of the feet (i.e. the feet do not move exactly straight when lunging forward). This angle is typically about 20 degrees [4]. Since it stays almost unchanged throughout the gait cycle, its effect on foot ankle rotation estimation proved to be negligible. Though, other information, such as the principle component of the angular rotation, which is likely to be around the ankle rotation axis, may be incorporated the into the filter to estimate the toe out angle as well [72].

5.2.6. Foot Ankle Rotation Axis and Rate Estimation

After we estimated the foot orientation vector ($\boldsymbol{v_f}$) corresponding to the anterior-posterior axis, since we know the gravity direction vector ($\boldsymbol{v_g}$), it is straight-forward to compute the ankle rotation axis ($\boldsymbol{v_a}$) corresponding to the medial-lateral axis, by applying cross-product to the former two vectors. What we get is a foot-local coordinate

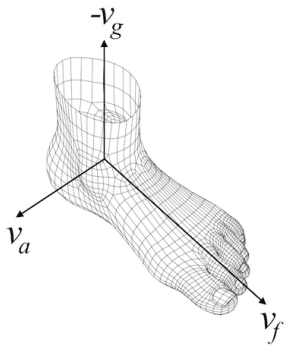


Figure 5.6. Foot-local coordinate system.

system with three perpendicular basis vectors as shown in Figure 5.6.

Extracting the rotation rate about the ankle axis $\boldsymbol{v_a}$ is a little trickier. The underlying error-state Kalman filter provides us with rotation matrices which map the sensor body coordinate system to the local Earth coordinate system. These matrices can be converted to orientation changes of the sensor at each time interval in the local coordinate system (delta rotations). The problem is extracting the rotation around only the ankle axis and eliminating the remaining rotations around any other axes. Quaternions, which are one of the standard ways of representing 3D rotations, offer us a convenient way to do this. Therefore, we first extract the delta rotations in quaternion representation: The orientation estimates of the error-state Kalman filter in rotation matrix form ($\hat{\boldsymbol{R}}_t$, see Equation 5.15) are converted to the quaternion representation. Then, using the two quaternions corresponding to two consecutive orientation estimates, we extract the delta rotation quaternion for time t by

$$\boldsymbol{\Delta r}_t = \boldsymbol{r}_t \boldsymbol{r}_{t-1}^{-1} \tag{5.27}$$

where $\boldsymbol{r}_t$ and $\boldsymbol{r}_{t-1}$ are the orientation estimates at time t and $t-1$ in quaternion form, respectively, and $\boldsymbol{r}_{t-1}^{-1}$ is the quaternion inverse of $\boldsymbol{r}_{t-1}$. The resulting delta rotation

quaternions are then projected to the ankle axis by

$$\boldsymbol{p} = (\boldsymbol{v} \cdot \boldsymbol{v_a})\boldsymbol{v_a} \tag{5.28}$$

$$\boldsymbol{q} = (\boldsymbol{p}, w) \tag{5.29}$$

$$\boldsymbol{q_a} = \boldsymbol{q}/\|\boldsymbol{q}\| \tag{5.30}$$

where $\boldsymbol{v}$ and w are the vector and the scalar components of the input delta rotation quaternion ($\boldsymbol{\Delta r}_t$), respectively, and $\boldsymbol{q_a}$ is the resulting rotation around the ankle axis represented as a quaternion.

To assess the accuracy of the proposed ankle axis rotation extraction method, we collected data from a sensor positioned on the foot with the x axis aligned with the ankle rotation axis, essentially fulfilling the perfect sensor placement assumption made by many existing studies on FO/IC detection [10], which allows them to directly use the x axis of the gyroscope readings directly as the ankle axis rotation rate. We compared the x axis rotation rates with the extracted rotation rates. Figure 5.7 shows the comparison for a single stride data, taken from a turning step (approximately 30 degrees) of the left foot. A turning step is deliberately chosen to make the case more challenging. The observed differences are minor, as visually demonstrated by the overlap of the two curves, indicating the success of our approach. The root mean square error (RMSE) of this example is 0.08 radians per second.

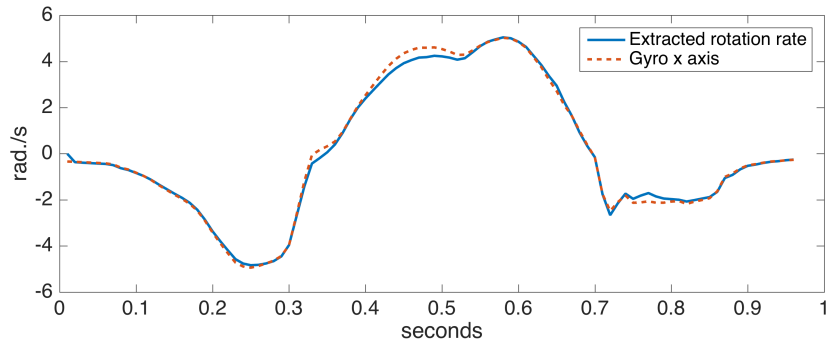


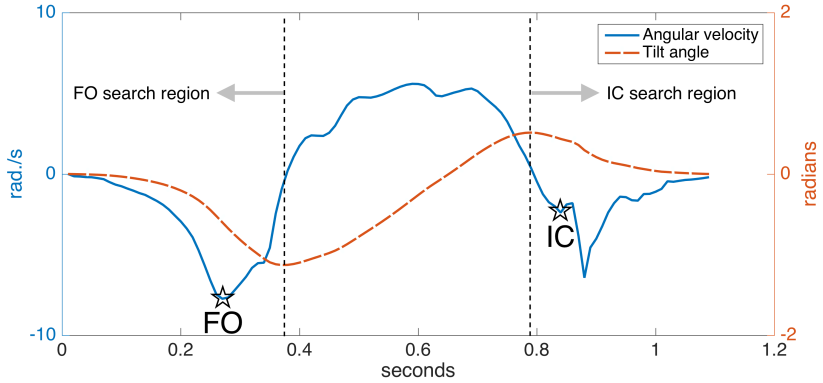
Figure 5.7. Extracted ankle axis rotation rate vs. x-axis gyroscope data of a correctly positioned sensor.

5.2.7. IC/FO Events Detection

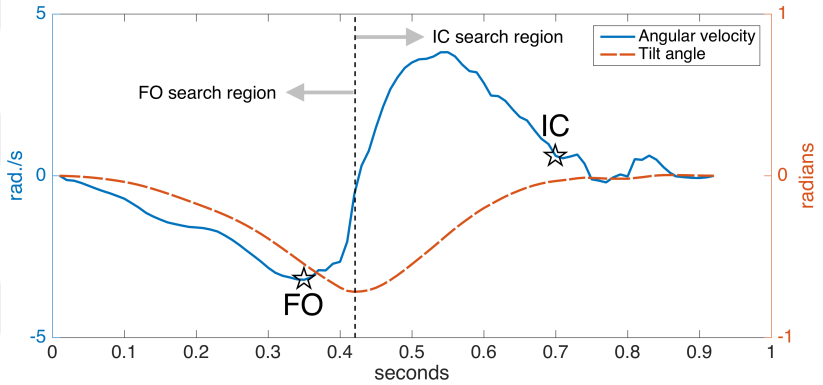
In healthy gait, rotation around the ankle axis (in short, tilt angle) changes as follows, assuming we are looking from the lateral (right) side at a person walking towards the right: Starting from the foot-flat phase, the foot begins to turn clockwise with the toe as the contact point, foot leaves the ground (FO) and the clockwise rotation begins to slow down, then it reverses to counter-clockwise direction as the foot lunges forward; near the end of the forward motion the toe elevation exceeds the heel elevation (toe lift), and the rotation reverses again to clockwise direction followed by a heel strike. The tilt angles and the angular velocity (the derivative of tilt angle) during a normal gait cycle is shown in Figure 5.8a. Notice there are one negative and one positive peak in the tilt angle, corresponding to the instances that the angular change reverses direction. These instances correspond to right after the FO and right before the IC respectively. Hence they can be used to limit the FO and IC search regions, since it is guaranteed that there can be no FO or IC events in-between [4].

In [10] and [72], it is presented that the two prominent negative peaks in the angular velocity marks the FO and IC events with sufficient accuracy. This means that the foot reaches the maximum angular speed as it leaves the ground. Our approach is also based on this observation. However, around the IC event time, we usually observe two consecutive negative peaks, the first one due to the impact of the heel strike and the second on due to the angular speed reaching its maximum right after the heel strike. So if these two peaks can be detected, the first one marks the IC [10]. An example of the detected FO and IC events are presented in Figure 5.8a.

While the observations above are valid for healthy gait, they are partially true for pathological gait. Especially for Parkinson's disease patients in later stages, the heel strike is not observed as the foot strikes the ground all at the same time (in some extreme cases, even the toe may strike first). Hence there is no toe lift to enforce the heel to be the first point of contact. This means that there is no positive peak in the tilt angle, and the negative IC peaks in the angular speed may not be observed



(a)



(b)

Figure 5.8. Detected FO & IC events, (a) healthy gait, (b) pathological gait.

(Figure 5.8b). Therefore, the previously outlined algorithm is not valid for detecting the IC event in such cases and has to be extended.

Since in the absence of toe lift, the foot strikes the ground almost all at once, we may use the foot elevation (clearance) information to detect if the foot has contacted the ground. Thankfully, the underlying error-state Kalman filter provides us with this information. So if we detect no toe lift, we may find the IC event by detecting the time instance when the foot elevation drops to a substantially low level (e.g. a few millimeters). An example of the FO and IC events detected in the case of pathological gait is presented in Figure 5.8b. Note that the swing times (the duration between FO and IC) in this case are much shorter than the healthy case as expected.

Once we have detected the FO and IC events, it is straightforward to determine the two major gait phases: swing time and stance time. Swing time corresponds to

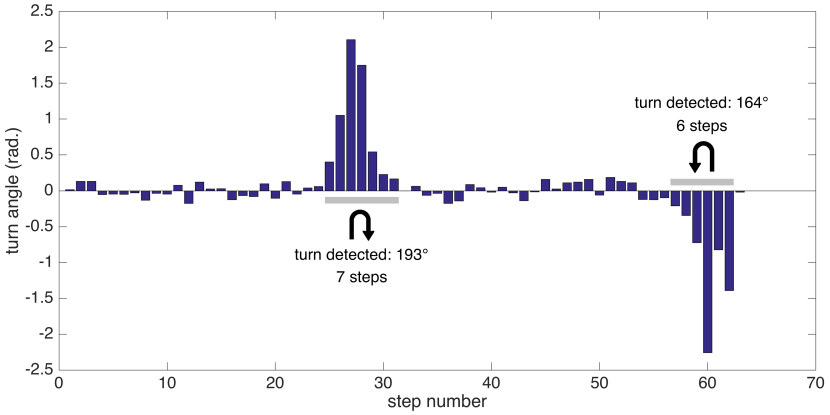


Figure 5.9. Turn angles for individual steps and detected substantial turns.

the period starting from the FO and ending at the IC, and stance time vice versa.

5.2.8. Detection of Turning Steps

Extracting the foot orientation has another benefit: the ability to detect turning steps and extract other parameters specific to them. We employ a simple method for detecting turns: We try to find consecutive turning steps (with angle changes from start to end of a step exceeding a certain threshold). Since our test scenarios include 180 degrees turns at the ends of a corridor, we specifically aim to detect these turns, which are especially challenging for patients experiencing pathological gait.

In summary, we can detect the following parameters related to turning: The number of steps to complete a specific turn (depending on the data collection session), and turning rate (degrees/sec). An example of substantial turn detection is presented in Figure 5.9.

5.2.9. Extraction of Spatio-Temporal Gait Parameters

After the IC and FO events are detected, their time instances can be used to determine stance and swing times. The IC event times can further be used to segment strides, making the connection between the spatial and temporal elements of gait, which in turn enables the extraction of stride length, clearance, cycle time, cadence

and speed. The parameters of stance and swing times, stride length and clearance are computed per stride and per foot, and hence their variabilities (standard deviation) can also be computed. Turning rate is a direct output of the turning steps detection module, as the total turn angles are divided by the total amount of time it takes to complete a turn.

5.2.10. Average Lateral Stride Profile Visualization

Apart from the numerical gait parameters, a visual representation of the average lateral stride profile (looking through the medio-lateral axis) for each feet is also beneficial to assess the position evolution of the feet through a stride. The aim is to process all the strides taken during a data collection session, and aggregate them into an easily comprehendible visual representation for both feet. The lateral view provides us with a glance at both the stride length and the clearance (foot elevation) changes during the swing phase. Being able to see the average profiles separately for each feet also allows the clinicians to spot any left-right asymmetries.

Changes in the walking speed and stride length in a session does not necessarily point to gait abnormalities, as people tend to modify these at will when walking at a leisurely mode. Hence the durations of individual strides may vary. Therefore, simply taking the average of position values belonging to the same time instance does not yield the intended results, as it tends to smooth out the secondary peaks (corresponding to the toe-lift just before IC) in the case of strides with different lengths. This information loss can be averted by taking a solely spatial approach rather than incorporating time information: We select a specific number of points (typically higher than 100) distributed uniformly on the individual stride profiles, i.e. the neighboring points are equidistant. Then, we average the points that correspond to the same index and achieve spatial aggregation. This way, both the primary (elevation right after FO) and the secondary (toe lift just before IC) peaks are preserved. To show the elevation variability among individual steps, we also visualize the standard deviation curves as dashed lines. Consequently, we incorporate as much spatial information as possible to

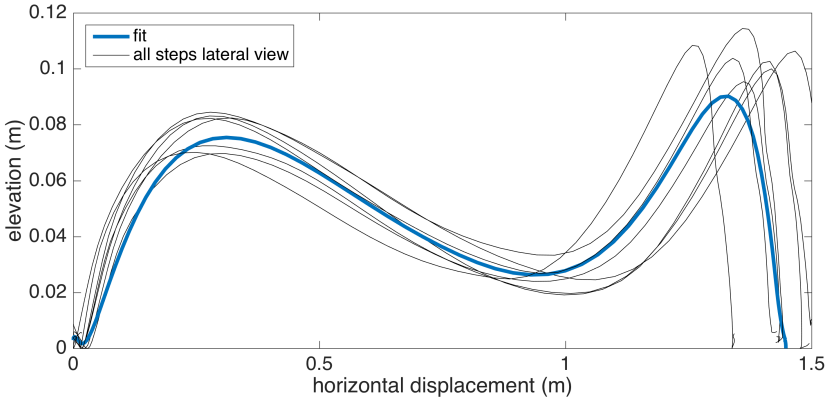


Figure 5.10. Example average stride profile fit over individual stride profiles.

an uncluttered and easily readable figure. An example is presented in Figure 5.10. The individual stride profiles are also drawn to give an idea on the underlying data used to generate the average profile.

To give an insight on how the visualization may be used for clinical assessment purposes, we also provide a real example, that compares an healthy elderly with a PD patient (Figure 5.11). It should be noted that, differentiating between healthy and pathological gait is not within the aims of this study, so the selection of patients for this figure is for demonstration purposes only. On the other hand, such an extreme case highlights the type of differences that the visualization may reveal. Both subjects are male and their ages are similar (76 and 83 respectively). The first difference to note is the big difference between stride lengths. Another important difference is that the secondary peak (right-most) in the PD patient is much lower compared to the first peak, indicating a difficulty performing the toe lift at the end of the swing phase.

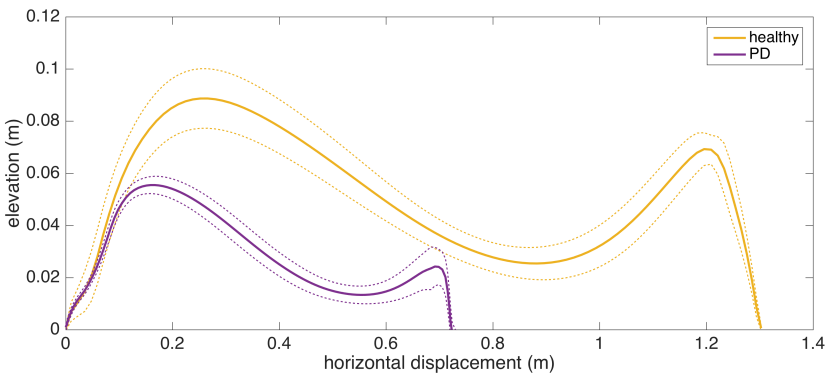


Figure 5.11. Comparison of average stride profiles of healthy and PD subjects.

This is typical of PD patients, and in severe cases the toe-lift completely disappears, meaning that the subject places the foot all at the same time without a pronounced heel strike. Both of these symptoms describe what is referred to as the Parkinsonian shuffling gait which is commonly observed in PD patients at later stages.

All the methods and analyses detailed in this chapter are implemented and executed using MATLAB R2018a software [75].

5.3. Experiments

We conducted a two-phase experimental study to validate the numerical accuracy of the extracted gait parameters and to demonstrate what the parameters can tell us clinically. In the initial system validation phase, we compare the stride length and swing time estimation performance of our system with a reference system (infrared depth-camera based gait analysis system supported by a slow motion camera). The data used for the validation is comprised of a disjoint dataset from 22 subjects including healthy subjects and patients with various neurological disorders. The results are presented in the next section. In Section 5.3.2, we present the extensive output of our system from 17 patients selected among our complete dataset (introduced in Chapter 4), and we discuss the clinical significance of the extracted parameters supported by the interpretations of a neurologist. With these two experimental studies, we aim to show the usability of our system, both technically and clinically.

5.3.1. Comparative Validation with Kinect and Slow Motion Camera

To assess the numerical accuracy of the extracted parameters, we conducted a numerical accuracy evaluation study to compare the output of our system with a system based on a Microsoft Kinect depth camera (for stride length comparison) and a slow motion camera (for stance and swing times comparison). The accuracy of the Microsoft Kinect depth camera [76] for gait analysis purposes has been well investigated in the literature [77–80]. Especially for estimating stride length, good validation results have

been reported when compared with the gold standard instrumented walkways and camera-based motion capture systems. In [77] and [80], mean absolute displacement errors of 2.5 cm and 2.9 cm per stride are reported, respectively. The applicability of Kinect as a tool for analyzing pathological gait, particularly PD, is also explored in [81–83], with good results. Considering these characteristics, Microsoft Kinect serves as a viable alternative that can be deployed in a non-hospital setting for estimating stride lengths. However, it should be noted that the output of the Kinect system still cannot be treated as the ground-truth, as opposed to a gold standard system. Therefore, in our validity analysis, we employ agreement analysis methodology, namely Bland-Altman and correlation plots, and do not treat Kinect as the absolute reference.

Even though Microsoft Kinect is a good gait analysis system alternative, it does not provide the same level of portability and convenience as an IMU system does. It still requires infrastructural setup (a tripod to mount the device, a power source and a wired connection to a computer for data collection) and its operational range is limited to 1.5–4 meters where the infrared depth sensors are the most accurate [79], though this range can be extended to some degree with complex visual tracking algorithms. Hence, we employ Microsoft Kinect only for validating the spatial accuracy of the IMU-based system, and not as a part of the core system.

We specifically used the Microsoft Kinect v2 camera, mounted on a tripod at a height of 0.7 m, to record the patients moving through a corridor towards the camera (along the anterior-posterior direction). We only considered strides within the most accurate operational range of 1.5–4 meters, since we want the Kinect data to be as reliable as possible, to be used as a reference. The spatial accuracy of the Kinect data further increases during the periods where the feet are stationary (i.e. the zero-velocity periods). Hence, extracting the displacement (computed via the depth readings) between two consecutive zero-velocity periods of a specific foot yields very accurate stride length estimations. Further details of the Kinect-based data collection setup can be found in [84], where we also explored the applicability of this system as a stand-alone gait analysis solution.

For validating the temporal parameters such as swing, stance and cycle times, the Kinect system proved to be not accurate enough. For instance, in [77], high absolute cycle time errors of 0.24 seconds are observed. Therefore, we decided to additionally employ a slow-motion camera (recording at 240 frames per second) placed on the floor beneath the Kinect camera. We conducted a frame-by-frame analysis of the recordings to determine the IC/FO times, and consequently determined swing, stance and cycle times for each stride. It should be noted that, the accuracy of the detected IC/FO times directly determines the accuracy of the computed swing and stance times, since they are defined as the complementing periods between consecutive IC and FO events (see Chapter 2, for detailed definitions).

We collected disjoint validation data from a total of 22 subjects; 16 of whom (eight males, eight females) are healthy, and the remaining six (three males, three females) suffer from different neurological conditions with gait implications; particularly, two subjects with FTD, one with VaD, one with VaMCI, one with NPH and one with PD. The healthy subjects' average age is 43.9 ± 15.7 (range: 25–76) and their average height is 1.68 ± 0.08 meters. The subjects with neurological conditions have an average age of 50.6 ± 18.3 (range: 52–79) and an average height of 1.67 ± 0.08 meters.

Whenever possible, the subjects were instructed to strap the IMUs on their feet themselves, with minimal intervention, to increase the sensor placement variability. The subjects were then asked to walk in the designated test area at their preferred pace. Three to five walking sessions were conducted for each subject to increase the amount of data.

To demonstrate the correlation and the agreement between the reference system and our system, we generated correlation and Bland-Altman plots [85], which is a standard method of analyzing the agreement and the differences between two measurement methods [86]. The method differences are plotted against the averages, together with the limits of agreement (LOA), corresponding to the 95% confidence interval of the differences. We employed the Kolmogorov-Smirnov test, which is a nonparametric

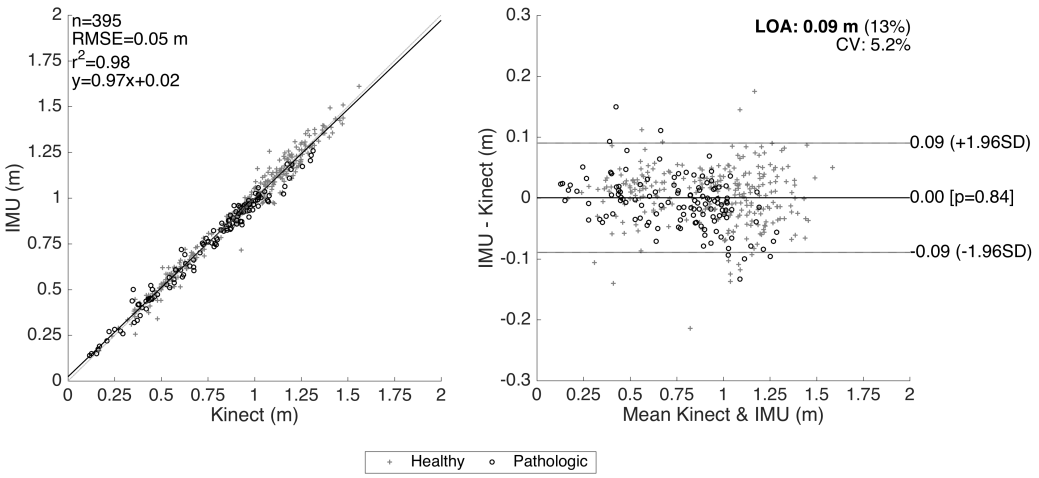


Figure 5.12. Correlation and Bland-Altman plots for stride length validation.

statistical test that aims to determine whether a variable follows a given distribution, based on the maximum absolute difference between the empirical cumulative distribution functions, to ensure the normality of the data before the analyses.

The results for the validation of stride lengths are presented in Figure 5.12. The healthy and pathological data are plotted with separate markers. The linear regression on the correlation plot demonstrates a good fit with $r^2 = 0.98$, and the slope of the fit (0.97) shows that there is no significant bias proportional to the magnitude of the measured quantity. The root mean square error (RMSE) is 0.05 m. The LOA are on the average 0.09 m per stride, which is clinically acceptable. Moreover, there is negligible bias (mean of differences is 4.6×10^{-4} m). The characteristics of the method differences also do not change significantly over the range of the measurements, indicating no considerable proportional bias. There is also no significant difference between the error characteristics of the healthy and pathological data.

The results for the validation of swing times are presented in Figure 5.13. Even though we also compiled the validation results for the stance times (and consequently the cycle times as the sum of the two), we only present the validation results for the swing times, since the stance time errors are determined to be proportional to the swing time errors (in the opposite direction), as they complement each other to form a cycle. Similar to the stride length validation results, a good correlation fit (with RMSE =

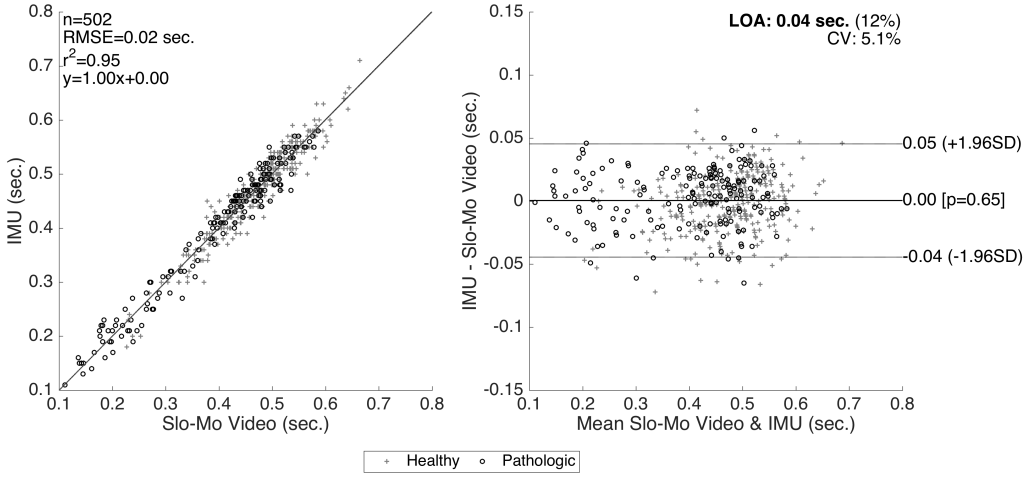


Figure 5.13. Correlation and Bland-Altman plots for swing time validation.

0.02 sec., $r^2 = 0.95$ and slope of 1.0) is observed. There is no considerable bias (mean of differences is 4.7×10^{-4} sec.) or significant changes in the error characteristics over the range of the measurements. The LOA (on the average 0.04 sec.) are clinically acceptable. Similar to the stride length validation results, there is no significant difference between the accuracy of the healthy and pathological data, which is an evidence towards our system's applicability for abnormal gait as well.

5.3.2. What Can the Gait Parameters Tell Us?

To assess and demonstrate the clinical significance and accuracy of the extracted gait parameters, we present the parameters computed from a selected portion of our dataset (see Chapter 4 for the details on the dataset), and compare them to the actual clinical findings of the neurologist. We first present the discussion on the control group results, that will serve as a reference for the subsequently explained gait abnormalities. Then, we discuss the findings on the neurological disorder subjects individually, complemented with the diagnoses of the neurologist. The discussions in this section are for demonstrative purposes to give the readers an insight on how the parameters can be evaluated to detect abnormalities. A more systematic evaluation on the predictive power of the gait parameters can be found in Chapter 6.

5.3.2.1. Healthy Control Subjects. A group of 18 healthy control subjects (11 females, 7 males) are selected from the pool of 60 control subjects, for demonstrative purposes. The extracted gait parameters of the selected control group are presented in Table 5.1. The gender, age and height of each subject are also presented. This data may be treated as a reference for assessing the gait abnormalities of the neurological disorder subjects discussed in Section 5.3.2.2. The summary of the significant control group findings is as follows:

- Stride length is affected by age, height and gender, as well as the intended walking speed of the subject during data collection. Therefore, it is not possible to determine gait abnormality solely by looking at this parameter; it has to be assessed with respect to the subject's traits and other parameters. However, extreme low values may indicate abnormality. The average stride length among the control subjects is 1.16 ± 0.12 m, with the lowest observed value being 0.93 m. The average is well above one meter and extreme low values are uncommon. Therefore, the interpreter should look out for extreme values rather than small inconsistencies.
- Cadence is similar to stride length, as it is also affected by by age, height, gender and the subject's intended pace. But the effects are much weaker, suggested by the low variability (the average is 101.6 ± 7.9). As a person attempts to increase his/her pace, both the average stride length and cadence increases. Therefore, these two parameters should be interpreted with respect to each other. For instance, a low stride length value combined with high cadence might indicate the attempt to achieve a certain speed by compensating the small steps by a faster rate, which may be a sign of abnormality. The combined effect of these two parameters are reflected in speed. Cycle time parameter is inversely proportional to cadence, thus similar observations can be made for it.
- For the parameters that have separate left-right components, the most important observation for the control subjects is that there are no considerable asymmetries. The normal gait is left-right symmetric, and this property is reflected in the parameters. Asymmetries are mostly observed in the stance ratios and clearance values, and these two parameters usually also affect each other.

Table 5.1. Gait parameters extracted from control subjects.

ID	**Gender**	**Age**	**Height (m)**	**stride length (m)**	**cadence (steps/ min.)**	**cycle time (sec.)**	**L stance time (sec.)**	**R stance time (sec.)**	**L swing time (sec.)**	**R swing time (sec.)**	**L stance ratio**	**R stance ratio**	**speed (m/s)**	**L clearance (cm)**	**R clearance (cm)**	**turning rate (deg./s)**
C1	M	62	1.76	1.44	109.2	1.10	0.64	0.67	0.45	0.44	0.59	0.60	1.31	10.0	9.8	81.8
C2	F	68	1.62	1.08	102.5	1.17	0.70	0.69	0.48	0.48	0.59	0.59	0.92	5.8	6.0	48.9
C3	M	83	1.65	1.17	88.0	1.36	0.84	0.80	0.54	0.55	0.61	0.60	0.86	6.7	7.0	38.6
C4	F	77	1.50	0.93	110.7	1.08	0.65	0.64	0.44	0.43	0.60	0.60	0.86	4.8	4.6	27.6
C5	F	51	1.70	1.29	106.8	1.12	0.67	0.65	0.47	0.46	0.59	0.58	1.15	7.0	7.5	80.4
C6	F	80	1.62	1.14	109.0	1.10	0.66	0.64	0.45	0.46	0.59	0.58	1.04	6.0	6.4	56.6
C7	M	84	1.70	1.31	104.5	1.15	0.67	0.72	0.45	0.46	0.60	0.61	1.14	7.5	7.8	54.2
C8	F	50	1.65	1.30	104.6	1.15	0.63	0.66	0.52	0.49	0.55	0.57	1.13	6.9	6.9	64.8
C9	F	73	1.60	1.13	111.9	1.07	0.63	0.62	0.45	0.44	0.59	0.59	1.05	5.6	5.6	53.7
C10	F	60	1.63	1.15	106.4	1.13	0.67	0.65	0.47	0.46	0.59	0.59	1.02	5.8	5.8	51.6
C11	M	75	1.78	1.03	103.2	1.16	0.69	0.71	0.48	0.45	0.59	0.61	0.88	5.1	5.0	26.9
C12	F	70	1.66	1.10	103.6	1.16	0.71	0.69	0.46	0.46	0.60	0.60	0.95	5.0	5.1	43.5
C13	F	73	1.50	1.14	104.4	1.15	0.74	0.69	0.42	0.45	0.64	0.61	0.99	6.7	7.5	37.4
C14	M	69	1.78	1.32	95.9	1.25	0.73	0.73	0.53	0.51	0.58	0.59	1.05	8.2	8.8	38.2
C15	F	66	1.53	1.08	100.6	1.19	0.73	0.69	0.49	0.48	0.60	0.59	0.91	5.3	5.3	46.5
C16	M	68	1.76	1.16	83.1	1.44	0.86	0.84	0.60	0.59	0.59	0.59	0.80	7.0	7.0	30.3
C17	M	78	1.68	1.08	92.4	1.30	0.78	0.79	0.52	0.51	0.60	0.61	0.83	7.3	7.5	51.4
C18	F	66	1.55	1.06	92.4	1.30	0.82	0.80	0.49	0.49	0.62	0.62	0.81	6.0	6.6	40.7

- In addition to the similarity of the left and right stance ratios (no asymmetry) for the control subjects, we also observe that they are very close to the healthy stance ratio value of 0.6 over one (60%). The averages are 0.60 ± 0.017 for the left side and 0.60 ± 0.012 for the right side, with the variability being very low. Any significant deviation from the nominal value may indicate abnormality.

5.3.2.2. Neurological Disorder Subjects. We selected 17 subjects from the pool of 60 neurological disorder subjects, to demonstrate the clinical potential of our system. The gait parameters extracted from these subjects are presented in Table 5.2. The subjects' gait related sypmtoms are discussed individually, supported by the findings indicated by the gait parameters. The individual neurological conditions of the subjects can be found in Table 4.1, though we also mention these conditions in the clinical discussions below, whenever appropriate.

The standard deviation values for the parameters that are computed over multiple strides are also available, but omitted due to space constraints. These indicators are crucial to detect temporal variations, which should be minimal in healthy gait. In the discussions of the individual subjects below, the standard deviation values are provided if they indicate a clinical finding.

We aggregate multiple sessions of a subject into one if the sessions are conducted back-to-back and the gait characteristics do not deviate from session-to-session. However, for the patient with ID 61, we decided to compile the parameters separately, as two different sessions correspond to PD medication ON and OFF states respectively. The results of this subject is discussed in more detail in the upcoming text.

When interpreting the gait parameters, it is important to consider multiple related parameters together, as focusing on a single parameter might be misleading. Some parameters for the neurological disorder subjects overlap with the parameters of the control group when viewed individually, but abnormalities may be detected when a parameter is assessed together with other parameters. For instance, a low stride length

Table 5.2. Gait parameters extracted from neurological disorder subjects.

ID	Gender	Age	Height (m)	stride length (m)	cadence (steps/ min.)	cycle time (sec.)	L stance time (sec.)	R stance time (sec.)	L swing time (sec.)	R swing time (sec.)	L stance ratio	R stance ratio	speed (m/s)	L clearance (cm)	R clearance (cm)	turning rate (deg./s)
1	M	72	1.74	1.20	88.9	1.35	0.84	0.84	0.50	0.52	0.62	0.62	0.88	8.6	9.1	55.9
2	M	85	1.65	0.99	109.3	1.10	0.66	0.71	0.44	0.39	0.60	0.65	0.90	7.3	6.9	45.2
3	F	73	1.62	1.11	99.9	1.20	0.76	0.70	0.45	0.49	0.63	0.58	0.92	3.9	5.3	50.3
4	F	82	1.58	0.50	72.4	1.66	1.18	1.18	0.47	0.49	0.72	0.71	0.30	4.5	4.4	29.0
5	M	80	1.76	1.10	75.0	1.60	0.87	1.02	0.71	0.6	0.55	0.63	0.69	7.7	8.4	22.6
6	F	85	1.65	0.81	88.3	1.36	0.86	0.85	0.49	0.52	0.64	0.62	0.60	5.3	6.0	28.8
7	F	81	1.60	0.72	70.6	1.70	1.15	1.12	0.55	0.58	0.68	0.66	0.42	5.2	5.9	32.5
8	F	80	1.60	0.73	82.6	1.45	0.94	0.96	0.53	0.48	0.64	0.67	0.50	4.5	5.2	38.7
9	M	82	1.65	1.16	88.4	1.36	0.78	0.82	0.57	0.56	0.58	0.59	0.86	9.4	10.7	41.3
10	F	52	1.56	0.83	123.0	0.98	0.57	0.67	0.40	0.32	0.59	0.68	0.85	3.5	6.0	59.1
11	F	90	1.60	0.53	119.3	1.01	0.67	0.61	0.35	0.38	0.66	0.62	0.52	3.7	4.0	18.1
12	M	83	1.59	0.93	95.6	1.26	0.77	0.76	0.48	0.5	0.62	0.60	0.74	6.9	6.1	45.1
13	M	84	1.69	0.45	90.9	1.32	0.89	0.87	0.43	0.45	0.67	0.66	0.34	3.7	3.0	29.0
14	F	82	1.50	0.83	83.8	1.43	0.96	0.84	0.47	0.59	0.67	0.59	0.58	5.2	4.8	35.8
15	F	56	1.58	0.89	88.9	1.35	0.89	0.80	0.49	0.52	0.65	0.61	0.66	8.6	7.9	56.4
16	F	79	1.57	0.15	74.5	1.61	1.39	1.37	0.21	0.26	0.87	0.84	0.09	2.1	2.4	13.5
61-ON	F	51	1.65	0.82	98.6	1.22	0.85	0.88	0.37	0.33	0.69	0.72	0.67	3.4	3.3	30.2
61-OFF	F	51	1.65	0.55*	95.6	1.26	0.99	1.07	0.27	0.18	0.79	0.85	0.44	2.9	2.4	40.5

value may not necessarily indicate an abnormality, as the subject may be intentionally walking slowly. But, if we observe a high cadence value combined with a low stride length, it could indicate that there is a difficulty lifting the feet off the floor, and the subject is trying to compensate by taking steps faster. Another example would be the stance and swing times. Looking at these parameters individually would not tell us much, instead their ratio should be assessed (as reflected in the stance ratio parameter). The parameters that have right and left counterparts, such as clearance, should also be considered with respect to each other. An overall low clearance would not indicate an abnormality, since it is also affected by the pace or the intentional sure-footedness of the subject. An asymmetry between left and right may indicate a gait problem though.

Subject 1 has DLB and VaMCI at early stages. The parameters listed in Table 5.2 do not show a serious gait abnormality, however the patient exhibits high stance time variations (standard deviation of 0.21 seconds), which indicates an abnormally high temporal variation. This is also observed by the neurologist.

Subject 2 has DLB. Left-right asymmetry is observed with right and left feet stance ratios being 60% and 65%, respectively. The cadence is higher compared to a leisurely walk, but the stride length is within the normal range, suggesting that the subject walked fast intentionally. None of these findings point to a significant gait problem, which is also verified by the clinical observation.

Subject 3 has PD pronounced on one side, as the main clinical observation for this patient is the left-right asymmetry. This observation is reflected in the parameters, as there is significant feet clearance asymmetry (left: 3.9 cm, right: 5.3 cm), shown in Figure 5.14, and a difference between the left-right stance ratios.

Subject 4 has PD with classical Parkinsonian gait. The overall muscle rigidity causes magnetic feet, as reflected in the high stance ratios (72%) compared to the typical healthy stance ratio of 60%. The stride lengths and feet clearance are also low (0.5 m and 4.5 cm, respectively) which are also consistent with Parkinsonian gait.

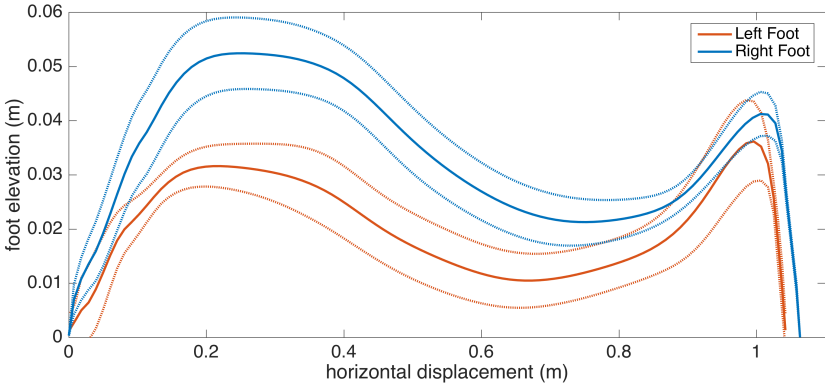


Figure 5.14. Feet elevation (clearance) asymmetry (Subject 3).

Subject 5 has VaD and DLB, and exhibits overall slow movement. The slowness is reflected in the cadence and speed parameters. Moreover, the turning rate is abnormally low (22.6 degrees per second), which may indicate problems associated with maintaining balance. There is also some degree of left-right asymmetry reflected in the stance ratio values.

Subject 6 has been diagnosed with NPH, and has problems in maintaining balance, as pointed out by the neurologist. This is reflected in the low turning speed. The stance ratio values are slightly higher than normal, indicating a slight difficulty of lifting the feet off the ground, which may also be associated with balance problems.

Subject 7 also exhibit Parkinsonian gait. The movement is slow overall, as shown by the low stride length, cadence and speed values, as a result of muscle rigidity. This patient also has even footfall with less pronounced heel strikes, which is also consistent with Parkinsonian gait, as demonstrated in the lateral stride profile (Figure 5.15).

Subject 8 suffers from VaD, DLB and also exhibit Parkinsonism symptoms. The stride lengths are low, contributing to the overall slow movement. The stance ratios are slightly higher than normal, with the right stance times slightly higher than the left, combined with decreased feet elevation.

Subject 9 has VaD with minimal gait-related symptoms. The parameters also do not indicate any significant abnormality.

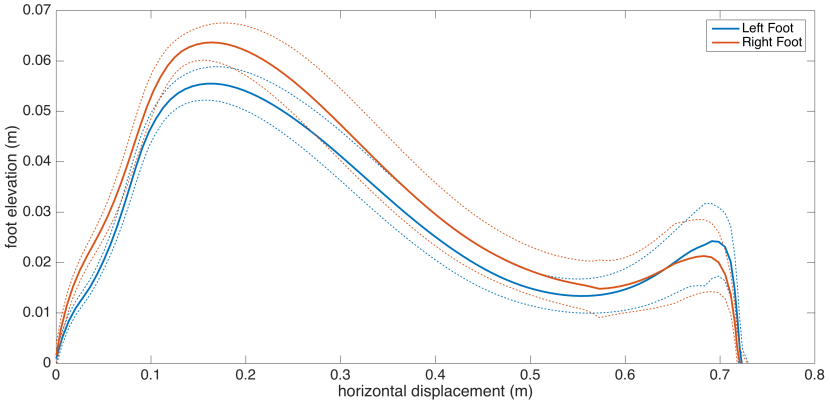


Figure 5.15. Even footfall indicated by lower secondary peaks (Subject 7).

Subject 10 is a 52-year-old early-onset PD patient, showing typical gait symptoms of PD such as decreased stride lengths, even footfall and right-left asymmetry (both indicated by the feet clearance and stance ratios). One important observation is the high cadence values, which indicates that the patient tries to compensate the decreased stride lengths with frequent steps, as also clinically observed.

Subject 11 is also a PD patient exhibiting gait-related symptoms similar to Subject 10. But stride lengths are even smaller, as also affected by the subject's age. There is a slight stance ratio asymmetry (left: 66%, right: 62%), confirming the clinical observation of higher left-sided rigidity.

Subject 12 has early stage PD with right side onset. The left-right asymmetry is apparent in the slightly lower right clearance value of 6.1. The remaining parameters do not indicate any abnormalities.

Subject 13 suffers from VaD with Parkinsonism symptoms. The magnetic feet are indicated by the high stance ratios and low feet clearance values. The stride lengths are very low. Left heel strikes are absent (even footfall), which is consistent with the clinical observation of slight left dominance of the extrapyramidal symptoms.

Subject 14 has DLB, causing left-right asymmetry, as indicated in the higher left stance ratio. The difference between left and right swing times are especially high (20% difference), showing an abnormality with foot swinging, which is confirmed by

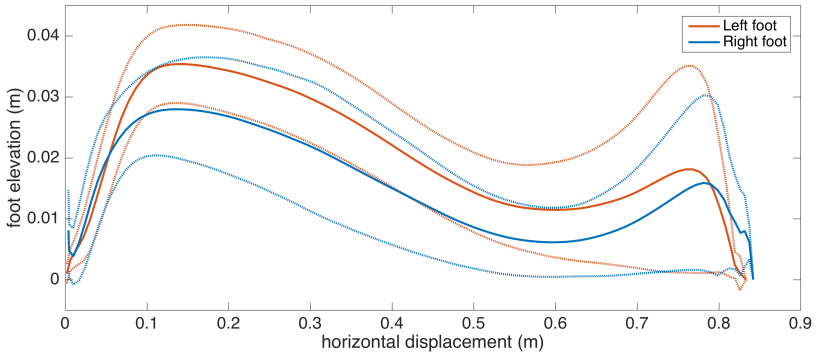
the clinician. The clearance values are also abnormally low.

Subject 15 is a young FTD patient at age 56, showing some left-right asymmetries reflected in the stance ratio values. Her gait also exhibits high temporal variations, as reflected in the stance time standard deviation value of 0.19 seconds.

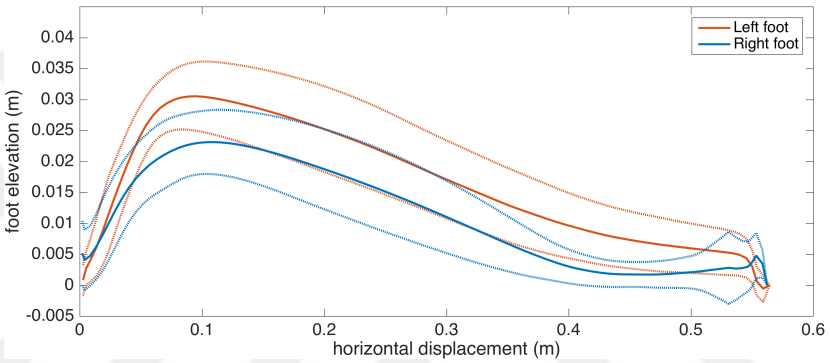
Subject 16 suffers from NPH, with extreme pathological gait. The stride length and clearance values are very low, as is also speed. The stance ratio values are very high ($> 80\%$), indicating magnetic feet. The turning rate is also very low (13.5 deg./sec.).

We were able to collect medication ON and OFF state data from Subject 61, who is a PD patient. The ON and OFF sessions are denoted by subject identifiers 61-ON and 61-OFF in Table 5.2, respectively. The data collection times were 2 hours apart. The medication ON state denotes the period during which the medication is active and the symptoms are mitigated. Assessing how and to what extent the symptoms are mitigated is especially important to be able to adjust the medication dosage of PD patients quickly and accurately. Also, excess dosage may cause motor complications such as dyskinesia, which further increases the significance of monitoring ON/OFF periods. The typical medication titration procedure for the clinicians is the feedback from the patient or the caregiver, which may be subjective and hence require a few weeks to collect and validate. Our system provides a faster and more objective method.

The ON state lateral stride profile is presented in Figure 5.16a. Even though the feet elevation and stride lengths are generally low, there is still a pronounced heel strike as the patient can still lift her toes before the IC. However, as fatigue kicks in about the middle of the session, gait becomes more dysfunctional. The toe lift decreases (as reflected in the increased standard deviation curves towards the secondary peak of the step profiles). This behavior is also apparent in the change of the stance and swing time ratios through the session, presented in Figure 5.17. The stance times get longer as the feet of the patient become harder to lift off the ground. In the OFF state, the heel strikes disappear completely (Figure 5.16b), and the feet are stuck on the ground for



(a)



(b)

Figure 5.16. Lateral stride profile of a PD patient (Subject 61), (a) ON state, (b) OFF state.

extended durations (indicated by the high stance ratios and low feet clearance values), consequently leading to foot dragging.

5.4. Conclusion

In this chapter, we proposed a robust inertial sensor-based gait analysis system suitable for non-hospital settings, that is able to extract a rich set of standard spatio-temporal gait parameters. The system is completely mobile with no requirement of an infrastructural element. The extracted parameters are supported by a novel lateral stride profile visualization method, which enables the instant visual interpretation of the underlying spatial gait characteristics.

We conducted a two-phase experimental study to validate the numerical accuracy of our system, and to provide individual case reports of various neurological disorders

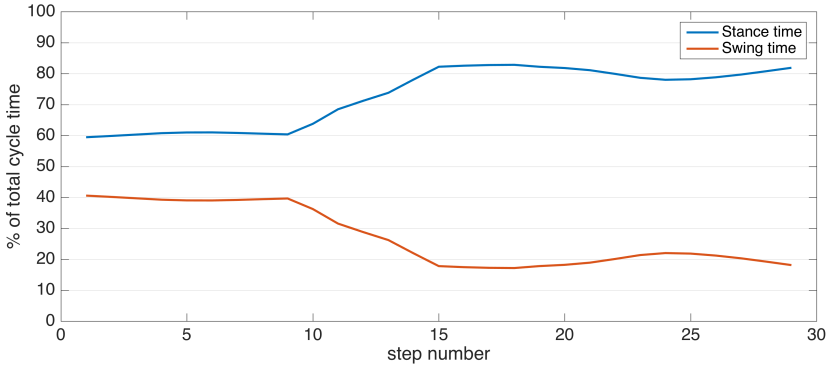


Figure 5.17. Change of stance and swing time ratios due to fatigue (Subject 61).

that demonstrate the system's clinical applicability. The results indicate that our system can indeed capture various gait pathologies in a non-hospital setting. They also strengthen the position of the wearable inertial sensors in the gait analysis scene, demonstrating their potential as alternatives to the gold standard systems.

In the next chapter, we extend the capabilities of our system by extracting higher level gait parameters that quantify asymmetries and temporal variations. Furthermore, we conduct a systematic feature selection study to identify the most important parameters for neurological disorders. The selected set of parameters are then used for the classification of neurological disorder patients and healthy control subjects, which further validates our system's success in detecting pathological gait traits.

6. IDENTIFYING IMPORTANT GAIT PARAMETERS FOR NEUROLOGICAL DISORDERS

In this chapter, we utilize various feature selection and predictor importance analysis methods to determine the predictive power of the spatio-temporal gait parameters in terms of identifying gait pathologies in neurological disorders. The material presented in this chapter is submitted for publication and currently under review.

6.1. Introduction

Patients with neurological disorders have increased tendency for gait disturbances, and neurodegenerative diseases like Parkinson's disease and dementia are common in the elderly [87], making gait analysis valuable for a substantial portion of the world population. Pathological gait has significant implications on the quality of life, leading to a decrease in mobility, self-esteem and self-independence [88]. Problems in gait are also accompanied by increased fall risk, which may result in injuries, institutionalization and even death [89]. Gait analysis methods enable the detection and assessment of such abnormalities and risks, guiding appropriate treatment and other means of coping with these negative implications. Detection of subtleties in gait can even guide differential diagnosis for neurological disorders [90], which is crucial for formulating the correct treatment.

Pathological gait conditions caused by neurological disorders have been examined in the literature, as there are studies focusing on disorders including Parkinson's disease [10, 18, 33, 91], cerebral palsy [92], dementia [93], multiple sclerosis [94] and even Alzheimer's disease [14]. Almost all of the existing work focus on a specific disorder and do not attempt to find gait-related commonalities in multiple conditions. One of the aims of this chapter is to fill this gap by identifying common gait factors observed in a variety of neurological disorders, that may help differentiate them from other non-neurological gait-affecting conditions.

Fortunately, the number and variety of spatio-temporal gait parameters extractable by inertial sensors increase as new gait analysis proposals are put forward in the literature. This can be both an advantage, as more information leads to better assessments, and a drawback, since the increased complexity may intimidate researchers new to the field. Moreover, having more features does not necessarily mean higher estimation accuracies, as they may tend to produce overfitted models, especially in cases of limited cohorts. Feature selection is a critical step in order to eliminate these problems.

In this chapter, we aim to investigate several feature selection and predictor importance analysis methods applicable on gait parameters extracted via an inertial sensor-based system. We focus on patients with neurological disorders, and assess the importance of the parameters in terms of detecting common gait abnormalities. Ultimately, we come up with a reduced set of parameters that can be used as a starting point in future studies. We also show that this set is at least as informative as the full set of parameters for distinguishing between pathological and healthy gait, proving that the loss of information due to the unselected parameters are minimal.

6.2. Methods

For this chapter, our whole dataset consisting of 60 neurological disorder subjects and 60 control subjects is used (see Chapter 4). The gait analysis methodology presented in the previous chapter is employed to extract spatio-temporal gait parameters, which will serve as the predictors that are subjected to feature selection algorithms.

The strides are automatically segmented by the gait analysis system, and the gait parameters are computed separately for each stride. The estimated gait parameters include stride length, cadence, cycle time, stance time, swing time, stance ratio, speed and clearance, which are pre-processed via the methods detailed in the next section to come up with aggregated gait parameters. Among these parameters, we aim to identify the important ones that define the pathological gait in neurological disorders.

6.2.1. Gait Parameters Pre-processing

The parameters extracted for individual strides are averaged over the whole data of a subject to compute the mean and standard deviation for a parameter. The parameters with separate left and right side components are also averaged and stored separately. To delateralize the parameters while preserving their sidedness, we also compute symmetry indices (SI) [95] for relevant parameters by

$$\mathrm{SI} = \frac{|X_L - X_R|}{0.5 \cdot (X_L + X_R)} \tag{6.1}$$

where X_L and X_R correspond to the average left and right components of a parameter, respectively. The value of $\mathrm{SI} = 0$ indicates perfect symmetry.

Furthermore, the standard deviation of the parameters are normalized by their respective means to produce coefficient of variation (CV) values. This approach is commonly used in numerous gait analysis studies [96]. The resulting 17 gait parameters are presented in Table 6.1, which includes the short names that will be used to reference these parameters in the remainder of the chapter, and their detailed definitions.

6.2.2. Predictor Selection

We use the gait parameter and predictor terms interchangeably, since the parameters are used as predictors for the existence of a gait abnormality, in the presented methods. The predictor selection procedure first involves correlation and multicollinearity analyses to eliminate the predictors that are representable by the linear combinations of other predictors, i.e. to mitigate the redundancy of predictive information.

We first analyze the pairwise correlations of the gait parameters by computing Pearson correlation coefficient ρ values within different predictor pairs. This step is helpful to show any direct redundancies and allows us to support them with intuitive reasoning as to why two gait parameters are correlated.

Table 6.1. Aggregated gait parameter names and definitions.

Short Name	**Units**	**Definition**
cadence	steps/min.	Number of steps taken in a minute; i.e. walking rate.
cycleTimeAvg	seconds	Time between successive floor contacts of the same foot (averaged).
speed	meters/sec.	Average walking speed.
strideLengthNormAvg	unitless	Distance between successive heel contacts of the same foot (averaged). Normalized by each subject's height (causing unit loss).
stanceTimeAvg	seconds	The duration for which the foot remains in contact with the floor (averaged).
swingTimeAvg	seconds	The duration for which the foot is not in contact with the floor, i.e. it is in motion (averaged).
stanceRatio	unitless	Stance time divided by cycle time (averaged).
clearanceAvg	centimeters	The maximum elevation the foot achieves during the swing phase (averaged).
strideLengthCV	unitless	Coefficient of variation for normalized stride length.
cycleTimeCV	unitless	Coefficient of variation for cycle time.
stanceTimeCV	unitless	Coefficient of variation for stance time.
swingTimeCV	unitless	Coefficient of variation for swing time.
clearanceCV	unitless	Coefficient of variation for clearance.
stanceTimeSI	unitless	Symmetry index for stance time.
swingTimeSI	unitless	Symmetry index for swing time.
stanceRatioSI	unitless	Symmetry index for stance ratio.
clearanceSI	unitless	Symmetry index for clearance.

The next step is to perform multicollinearity analysis to eliminate redundancies caused by multiple predictors at the same time. We compute variance inflation factors (VIF) for each predictor. Then, we iteratively remove the predictors with high VIF values and recompute till we reach an acceptable set of predictors with reasonably low VIF values. This procedure allows us to eliminate redundancies as much as possible while preserving the overall informativeness of the predictor set.

The predictor set resulting after the multicollinearity analysis is subjected to four different methods that can be used for the purposes of predictor selection: ANOVA, stepwise logistic regression (LR), LASSO logistic regression and random forest (RF). The whole dataset comprised of 60 neurological disorder patients and 60 healthy subjects is used as input for the subsequent feature selection methods.

ANOVA (analysis of variance) is used to assess the individual statistical significance of the predictors in terms of gait abnormalities. The normality of the data is confirmed by the Lilliefors test, beforehand. The computed p-values are used to determine the predictor selection outcome of this method, with the threshold of $p < 0.001$.

Even though, ANOVA is a powerful method to assess the the predictors individually, the significance of multiple predictors conditioned on the response is also important. A predictor that is not significant by itself may prove to be informative with the existence of other predictors. Therefore, classification methods that are able to perform multivariate cuts in order to discriminate between different states of gait are also important. For this purpose, we employ logistic regression, which is a binary classifier based on determining a linear discriminant using least squares regression. An advantage of LR is its transparency that allows us to see the predictors' contributions to the final model. LR itself is not sufficient for predictor selection. An extension on LR is stepwise LR, which involves iteratively building multiple LR models, at each step adding or removing predictors based on their contributions. The model converges on a predictor set which we determine as the outcome of this method. In our analyses, the stepwise procedure starts with a constant model with only the intercept and iteratively

builds upon that by adding or removing predictors until convergence.

Another extension of LR is LASSO (least absolute shrinkage and selection operator) LR [97]. LASSO is a regularization method which prevents overfitting by tuning down the coefficients of the relatively unimportant predictors as far to the point of zero, essentially eliminating them from the model. It does this by adding a penalty term to the error minimizing objective function, equal to the sum of the absolute values of the coefficients, i.e. the success of the model is penalized as more predictors with large coefficients are present in the model. This penalty term is scaled by parameter λ, which is estimated by cross-validation with 10 folds. We select the model with minimum-plus-one standard error computed over the average of the folds, corresponding to $\lambda = 0.05$, to favor model simplicity (fewer selected predictors) over accuracy.

The final model we use for predictor selection is random forest [98], i.e. bootstrap-aggregated decision trees, which are essentially an ensemble of decision trees trained on randomly selected sets of predictors and input data. This approach avoids overtraining while providing means of assessing predictor importance by utilizing the data not used while training a specific tree (out-of-bag data). Although RF is essentially a classifier, it is also suitable to assess feature importance via observing the effect of manipulating different features on a multitude of trees [99]. We specifically use out-of-bag predictor importance estimates by permutation, which relies on randomly permuting the values of a particular predictor and examining its effect on the out-of-bag classification error. If a predictor is significant, permuting its values should have a drastic increase in the error. This method allows us to produce predictor importance estimates on a continuous scale, which could then be thresholded to obtain a set of selected predictors. We train 1000 trees, with 6 predictors randomly sampled for each tree having minimum leaf size of one sample.

These four models provide four different sets of selected predictors. We further analyze these sets to determine the commonalities and differences, to come up with the ultimate reduced set of predictors.

6.2.3. Validation of Selected Predictors

To validate the informativeness of the ultimate set of selected predictors, we analyze the accuracy of two powerful classifiers, support vector machine (SVM) [100] and random forest in terms of detecting pathological gait. SVM is selected because of its black box nature to complement the previously utilized methods which are transparent. We utilize the linear SVM kernel. Random forest is trained with the same parameters as in the predictor selection step. Both models are trained using leave-one-out cross-validation to cover the whole dataset while keeping the test and training sets separate. It should be noted that, the ideal validation setting would be to utilize a completely separate test dataset which is not seen during feature selection, in order to avoid overfitting the hyper-parameters to the test set. However, this was not possible due to the limited data consisting of only 120 samples (one sample consisting of a single set of aggregated parameters for each subject), as it would lead to some valuable neurological cases not being considered during feature selection.

We build two different models for each classifier: One with the selected (reduced) set of predictors, the other one with the full predictor set. We compare the classification power of the reduced predictor set with the full predictor set, for each classifier. We aim to show that the selected predictors lead to a classification accuracy at least as good as the case where we use the full predictor set as the input.

All the methods and analyses detailed in this chapter are implemented and executed using MATLAB R2018a software [75].

6.3. Results

6.3.1. Multicollinearity Analysis

The pairwise correlation coefficients (Pearson ρ) are presented in Figure 6.1, in matrix format. Lighter shades indicate higher correlation. The pairs with unusually

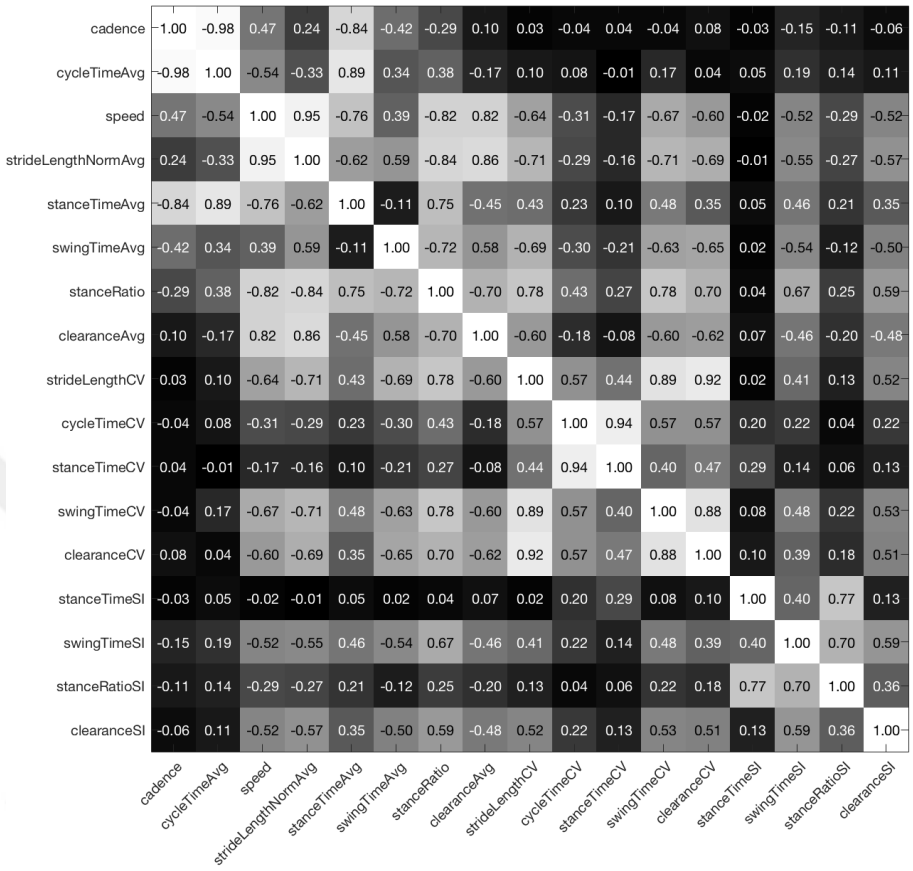


Figure 6.1. Pairwise Pearson correlation matrix for gait predictors.

high correlation ($\rho > 0.90$) include *cadence-cycleTimeAvg*, *speed-strideLengthNormAvg*, *strideLengthCV-clearanceCV* and *cycleTimeCV-stanceTimeCV*.

Cadence and cycle time both represent gait frequency in different ways and are inversely correlated, as deduced from their definitions. The relationship between cadence and cycle time can be expressed as $\text{cycle time (sec.)} = 120/\text{cadence (steps/min.)}$ [4]. Therefore, removing either of these predictors would not lead to any loss of information.

Speed and stride length also have a high correlation even though speed is not solely determined by stride length. It also depends on cadence (i.e. step frequency). However, the correlation between speed and cadence is low (0.47), indicating that stride length is the dominant factor.

Table 6.2. Multicollinearity analysis with variance inflation factors.

Gait Parameter	**Initial**	**1st**	**2nd**	**3rd**	**4th**	**Final**
cadence	67.1	62.2	14.4	14.3	3.4	3.4
cycleTimeAvg	1011.3	-	-	-	-	-
speed	67.4	67.3	62.6	-	-	-
strideLengthNormAvg	44.4	44.4	41.4	7.4	6.7	6.7
stanceTimeAvg	890.2	77.8	-	-	-	-
swingTimeAvg	207.4	35.5	35.4	27.9	7.6	7.6
stanceRatio	57.8	57.1	39.6	33.4	-	-
clearanceAvg	6.4	6.3	6.2	4.4	4.4	4.3
strideLengthCV	11.2	11.1	10.2	10.1	9.7	9.7
cycleTimeCV	17.8	17.8	16.9	16.2	15.6	-
stanceTimeCV	13.7	13.7	13.5	13.4	13.2	1.8
swingTimeCV	9.1	8.4	7.7	7.5	7.2	6.0
clearanceCV	10.1	10.1	9.7	9.2	9.0	9.0
stanceTimeSI	4.2	4.2	4.0	3.9	3.9	3.9
swingTimeSI	6.6	6.6	6.5	6.4	6.4	6.1
stanceRatioSI	7.8	7.8	7.7	7.4	7.3	7.0
clearanceSI	1.9	1.9	1.9	1.9	1.9	1.9

Variations in stride length and clearance are also highly correlated. Both of these parameters represent variations in the spatial domain, so it is intuitive that the stride-wise instabilities in complementing horizontal and vertical dimensions are dependent on each other.

Cycle time CV and stance time CV do not have a direct relationship; however, increased variations in stance times may influence cycle time CV, since stance period typically constitutes the majority of the gait cycle [101]. We do not yet remove any predictors based on these results, and intend them to serve only as supporting information for the subsequent multicollinearity analysis step.

Table 6.3. Descriptive statistics of predictors and ANOVA results.

Gait Parameter	**Mean**	**Std.**	**Min.**	**Max.**	**F-score**	***p*-value**
cadence	96.31	11.85	67.90	140.80	6.28	$p = 0.014^{*}$
strideLengthNormAvg	0.97	0.28	0.16	1.38	87.39	$p < 0.001^{***}$
swingTimeAvg	0.47	0.07	0.13	0.66	10.68	$p = 0.001^{**}$
clearanceAvg	5.75	1.97	0.90	10.10	31.97	$p < 0.001^{***}$
strideLengthCV	0.09	0.08	0.03	0.65	32.21	$p < 0.001^{***}$
stanceTimeCV	0.12	0.05	0.03	0.32	7.70	$p = 0.006^{**}$
swingTimeCV	0.09	0.08	0.02	0.61	25.99	$p < 0.001^{***}$
clearanceCV	0.13	0.09	0.04	0.74	34.47	$p < 0.001^{***}$
stanceTimeSI	0.04	0.04	0.00	0.16	5.55	$p = 0.020^{*}$
swingTimeSI	0.06	0.07	0.00	0.43	22.48	$p < 0.001^{***}$
stanceRatioSI	0.03	0.03	0.00	0.14	21.15	$p < 0.001^{***}$
clearanceSI	0.09	0.11	0.00	0.73	31.46	$p < 0.001^{***}$
						$^{***}p < 0.001$, $^{**}p < 0.01$, $^{*}p < 0.05$

The initial VIF values of the predictors are presented in Table 6.2. Some predictors have high VIF values, indicating high multicollinearity. We employ an iterative process where we remove the predictor with the greatest VIF at each iteration and recompute the VIF values of the remaining predictors at each step, until we reach the final VIF values which are within reasonable limits. The values after each iteration are also presented in Table 6.2, along with the initial and final values. The ultimately removed predictors are presented with dashes in the final VIF column of the table, and are *cycleTimeAvg*, *speed*, *stanceTimeAvg*, *stanceRatio* and *cycleTimeCV*. These results indicate that these parameters can be reconstructed from the remaining parameters with reasonable accuracy, and hence are not very informative.

6.3.2. Predictor Selection

After multicollinearity analysis, we selected 12 gait parameters as predictors out of the full set of 17 parameters. The resulting p-values from the ANOVA procedure and

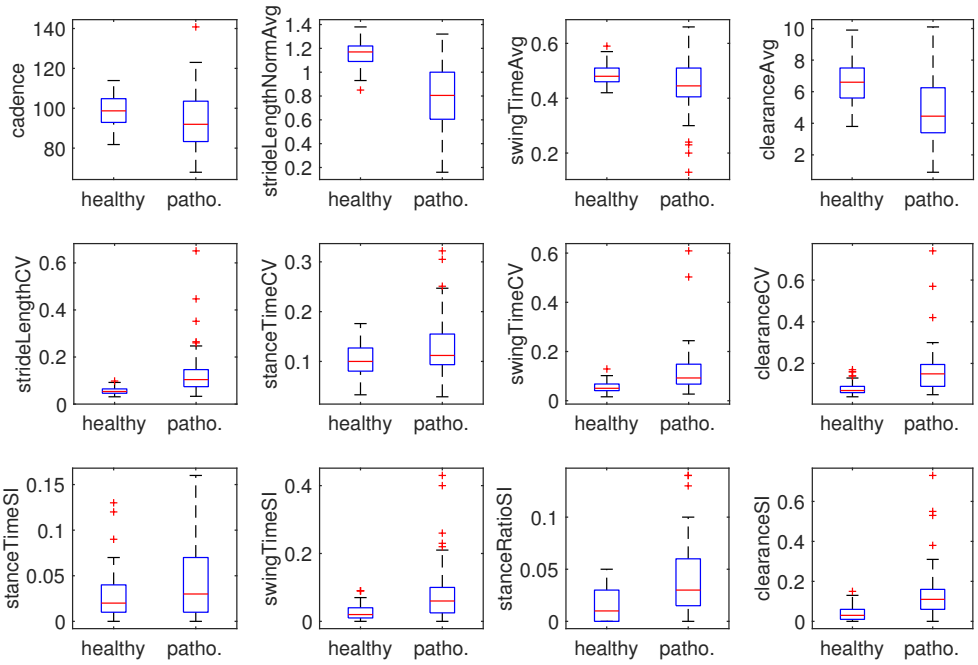


Figure 6.2. Box plots for gait predictors.

some descriptive statistics for these remaining predictors are presented in Table 6.3. Three different levels of significance are highlighted in the table. The threshold of $p < 0.001$ is determined to be the predictor selection criteria for this method. The selected predictors are *strideLengthNormAvg*, *clearanceAvg*, *strideLengthCV*, *swingTimeCV*, *clearanceCV*, *swingTimeSI*, *stanceRatioSI* and *clearanceSI*. The box plots of each predictor are also presented in Figure 6.2, to additionally provide a visual aid to assess the descriptiveness of the predictors and to shed light on their distributions.

The stepwise LR procedure converges to a simple model including only the predictors *strideLengthNormAvg*, *strideLengthCV*, *stanceRatioSI* and *clearanceSI*, with estimates -6.97, 46.09, 31.24 and 26.87, respectively. The intercept is 1.56.

LASSO LR produces a more complex model with the following predictors having nonzero coefficients: *strideLengthNormAvg*, *strideLengthCV*, *stanceTimeCV*, *clearanceCV*, *stanceRatioSI* and *clearanceSI*, with estimates -5.48, 0.91, 5.42, 2.87, 14.41 and 8.40, respectively. The intercept is 3.61.

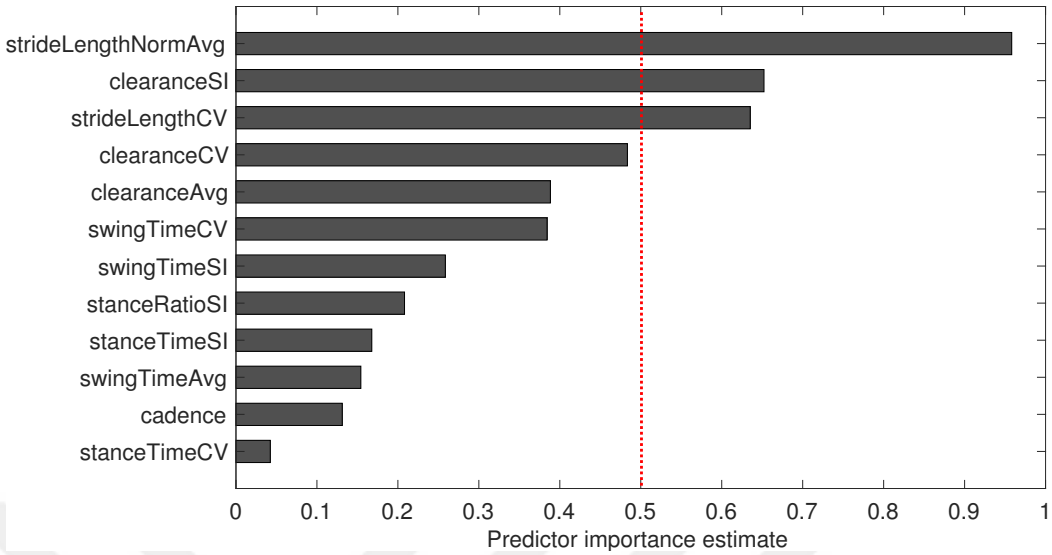


Figure 6.3. Random forest predictor importance estimates.

Random forest produces the predictor importance estimates presented in Figure 6.3. With a threshold value of 0.5, positioned at a relatively high cutoff margin, the selected predictors include *strideLengthNormAvg*, *clearanceSI* and *strideLengthCV* in decreasing importance.

The list of selected predictors for all four of these methods are presented in Table 6.4. The intersection, union and majority of these selections among all methods are also presented. A detailed discussion on this table can be found in Section 6.4.

6.3.3. Validation

To validate the applicability of the selected features in terms of detecting abnormal gait, we train and test separate SVM and RF classification models. The set of selected predictors used as input to these models are based on the intersection criteria (predictors commonly selected by all methods) presented in Table 6.4, including *strideLengthNormAvg*, *strideLengthCV* and *clearanceSI*. The full set includes all 12 predictors remaining after the multicollinearity analysis.

The receiver operating characteristic (ROC) curves of the four models are depicted in Figure 6.4. The RF classifier trained with the selected predictors perform

Table 6.4. Gait predictors selected by feature selection methods.

Gait Parameter	**ANOVA**	**Stepwise LR**	**LASSO LR**	**RF**	**Intersection**	**Union**	**Majority**
cadence							
strideLengthNormAvg	✓	✓	✓	✓	✓	✓	✓
swingTimeAvg							
clearanceAvg	✓					✓	
strideLengthCV	✓	✓	✓	✓	✓	✓	✓
stanceTimeCV			✓			✓	
swingTimeCV	✓					✓	
clearanceCV	✓		✓			✓	
stanceTimeSI							
swingTimeSI	✓					✓	
stanceRatioSI	✓	✓	✓			✓	✓
clearanceSI	✓	✓	✓	✓	✓	✓	✓

very close the one trained with the full set, with an area-under-the-curve (AUC) value of 0.909 compared to 0.906. The classification accuracies are 0.83 and 0.85, for the selected set and the full set, respectively. Similar results are observed for the SVM model, with 0.919 and 0.925 AUC values for the selected set and the full set, respectively. The classification accuracies are 0.88 for both cases.

These results indicate that the selected predictors are sufficient to produce competing and even superior classification performance to detect pathological gait, compared to the performance of the full set. Comparing the SVM and RF models, we observe that both of them perform reasonably well, with SVM having slightly better AUC and accuracy values.

6.4. Discussion

The multicollinearity analysis shows that some gait parameters can be removed without loss of information (Table 6.2). Cadence and average cycle time can be interpreted as different representations of gait frequency. Cycle time is further decomposed into stance and swing phases. These four temporal parameters are tightly coupled [4], and keeping only two of them (*cadence* and *swingTimeAvg*) are sufficient to infer the

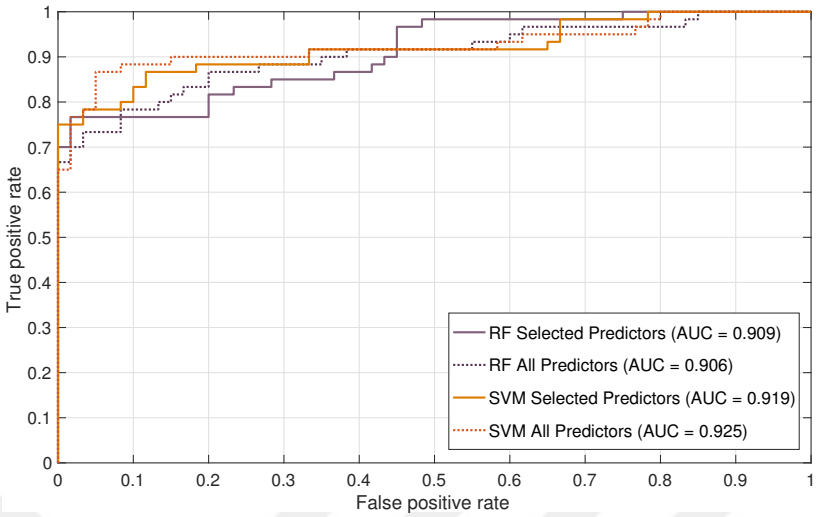


Figure 6.4. ROC curves for validating selected predictors.

remaining two (*cycleTimeAvg* and *stanceTimeAvg*). Moreover, stance ratio is directly derivable from these parameters and hence can also be removed. Having cadence and average stride length allows us to infer speed as well, since it is influenced by both gait frequency and stride length. These deductions based on the definitions of the parameters shed light on why the multicollinearity analysis suggests the removal of average cycle time, speed, average stance time and stance ratio.

Among the symmetry and variation related parameters, only cycle time variation (*cycleTimeCV*) is removed. Since the gait cycle is composed of stance and swing phases, variations in these phases influence variations in the whole cycle. Another interesting observation is the high correlation between *stanceTimeCV* and *cycleTimeCV* (0.94) as seen in Figure 6.1. Stance phase constitutes more than half of a gait cycle, specifically about 60% in normal gait [102]. This ratio is shown to be even greater in Parkinson's disease patients [103]. Hence *stanceTimeCV* is sufficient to explain the majority of variations in cycle times.

Out of the 12 gait parameters remaining after the multicollinearity analysis step, only three gait parameters are selected commonly by all methods: *strideLengthNormAvg*, *strideLengthCV* and *clearanceSI*. None of the parameters that represent the average value of a specific parameter, except for strideLengthNormAvg, are deemed important by the majority of the predictor selection methods. This indicates a ten-

dency to favor symmetry or variation related parameters to identify pathological gait.

Temporal irregularities in gait, which are represented by the CV parameters in our study, have also been shown to be indicators of abnormality in other studies, especially for neurological disorders [104–106]. Either a consistent existence of variation, or a change over time as the subjects walks (such as progressive diminishing of stride lengths, difficulties in gait initiation or freezing of gait) may be observed in neurological disorder patients [107]. Both of these conditions result in increased variation values. In line with these observations, *strideLengthCV* is commonly selected by all methods. Other variation related parameters, such as *clearanceCV*, are also selected by some methods, making them important candidates to represent gait abnormalities.

Left-right asymmetries are also important to identify pathological gait, and two symmetry related parameters are selected by the majority of the methods: *stanceRatioSI* and *clearanceSI*. Indeed, left-right asymmetries are observed in many neurological conditions, as disorders like Parkinson's disease may exhibit motor symptoms differently in distinct parts of the body, with varying left/right or upper/lower body onsets [108]. Stance ratio is a composite parameter influenced by both swing and stance time, hence stance ratio asymmetries may indicate anomalies in either swing or stance times. However, none of the methods selected *stanceTimeSI*, indicating that swing time asymmetries are more commonly observed. Unlike orthopedic conditions which may result in increased sensitivity to the loading responses that lead to asymmetries in stance times [109], neurological conditions may result in swing time anomalies [110].

Moreover, it should be noted that, none of the average temporal parameters (*swingTime* and *cadence*) are selected as important measures for pathological gait [111]. Instead, the temporal asymmetry between two feet (*stanceRatioSI*) is determined to be a more informative measure.

The accuracy of the models trained for the purposes of validation show that the selected parameters are important to represent gait abnormalities. This is also

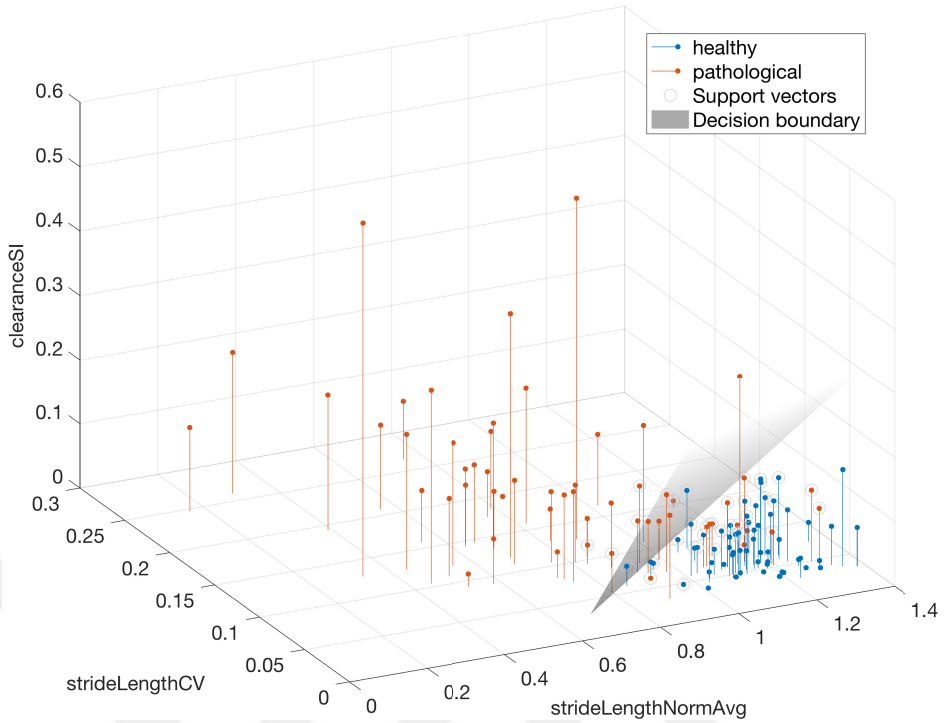


Figure 6.5. 3D visualization of selected parameters (SVM with linear kernel).

apparent in their visualization presented in Figure 6.5, along with the linear SVM decision boundary. To see if a more complex model would lead to better inference accuracies, we also trained a non-linear SVM with the radial basis function (RBF) kernel (Figure 6.6). The performance of this model is very close to the linear model (AUC: 0.907, accuracy: 0.88), hence the simpler linear model should be preferred.

It should be noted that, the primary aim of this study is not to automatically classify normal and pathological gait, but rather to determine the key spatio-temporal gait parameters in terms of identifying gait abnormalities. Our results may aid the researchers to select parameters in order to detect higher level phenomena such as disease progression or fall risk which may have connections to common abnormalities observed in neurological conditions. The selected parameters should not be considered as an absolute set to represent pathological gait characteristics, but instead as a mere starting point in further studies. In this respect, the continuous importance estimates of RF (Figure 6.3) are especially important, since they can be used to guide further addition and removal of predictors depending on the specific requirements of the problem.

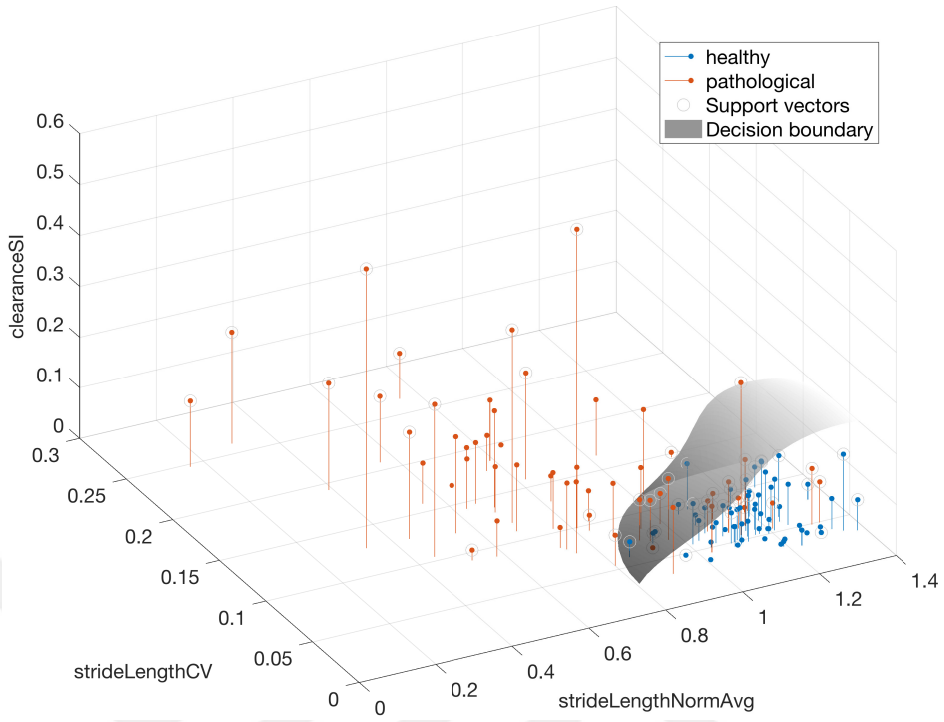


Figure 6.6. 3D visualization of selected parameters (SVM with RBF kernel).

6.5. Conclusion

In this chapter, we presented a thorough predictor importance analysis study to determine the contributions of different spatio-temporal gait parameters to common pathological gait traits observed in neurological disorders. The results indicate that the left-right asymmetries in clearance, temporal variations in stride lengths and average stride length values are especially important to detect pathological gait in neurological disorders. The predictive significance of the selected parameters are validated with two machine learning models, random forest and support vector machine. Our findings can serve as a guide to predictor selection for future studies focusing on assessing gait-related implications of neurological disorders. They also demonstrate the power of the gait parameters extractable by inertial sensors to identify specific gait pathologies.

In the next chapter, we utilize the gait parameters in a higher level inference objective, attempting to identify the patients with higher risk of falls among the neurological disorder subjects. We employ more sophisticated machine learning methods, e.g. deep learning, and try to achieve an automated fall risk assessment system.

7. FALL RISK ASSESSMENT

In this chapter, we propose an automated fall risk assessment system that utilizes the spatio-temporal gait parameters extracted by our gait analysis system as input features. We explore the applicability of deep learning methods and attempt to come up with a classifier with high inference accuracy. A manuscript based on the work presented in this chapter is currently under preparation; except for Section 7.4 that is adapted from our existing publication [112], which explores the transformation of the proposed fall risk assessment into a pervasive healthcare service.

7.1. Introduction

Accurate fall risk assessment is crucial in order to prevent fall-related psychological and physiological consequences, especially for the geriatric population [113]. The falls incur hospitalization and treatment costs to the families and indirect costs to the society in terms of expanded need for caregivers and additional facilities [114]. Fall risk assessment is important to predict falls and take preventive measures, which may include treatment adjustments, walking aids, exercise routines, changes to the living environment to eliminate hazardous elements, and caregiver support [65].

Fall risk assessment is a technically challenging problem, since not all gait abnormalities are indicative of a high fall risk. Moreover, some fall risk factors may present themselves intermittently, hence requiring continuous and real-time monitoring of gait, which our gait analysis system, presented in Chapter 5, can provide. Short outpatient visits may not be sufficient for the clinicians to detect these factors and objectively assess them, thus requiring remote monitoring in non-hospital settings. Wearable inertial sensors and the gait analysis methods associated with them become invaluable to facilitate fall risk assessment under these conditions.

As dissected in Section 3.2, the existing work on fall risk assessment with inertial sensors rarely employ sophisticated machine learning methods, leading to poor

classification accuracies. Misclassifying a high fall risk patient as low risk could have serious implications, discouraging much needed interventions. Hence, achieving a high inference accuracy is crucial, requiring powerful methods such as deep learning.

Currently, there is only one study [57] exploring deep learning methods, specifically long short-term memory (LSTM) neural networks, for fall risk assessment. The authors attempt to use the raw inertial data directly as input to the classifier, nonetheless fail to achieve high inference accuracies. Deep learning methods do indeed have the potential to learn domain knowledge from the raw data directly [115], however this seems to be not the case for fall risk assessment. Therefore, we pursue a different direction, and employ the spatio-temporal gait parameters extracted by our gait analysis system as input to the machine learning classifiers. The domain knowledge infused in the gait parameters proved to be beneficial and resulted in a superior classification accuracy. We utilize the LSTM classifier and compare its performance against more traditional classifiers such as hidden Markov models (HMM) and support vector machines (SVM). The methods are detailed in Section 7.2, and the results are presented in Section 7.3, where we also discuss our findings with respect to the existing studies. The results also indicate that the gait parameters extractable by wearable inertial sensors are convenient for a higher level inference objective, strengthening their merit.

In this chapter, we also explore how a pervasive healthcare application like fall risk assessment can be transformed into a service that can be used by multiple users in a real life setting. We propose a multi-tier computing and communication architecture that utilizes the edge computing and software-defined networking paradigms to efficiently serve many patients and clinicians with a high quality of experience. The details on the proposed architecture and its performance evaluation is presented in Section 7.4.

7.2. Methods

The data from the 60 neurological disorder subjects in our dataset (see Chapter 4) is used for the analyses in this chapter. The subjects are divided into high fall risk (30

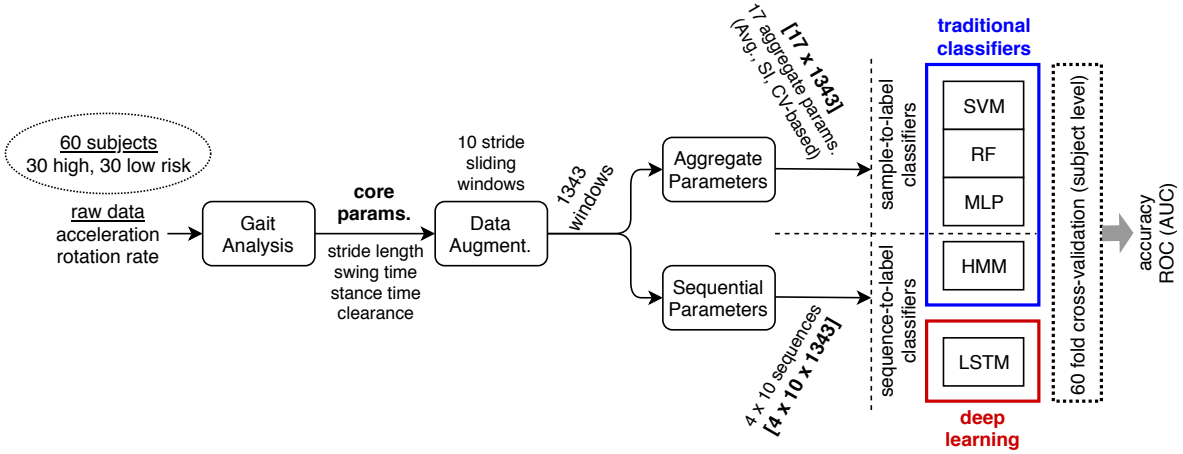


Figure 7.1. Data processing pipeline for fall risk assessment.

subjects) and low fall risk (30 subjects) categories based on their history of falls or their usage of a walking aid in daily life, which are common representatives for the ground truth of fall risk [116]. We employ the gait analysis system proposed in Chapter 5 to extract the gait parameters that will be used as input to the machine learning classifiers. A sliding window-based data augmentation approach is used to increase the number of samples and to introduce variations into the data useful for model training. The gait parameters are then transformed into either aggregated parameters or sequences depending on the input expectations of the classifier. Then, we utilize an LSTM classifier and a number of more traditional classifiers to infer fall risk. The overall data processing pipeline of our methods are illustrated in Figure 7.1. The following sections describe these methods in the same sequential order of the depicted pipeline, with the exception of the gait analysis module, which is explained in Chapter 5.

7.2.1. Data Augmentation

A sliding window-based approach is employed for data augmentation purposes. After the segmentation of strides, the time-consecutive strides are grouped to form data windows containing 10 strides (5 left, 5 right strides) each. The window is shifted 2 strides (1 left and 1 right stride) to construct the next data window. Consequently, multiple data windows can be extracted from the recording of a single subject.

The utilized data augmentation approach has several advantages. First, the total number of data samples is increased, which is a prerequisite for complex machine learning models, specifically deep learning models such as long short-term memory neural networks [117]. Second, it introduces variations for individual subjects in the data which tend to improve the generalization performance of a machine learning classifier [118]. Third, the sliding window-based approach allows frequent and real-time inferences, which is especially important for fall risk prediction to be able to make timely interventions [65]. Consequently, we were able to extract a total of 1343 windows from the data of 60 subjects. The next step is to extract features from each of these windows in a way suitable for the target classifier, so that each window is transformed into a data sample of multiple dimensions. We employ different approaches for sample-to-label and sequence-to-label classifiers, as explained in the next two sections.

7.2.2. Aggregated Gait Parameters

Sample-to-label classifiers aim to infer a single label for a single data sample. Each sample may have multiple dimensions corresponding to different features, however the dimensionality has to be kept in check to avoid overtraining issues. Therefore, we process the gait parameters belonging to individual strides in each window to come up with aggregated features.

We specifically use the parameter aggregation method detailed in Section 6.2.1. The only difference is that only the gait parameters in a window are used to extract the aggregated parameters for that window, whereas in Chapter 6, the whole data of a subject were used to come up with a single aggregated parameter set for each subject. To summarize, the parameters for the 10 strides comprising a window are averaged to produce the mean and standard deviation of a specific parameter. The standard deviation values are converted to coefficients of variation (CV), by normalizing them with their respective means. The parameters belonging to five right and five left strides within a window are also averaged separately and symmetry indices (SI) are computed. As a result, we achieve a set of 17 parameters in three categories: average-

Table 7.1. Aggregated gait parameters.

Average-based	**Variation-based**	**Asymmetry-based**
avg. stride length	stride length CV	stance time SI
avg. cycle time	cycle time CV	swing time SI
avg. stance time	stance time CV	stance ratio SI
avg. swing time	swing time CV	clearance SI
avg. clearance	clearance CV	
stance ratio		
cadence		
speed		

based, variation-based and asymmetry-based. The resulting parameters are listed in Table 7.1, while their detailed definitions can be found in Table 6.1.

7.2.3. Sequential Gait Parameters

Contrary to sample-to-label classifiers, sequence-to-label classifiers such as LSTM networks can accept sequence data directly. Therefore, as an alternative to aggregated features, we also construct sequences of gait parameters. The parameters corresponding to 10 strides in a window are arranged as a sequence in chronological order, resulting in a series of parameters alternating for the left and right feet. This process is performed for four core gait parameters, *stride length*, *clearance*, *stance time* and *swing time*, hence the resulting data samples consist of four-dimensional sequences of length ten. A single sequence can capture both the temporal variations and the asymmetries in gait, since it contains elements from both different time instances and sides. This approach also do not suffer from the potential information loss in the aggregation approach. For instance, a CV parameter with a high value could be due to either the stride-to-stride variability present throughout the window, or due to a progressive deterioration. This distinction cannot be captured in a single parameter value. On the other hand, such an information is preserved in the sequence form, and a sequence-to-label classifier can make use of it to make better inferences.

7.2.4. Machine Learning Classifiers

The aim of this study is to explore the applicability of deep learning, specifically LSTM networks, for the problem of fall risk inference and to compare its performance to more traditional machine learning models. In this section, we present the details of the different classifiers employed in this study. We selected a variety of traditional classifiers with different strengths and modes of operation to ensure a comprehensive comparison study. Depending on the type of the classifier, either the aggregated or the sequential gait parameters are used as the input features. The traditional vs. deep learning classifier distinction and the type of the classifiers, namely sample-to-label or sequence-to-label, are highlighted in Figure 7.1.

The hyper-parameters of the classifiers are determined with leave-one-subject-out cross-validation, corresponding to 60 folds, where each fold is comprised of validation data from a single subject, and training data from the remaining 59 subjects. Cross-validation at the subject level is a valid and common strategy used in similar studies that have distinct data for individual subjects [119]. This approach is also beneficial to make sure that a single subject's data is not mixed into both the test and the training sets. Failing to do so could result in falsely boosted accuracies that result from learning the identity of the subjects, rather than learning the intended fall risk. The settings that give the best pooled fold classification accuracy are selected as the ultimate hyper-parameters for a specific model. For brevity, we do not present the classification results for all the different settings explored in this study; although we present the list and range of hyper-parameters we experimented with, to enable reproducibility. The results of the best performing settings are shown and discussed in Section 7.3.

7.2.4.1. Traditional Classifiers. As the traditional machine learning models, we employ three sample-to-label classifiers, namely support vector machine (SVM), random forest (RF) and multilayer perceptron (MLP); and one sequence-to-label classifier, namely hidden Markov model (HMM).

Support vector machine is a binary classifier that aims to find the optimal separating hyperplane that maximizes the margin between the two class instances [100]. Via the use of kernel functions, the data can be mapped to a higher dimensional space, which enables SVM to compute non-linear decision boundaries. We explored the linear and radial basis function (RBF) kernels, and experimented with different values of box constraint parameter (misclassification cost, commonly known as parameter C) in the range of 1–10 with increments of one. Ultimately, the RBF kernel with a box constraint value of one yielded the best accuracy. The kernel scale factor parameter is learned by the model from the training data via a heuristic procedure that uses subsampling, and hence is not manually set. The data is standardized beforehand to have a mean of zero and a standard deviation of one, for each input feature.

Random forest, i.e. bootstrap-aggregated decision trees, is essentially an ensemble of decision trees, each trained on a randomly selected portion of features and samples [98]. This approach greatly combats overtraining issues. We explored different number of trees in the range of 50–500 with increments of 50. We also experimented with the number of predictors randomly selected for each tree, for values 3–6; along with the minimum leaf size values of one to six samples. The ultimately selected model contains 100 trees, with four predictors randomly selected for each tree, having a minimum leaf size of three samples. The data is not standardized for this method, since RF does not suffer from feature scale differences.

Multilayer perceptron is a feedforward artificial neural network with at least three layers corresponding to the input layer, hidden layer(s) and the output layer. The hidden layer(s) employ activation functions to be able to capture nonlinear associations in the data, hence MLPs can compute nonlinear discriminants between classes. This model is selected to represent a shallow neural network counterpart as opposed to the employed deep learning method. The hyperbolic tangent sigmoid function (tanh) is used as the activation function in the hidden units. The scaled conjugate gradient backpropagation algorithm is used to train the network. We chose to employ a simple MLP with a single hidden layer, and did not explore deeper networks with more hidden

layers, to maintain a shallow neural network alternative. We experimented with different values of hidden units in the range of 5–20, with increments of one. The final model contains ten hidden units. We also tried different numbers of training epochs in the range of 50–100, with increments of ten, and 70 epochs yielded the best performance. The data is standardized before training.

SVM, RF and MLP are all sample-to-label classifiers that do not directly accept sequence data. Hence, the aggregated gait parameters are used as the input features for these methods. To enable a fairer comparison with the LSTM method, which is a sequence-to-sample classifier, we also train an HMM. Both LSTM and HMM are configured to operate on the same sequential gait parameters data.

Hidden Markov models are dynamic Bayesian networks which model the underlying process as a set of hidden states and visible observations. To realize sequence-to-label classification, a separate HMM is trained for each class and the likelihoods of the test sequence over these models determine the label of the sequence, i.e. the label of the most likely model is selected as the output class. In this study, we specifically employ HMMs with Gaussian mixture outputs, since the gait parameter features (corresponding to the observations in the model) are continuous and likely to be modeled better with a combination of Gaussians. We train two different HMMs corresponding to two target classes, low and high fall risk, and the labels are assigned according to the model that fits the test data best. We explored different numbers of hidden states in the range of 2–6. We experimented with mixtures of five to 15 Gaussians to model the observations, with each Gaussian limited to have a diagonal covariance matrix. Ultimately, the number of hidden states is selected to be three, and the number of observation-modeling Gaussians is selected to be ten. The expectation maximization procedure that estimates the transition and emission models was terminated after at most five iterations, although the procedure employs a convergence criteria to terminate early, in order to avoid overtraining.

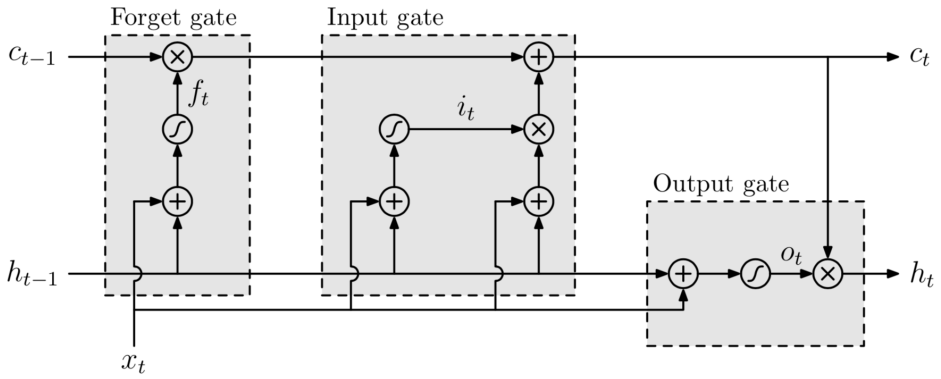


Figure 7.2. Schematic representation of an LSTM module [57].

7.2.4.2. Long Short-Term Memory Networks. LSTM networks are an extension on recurrent neural networks (RNN), featuring a memory cell that can store information on previously seen data instances [120]. The major advantage of an LSTM network over a traditional RNN with a single memory unit is that it can also remember long term dependencies within the data, using the concept of gating which regulates the information flow into and out of the memory cell. Specifically, non-linear input, output and forget gates are used to control and access the stored information [121]. LSTM networks can be used for either sequence-to-sequence classification where labels are generated for each time instance, or for sequence-to-label classification where a sequence is used to predict a single label. We use the latter mode, since we aim to estimate a single fall risk label for each data sequence window.

A schematic diagram of a recurring LSTM module is given in Figure 7.2, where x_t is the input data at time t, h_t is the output, c_t is the memory cell which is manipulated by f_t, i_t and o_t, corresponding to the forget, input and output gates, respectively.

LSTM networks are widely adopted for language modeling [122] and speech recognition [123]. More related to the topic at hand, they have recently gained popularity for gait biometrics [124], and for human action and activity recognition, either based on computer vision [125] or wearable sensors [126]. To the best of our knowledge, there is only one study in the existing literature that employs an LSTM network (or any other deep learning method) for fall risk assessment with wearable sensors [57] (details on this study can be found in Section 3.2). Therefore, in the subsequent discussions,

we will directly refer to this study to highlight the differences of our approach, and use it as a reference point for the accuracy evaluation.

For this study, we specifically use a bi-directional LSTM network, where the whole data sequence in a window is known in advance to produce a fall risk label, which is the suitable mode of operation for sequence-to-label classification. The sequential gait parameters detailed in Section 7.2.3 are used as input to the model. We employ a neural network architecture with a single LSTM module. We chose not to explore a more complex architecture, as the number of tunable hyper-parameters would increase drastically, which would be impossible to tune without overtraining issues, considering the limited size of our dataset.

The hyper-parameters we experimented with include the number of hidden units (in the range of 5–50, with increments of five), the training batch size (in the range of 50–300, with increments of 50), and the number of training epochs (in the range of 50–150, with increments of 25). The ultimate model contains ten hidden units, and is trained with a batch size of 100 sequences (windows) over 100 epochs. The Adam solver [127] is utilized for the training. The data is re-shuffled at every epoch, to avoid bias errors due to training data order.

7.2.5. Classifier Performance Evaluation

All of the classifiers are evaluated by the leave-one-subject-out cross-validation strategy, similar to the strategy used for hyper-parameter tuning. Separating the folds at the subject level prevents mixing of a subject's data into both the training and the test sets, and avoids the classifiers to learn the gait pattern of a subject rather than the intended fall risk. It should be noted that, the ideal evaluation strategy would be to have a completely separate test dataset that is not mixed with the validation set, in order to avoid learning from the test set in any way, which is reflected as the potential overfitting of the hyper-parameters in this case. However, due to the limited amount of data comprised of only 60 subjects, we could not designate a separate test set, as

that would mean losing some valuable and unique gait pathology cases in the training phase. Therefore, considering this deficiency, this study must be viewed as an initial attempt to demonstrate the potential of deep learning methods for the problem of fall risk inference, and the results presented in the next section should be interpreted with care. In the future, after we collect more data, we plan to employ a more adequate evaluation strategy with completely separate validation and test sets.

As the first classifier evaluation metric, we report accuracy, which denotes the ratio of the correct predictions over all predictions. The accuracy values are compiled for all the test data across the cross-validation folds, so that a single accuracy value can be measured for each classifier. Using solely the accuracy metric can be misleading as it may fail to capture classification biases, even though we have a fairly balanced dataset (629 low, 714 high fall risk windows). Therefore, we also compile receiver operating characteristic curves, and report area under the curve (AUC) values for each classifier.

All the methods and analyses detailed in this chapter are implemented and executed using MATLAB R2018a software [75]. We additionally employed the Bayes Net Toolbox [128], which is a Bayesian inference toolbox for MATLAB, to implement the HMM with Gaussian mixture observations.

7.3. Results & Discussion

The overall performance metrics for the fall risk classifiers are listed in Table 7.2. LSTM outperforms all other classifiers by a significant margin (accuracy of 0.890 compared to the nearest accuracy of 0.828 by HMM). The AUC values are correlated with the accuracy values, indicating that all the classifiers are fairly balanced, with the exception of SVM having a substantially lower AUC value of 0.858.

We also compiled the subject-wise accuracy values, as shown in the second column of Table 7.2, as a result of attempting to assign a single fall risk label to a subject's data collectively, rather than considering the labels of the individual samples. The majority

Table 7.2. Fall risk classifier performance results.

	Accuracy	**Subject Accuracy**	**AUC**
SVM	0.795	0.833	0.858
RF	0.806	0.800	0.894
MLP	0.821	0.883	0.904
HMM	0.828	0.867	0.912
LSTM	0.890	0.900	0.943

of the sample labels of a subject is selected to be the subject's fall risk label. LSTM outperforms the other classifiers considering this metric as well, correctly classifying 54 subjects out of 60, but HMM and MLP offer competing performances.

The subject-wise classification performances of the classifiers are listed in Table 7.3. The ID column references the subject identifiers listed in Chapter 4. The check marks indicate that the classifier was successful in correctly labeling a specific subject, while the cross marks indicate failure. Subjects 38, 51 and 59 were misclassified by all the classifiers. Subject 38 is a DLB patient with a low fall risk label, but exhibits many pathological gait symptoms, including a low average clearance value of 3.4 cm, a clearance symmetry index of 0.38 indicating high asymmetry and a low average stride length value of 0.69 meters. Similarly, Subject 59, who is a Hemiparesis patient, also has considerable gait abnormalities, including a low average clearance value of 4.3 cm and a stance ratio value of 0.65, albeit being labeled as a low risk subject. The fact that these patients do not have a history of falls may be due to the relative immobility and carefulness of the patients, as determined by the clinical investigation. So, these patients may in fact be high risk subjects.

On the other hand, Subject 51 is a high fall risk subject who is misclassified as low risk. This patient exhibits many gait abnormalities; however his gait is mostly left-right symmetric, which may have been learned by the classifiers as an essential fall risk indicator based on other high risk cases. We did not detect any other anomalies that could explain why this patient was consistently misclassified.

Table 7.3. Subject-wise classification analysis of fall risk classifiers.

Low Fall Risk Subjects						**High Fall Risk Subjects**					
ID	**SVM**	**RF**	**MLP**	**HMM**	**LSTM**	**ID**	**SVM**	**RF**	**MLP**	**HMM**	**LSTM**
1	✓	✓	✓	✓	✓	3	✗	✗	✗	✗	✓
2	✓	✓	✓	✓	✓	4	✓	✓	✓	✓	✓
9	✓	✓	✓	✓	✓	5	✓	✓	✓	✗	✓
10	✗	✗	✓	✓	✓	6	✓	✓	✓	✓	✓
12	✓	✓	✓	✓	✓	7	✓	✓	✓	✓	✓
15	✗	✗	✓	✓	✓	8	✓	✓	✓	✓	✓
17	✓	✓	✓	✓	✓	11	✓	✓	✓	✓	✓
18	✓	✓	✓	✓	✓	13	✓	✓	✓	✓	✓
22	✓	✓	✓	✓	✓	14	✓	✓	✓	✓	✓
23	✓	✓	✓	✓	✓	16	✓	✓	✓	✓	✓
25	✓	✓	✓	✓	✓	19	✓	✓	✓	✓	✓
26	✗	✓	✗	✓	✓	20	✓	✗	✓	✓	✓
27	✓	✓	✓	✓	✓	21	✓	✓	✓	✓	✓
33	✓	✓	✓	✓	✓	24	✓	✓	✓	✓	✓
34	✗	✗	✓	✓	✗	28	✓	✓	✓	✓	✓
35	✓	✓	✓	✓	✓	29	✓	✓	✓	✓	✓
36	✓	✓	✓	✓	✓	30	✓	✓	✓	✓	✓
37	✓	✓	✓	✓	✓	31	✓	✓	✓	✓	✓
38	✗	✗	✗	✗	✗	32	✓	✓	✓	✓	✓
40	✓	✓	✓	✓	✓	39	✓	✓	✓	✓	✓
41	✗	✗	✗	✗	✓	42	✓	✓	✓	✓	✓
44	✓	✓	✓	✓	✓	43	✓	✓	✓	✓	✓
45	✓	✓	✓	✓	✓	47	✓	✓	✓	✓	✓
46	✓	✓	✓	✓	✓	49	✓	✗	✗	✗	✗
48	✓	✓	✓	✓	✓	50	✓	✗	✓	✓	✓
53	✓	✓	✓	✓	✓	51	✗	✗	✗	✗	✗
56	✓	✓	✓	✓	✓	52	✓	✓	✓	✓	✓
57	✓	✓	✓	✓	✓	54	✗	✓	✓	✓	✓
59	✗	✗	✗	✗	✗	55	✓	✓	✓	✓	✓
60	✓	✓	✓	✓	✓	58	✓	✗	✓	✗	✗



Figure 7.3. Confusion matrices for fall risk classifiers, (a) SVM, (b) RF, (c) MLP, (d) HMM, (e) LSTM.

The cases that were mostly misclassified by the sample-to-label classifiers, but were correctly classified by both of the sequence-to-label classifiers include subjects 10, 15 and 26, which highlight the power of dynamic models. On the contrary, Subject 58 was classified correctly by SVM and MLP, while HMM and LSTM were not successful.

To enable an in-depth look at the individual sample-wise performance of the classifiers, their confusion matrices are presented in Figure 7.3, which are based on the pooled test inferences across the folds. SVM has a tendency towards classifying instances as high risk, as apparent from the number of instances predicted for each class. As a result of this bias, SVM's high risk classification accuracy (85.2%) is significantly higher than its low risk classification accuracy (73.1%). None of the other classifiers exhibit such a substantial balance problem. LSTM, having the highest accuracy and AUC values, is also fairly balanced, making it superior in this respect as well.

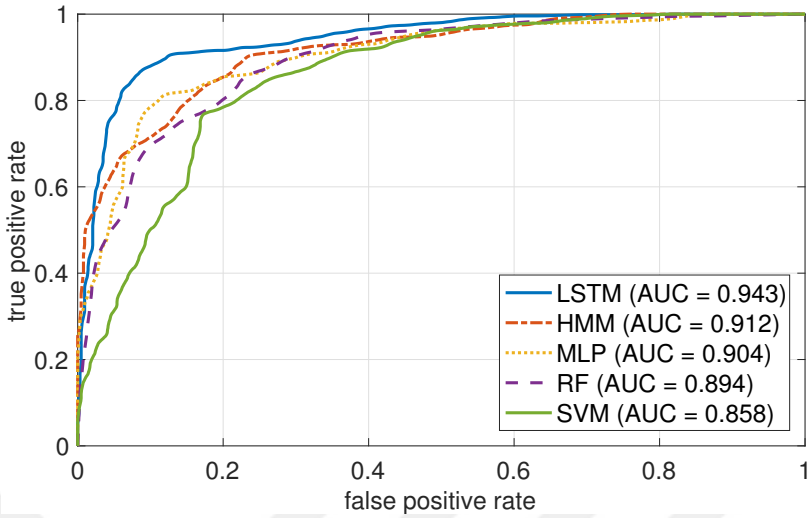


Figure 7.4. ROC curves for fall risk classifiers.

To alleviate the balance issues of the SVM classifier, we also experimented with different values of the misclassification cost hyper-parameter. With the cost of misclassifying a low risk instance as high risk set to twice as high as vice versa, the bias is mostly mitigated (high risk accuracy of 81.2% vs. low risk accuracy of 76.3%), however the overall accuracy drops to 78.9%. It should be noted that, even if such a cost adjustment had proved to be beneficial, one should be wary of making this adjustment, since misclassifying a high risk patient as low risk is more dangerous than the opposite case. Failing to spot a high fall risk condition could have serious health ramifications, whereas misclassifying a low risk patient as high risk would merely result in unnecessary precautions and interventions.

The ROC curves are presented in Figure 7.4, further demonstrating the balance characteristics of the classifiers. The positive class corresponds to the high fall risk class. SVM's deficiency is also apparent here, while LSTM demonstrates a superior performance, with an ROC curve well above the other classifiers. HMM and MLP exhibit similar performances while they are slightly better than the RF classifier, as also indicated by the accuracy and AUC values. MLP's higher accuracy and AUC values compared to the other sample-to-label classifiers, namely SVM and RF, show that artificial neural networks are indeed viable for the problem of fall risk assessment.

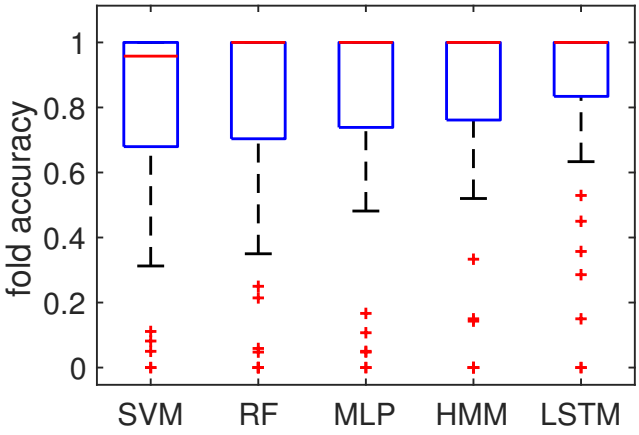


Figure 7.5. Box plots for fall risk classifier fold accuracies.

HMM and LSTM, which are sequence-to-label classifiers, perform at least as good as the sample-to-label classifiers, which indicates that preserving the sequence of gait parameters for the individual strides is beneficial for the classification performance. Even though the aggregate gait parameters attempt to store the temporal variation and left-right asymmetry related information via CV and SI parameters, they are apparently not sufficient to capture the factors leading to fall risk. The superiority of LSTM is not solely explained by this observation though, since it still outperforms HMM. This observation proves that deep learning methods, specifically LSTM networks, are indeed applicable to the problem of fall risk assessment.

To demonstrate and compare the fold-wise accuracies of the classifiers, we also compiled box plots to show the distributions of the fold accuracies, presented in Figure 7.5. The box plots are helpful to show whether the performance of a classifier is consistent across the folds, and whether the overall accuracy is the result of a stable performance or a few lucky folds. The LSTM classifier indeed demonstrates a stable performance with minimal fold-wise variation. The interquartile ranges denoted by the blue boxes agree with the overall accuracy values of the classifiers, as they also tend to shrink with increasing accuracy.

To quantify the fold-wise performance differences between two classifiers, we also utilized the Wilcoxon signed rank test, which is a nonparametric statistical significance

test for paired observations. It is suitable for fold-wise accuracy comparison [129], since the individual fold accuracies are indeed paired (the i-th fold of a classifier exactly corresponds to the i-th fold of another classifier), and the distributions tend to deviate from the Gaussian, since the maximum accuracy is naturally limited to 1.0. The tests show that LSTM is significantly better than all the other classifiers ($p < 0.05$), while the other classifiers do not exhibit a significant difference among themselves.

To the best of our knowledge, as of 2018, the only fall risk assessment study that utilizes deep learning methods is conducted by Nait Aicha et al. [57]. The authors directly use the raw acceleration data as input to the LSTM classifier, and do not attempt to extract any gait parameters or features as a pre-processing step. Apart from a pure LSTM architecture, they also experimented with a neural network consisting of an LSTM layer combined with a convolutional neural network layer (CNN), but did not observe any accuracy improvement, albeit some training time reduction thanks to the weight sharing imposed by the CNN. Ultimately, they were able to achieve an AUC value of 0.75 (the authors only report AUC values as the classifier performance metric).

Theoretically, deep learning methods such as LSTM networks do indeed have the power to infer domain knowledge automatically from the raw data, hence alleviating the need for feature engineering, provided there are sufficient data and the network architecture is complex/deep enough [115]. Similar to [57], using raw data directly was indeed our initial attempt at the problem of fall risk inference, as we utilized a two-layer LSTM network with 100 and 20 hidden units, respectively. We achieved an AUC value of 0.70, comparable to the value of 0.75 reported by Nait Aicha et al. Considering the much superior performance of our ultimate approach (AUC = 0.943), which utilizes sequential gait parameters as input, it is observed that incorporating the domain knowledge in the input features is invaluable for the problem of fall risk assessment. So, in practice, raw data proved to be not sufficient to achieve high classification accuracy, even for the deep learning methods. Our findings show that the domain knowledge inherent in the spatio-temporal parameters well-adopted by the medical community can be combined with the sophisticated methods of the computer science domain.

Another important experimentation setting evaluated by Nait Aicha et al. is splitting the training and test data randomly at the sample level, i.e. allowing the data of a subject to mix into both sets. A high AUC value of 0.94 is achieved via this setting; however, the authors argue that this is due to the model learning the identity of the subjects rather than the characteristics leading to fall risk. Indeed, when we experimented with randomly selected cross-validation folds at the sample level, we also observed a high AUC value of 0.961. The substantial performance increase associated with cross-set mixing confirms the reasoning of Nait Aicha et al., showing that this strategy is not viable to come up with a model that can operate equally well on data from unseen subjects. This finding also confirms the validity of our approach in determining cross-validation folds at the subject level, strictly preventing cross-set mixing. As a side note, the success of LSTM in identifying subjects hints at the applicability of inertial gait data for biometrics. However, we did not further pursue this objective since it is not in the scope of this thesis.

7.4. Fall Risk Assessment as a Pervasive Healthcare Service

In this section, we explore how the proposed fall risk assessment methods can be realized as a pervasive healthcare service. We propose a computing and communication architecture that can effectively carry out the healthcare routines that typically operate on the sensor data collected from wearable devices, in real life settings. The continuous fall risk assessment service is selected as the main use case; however, the proposed architecture can be employed for many similar pervasive healthcare applications.

With the advances in wearable devices and smart gadgets, pervasive healthcare applications have gained the means to become an integral part of daily life. The available applications include physical exercise assistants, sleep trackers and stress detectors, all aiming to give continuous feedback to their users for a healthier lifestyle. While smart watches and bracelets, with their onboard sensors, provide a convenient platform for ordinary users to track their own wellbeing; more specialized healthcare-dedicated sensors grant the clinicians the ability to remotely monitor their patients in

a quantified and objective manner. Fall risk assessment is a good example of such a remote patient monitoring application.

The spectrum of these services raises some requirements that need to be fulfilled. Conducting experiments and performing analyses in a laboratory environment is immensely different from the conditions on the field. Huge amounts of data are generated by the wearable sensors, but analyzing and turning all of them into relevant indicators of wellbeing is difficult. This is mostly due to the insufficient computation capabilities, limited storage capacity and battery constraints of the end-user devices. Even though the small form factor devices have become more powerful than ever, their performance is still unsatisfactory to execute all of the required healthcare service routines, as the complexity of the relevant algorithms also increases. Some healthcare services are time sensitive, requiring quick interventions depending on the health status of the patient, further escalating the computational requirements. The devices constantly generate health data that need to be stored for continuous and history-aware health analysis and the data collected from multiple tenants need to be adjoined to further increase the accuracy (e.g., retraining a machine learning model with new users' data), which necessitate a more central computation entity. Moreover, realizing the daily scenarios of healthcare services on the device quickly drains the limited available energy, restricts the mobility of the end-user and eventually deteriorates the overall usability. This problem may also disrupt the continuous monitoring of the patients by the medical experts and causes loss of critical medical data. Compromises can be made by utilizing simpler algorithms that respect these constraints, however the inference accuracy is bound to decline in return, which would render many healthcare applications inadequate.

All of these requirements necessitate a computation and communication architecture that can efficiently serve the specific needs of a healthcare application. A potential solution is cloud computing data centers. Even though they have powerful resources which are always available on-demand, offloading healthcare tasks to remote cloud servers may result in indefinite latencies due to wide area network (WAN) access. A relevant trend that provides a quick and efficient fix is edge computing [130], in which

computational resources are brought to the proximity of the end-users where the services are actually consumed. Edge computing is effective especially in the cases where accessing the cloud resources imposes a heavy burden on the system performance in terms of time sensitivity. The main mechanism for exploiting the edge computing resources is code offloading [131], where user devices delegate unit computational tasks to the edge servers. Employing the edge computing approach alone does not suffice for the overall seamless operation of the system. The distributed form of the edge servers may be inadequate in certain cases, while a centralized cloud infrastructure may take the responsibility of orchestrating the global environment effortlessly, such as distributing the improved version of a machine learning model, or maintaining long term data repositories.

The existing studies that utilize the edge computing paradigm for the healthcare domain include [132], which examines the applicability of edge servers as gateways between the cloud servers and body sensor networks, [133], which proposes a fall detection service executed on the edge, and [134], which introduces a wearable sensor-based activity recognition service exploiting edge servers. In [135, 136], the cooperation of edge servers and internet of things (IoT) devices are explored, which can serve as foundations for healthcare services. Even though these studies explore various aspects of possible healthcare service architectures, a complete multi-tier solution, that is flexible enough to be applicable for a variety of applications is still not achieved. Furthermore, the proposals usually remain to be proof-of-concept designs, and they are not tested and validated with realistic use cases and real data.

To address these challenging aspects, we propose a multi-tier computation and communication architecture. While the cloud servers are utilized for delay-tolerant and resource-hungry tasks such as improving the model and the long-term storage of the personal health records, the edge servers are utilized for executing the routines of the healthcare service itself. We may still benefit from mobile devices for simple operations such as pre-processing the raw sensory data, even though they are operating within restraining conditions. Software-defined networking (SDN) is a candidate solution for

administrating the complex internal operations within the network and orchestrating different resource layers. It separates the control plane from the data plane composed of the forwarding devices and concentrate the main logic on a software-based controller [137]. By making the networking resources programmable, the overall system performance can be improved with an effective and flexible resource allocation scheme.

Continuous fall risk assessment using wearable inertial sensors is a service that can benefit greatly from the edge computing aspect of the multi-tier architecture, since it requires near real-time analysis. The clinicians or caregivers should be alerted to any deviations promptly, to make timely interceptions possible. Access to the patient records history is also important, since fall risk is tightly related to changes in gait and motor functions over time. The long-term storage deems a central and reliable entity such as the cloud, while the short-term data could be stored on the edge to enable time-window analysis which is crucial for typical gait analysis implementations. Considering these properties, a fall risk assessment service can serve as a realistic use case to validate the applicability of the proposed architecture. The contributions and highlights of our work are summarized as follows:

- We propose a multi-tier architecture with both cloud and edge servers, which are orchestrated by a northbound SDN application that utilizes a novel load balancing algorithm to increase the quality of experience by minimizing service delays.
- The proposed architecture not only performs load balancing among the edge servers, but also distributes the submodules of a healthcare service pipeline across different tiers based on their individual requirements.
- The performance of the multi-tier architecture is evaluated in an emulation environment with the continuous fall risk assessment use case. The service is implemented and tested with real data from our dataset.

In the next section, we present the details of the multi-tier architecture. In Section 7.4.2, we show the performance evaluation results of the emulation study, compiled via the execution of the fall risk assessment service on the proposed architecture.

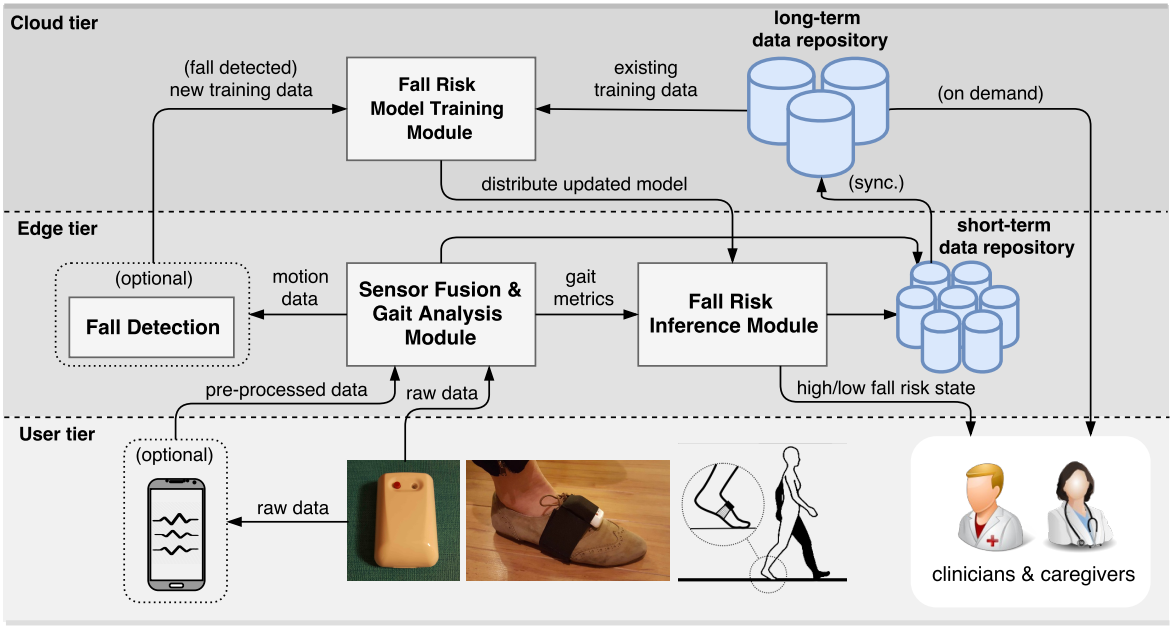


Figure 7.6. Multi-tier fall risk assessment service architecture.

7.4.1. Multi-Tier Computing and Communication Architecture

7.4.1.1. Fall Risk Assessment Service Architecture Overview. To facilitate a pervasive fall risk assessment service, we propose a multi-tier architecture that consists of edge, cloud and end-user device layers, depicted in Figure 7.6. The data collection, pre-processing and fall risk inference functionalities are distributed across multiple layers to ensure the best adaptation to the requirements and attain a high performance, both inference accuracy and network-wise.

Today's wearable sensors are typically empowered by wireless communication technologies, thus having the capability to directly interface with a variety of edge devices. For instance, the sensors used in our study (details presented in Chapter 4) are Bluetooth-enabled. Depending on the environment, the sensors may either transmit directly to the edge servers (such as Raspberry Pi computers equipped with Bluetooth dongles) or relay their data to the edge through a smartphone. In healthcare dedicated environments like hospitals, the former approach is viable, while in locations where direct connectivity with an edge server may not be possible, like in a house environment or outdoors, smartphones could be used to manage sensor-to-edge connectivity. Smartphones could further be facilitated to handle some portion of the data pre-processing;

however, it should be noted that smartphones are battery-constrained devices, thus the amount of delegated computation should be restrained accordingly.

After the sensor data reaches the edge, it is processed and stored. The data processing includes two stages that are executed for each user: Extraction of spatio-temporal gait parameters and fall risk classification using the parameters as input. In case of an escalation in the fall risk state of the user, the care-givers, clinicians or the relatives should be notified immediately to make timely interventions possible. The time-sensitive nature of fall risk assessment renders the edge as a suitable location to carry out the actual decision making.

The personal data of each subject should be stored on the edge for a few reasons. First, the sensory data history of the users is used to construct data windows, over which the parameters related to changes in gait and short-term trends are estimated. Second, the long-term history of extracted parameters and the inferred fall risk status of a user should be made accessible to the clinicians on demand, since it could guide continual interventions such as medication adjustment. Lastly, the stored data could later be used to improve the fall risk inference model, depending on the presence or absence of falls in the user's history. An example scenario is adding the historical data of a subject to the training dataset with the label of high risk, upon detection of a fall. Such additions to the training data require the retraining of the machine learning model. After the model is improved, it should be distributed to the edge servers with active users, in order to increase the service quality for all the users in system. Both of these steps are handled and orchestrated by the cloud due to its central position and superior capabilities. The cloud also maintains the long-term data repositories, to enable on-demand access by the clinicians.

7.4.1.2. SDN Control Plane Components and Northbound Application. The overall infrastructure, with the healthcare services deployed throughout different tiers, is controlled and orchestrated by the SDN control plane with the cooperation of northbound applications that can be customized according to the requirements of the managed

environment. The typical SDN design is organized in three different levels: data (forwarding) plane, control plane and application plane. While the forwarding plane is composed of typical networking devices without any logic implemented, the logically centralized control plane is responsible for orchestrating the underlying infrastructure. On top of these, the application plane implements the behavior of the network, and defines customized policies for the effective and reliable management of the network.

A northbound application implemented by the operators, ISPs or third-party developers can communicate with the SDN controller via the northbound API implemented by the controller itself. The instructions and policies defined by the northbound application are transferred to the controller through this interface. The received information is then translated into OpenFlow messages [137] by the controller and sent through the southbound interface to the forwarding plane.

One of the contributions of this work is the implementation of a northbound application to enable autonomous management of the resources in the network for healthcare services. The application is implemented through the Python API provided by Ryu SDN controller [138]. Its main functionalities include service discovery, topology discovery, resource allocation and load balancing. It should be noted that, the implemented application is capable of handling multiple types of healthcare services deployed on the architecture concurrently, even though our fall risk assessment use case includes only one service.

Considering the default operations of SDN, whenever an unmatched packet arrives at an OpenFlow-enabled switch, it is forwarded to the controller for the decision of a further action, in the form of an `OFPT_PACKET_IN` message. The northbound application receives a copy of the packet buffered at the switch and inspects the header fields. The algorithm determines the type of the requested service through extracting the information of destination TCP port number. In our design, each healthcare application is served through a unique TCP port number and service-oriented access is enabled without leaving the responsibility of service discovery to the user devices.

After determining the requested healthcare service, the load balancing procedure is invoked. First, the set of possible destinations that are ready to execute the routines of the requested service is retrieved. From the resulting set of the destination servers, the algorithm attempts to select one of the less-loaded servers in order to minimize the overall service delay. In order to achieve this, a separate thread in the application periodically retrieves and stores the recent CPU load information of the servers. The load balancing algorithm inspects the CPU loads information and selects one of the servers randomly according to the probability value calculated as

$$p_s(t) = \frac{\frac{\sum_s \alpha_s(t) - \alpha_s(t-1)}{\alpha_s(t) - \alpha_s(t-1)}}{\sum_s \frac{\sum_s \alpha_s(t) - \alpha_s(t-1)}{\alpha_s(t) - \alpha_s(t-1)}} \tag{7.1}$$

where $p_s(t)$ represents the probability of selecting server s for the offloading operation at time t and $\alpha_s(t)$ depicts the CPU load of server s at time t.

Following the destination server decision phase, the northbound application generates the necessary instructions for modifying the destination MAC and IP address fields of the packet, in order to route the request to the destined location properly. Since the northbound application has a topology learning module and updates the view of topology frequently, routing information is also ready to be generated by the controller. The effectiveness of the routing information can be enhanced by retrieving the network load information through OpenFlow messages.

The controller prepares the set of matching fields and list of actions to be applied on the request packet. This information is converted into `OFPT_FLOW_MOD` OpenFlow message to be added as a new entry to the flow rule table of the switch, that is awaiting for a directive to process the incoming request packet. The structure of the message is composed of the following variables:

- Hard Timeout = c seconds
- Matching Fields = [(destination TCP port = TCP port number for the requested service), (source IP address = IP address of the client requesting the service)]

- Priority = 50000 (maximum priority value)
- Actions = [(modify destination IP address), (modify destination MAC address), (physical output port)]

The hard timeout parameter controls the expiration of the flow rule, determining when it is deleted from the switch's flow table. For instance, if the hard timeout value is 60 seconds for a flow rule, the requests of a specific end-user are assigned to the same server for 60 seconds. After the flow rule is deleted for that source end-user device, the load balancing algorithm is re-triggered and the destination server is determined again in order to reallocate resources for the subsequent requests generated by that end-user.

The installed flow rule includes two matching fields: source IP address and destination TCP port number. If a packet is generated from the same client requesting the same service, it matches the generated flow rule and it is processed without consulting to the controller. The actions to be applied on the matching packets include modifying the packet's destination MAC address and IP address, and forwarding the packet through the specified physical port number. Also, the priority is set to its maximum value in order to eliminate the other matching flow rules, if there are any.

Similarly, another `OFPT_FLOW_MOD` message is sent to the corresponding switch to construct the reverse path routing from the server to the end-user. The northbound application is configured to manage TCP traffic streams, since reliability, sequence of messages and minimizing packet losses are key requirements for typical healthcare services. Therefore, to transmit the acknowledgement packets from the server to the end-user, the corresponding flow rule is installed with the same hard timeout value.

It should be noted that the `OFPT_FLOW_MOD` message does not apply to the packet that is already buffered at the switch, waiting for an action. Since the buffered packet did not match any flow rule yet, the recently installed flow rule does not affect its state. In order to apply the same operations on this packet, an `OFPT_PACKET_OUT` message is sent to the switch with the same set of variables.

7.4.2. Performance Evaluation in an Emulation Environment

To assess the viability of the proposed architecture, and to evaluate its performance under realistic conditions, we designed an experimental protocol that combines a real healthcare service (i.e. a fall risk assessment service) operating on real patients' data and an emulation framework that uses this data to measure various networking/operation metrics. In this section, we present the details of our experimental protocol and the performance evaluation results. We specifically describe the emulation environment, and explain how we use the collected fall risk data to achieve a realistic use case scenario. The network topology, parameters and the methods that are employed to extract the performance metrics are additionally explained.

7.4.2.1. Multi-Tier Network Emulation. The proposed system is implemented and executed on the Mininet [139] emulation environment, which is configured on a computer with Intel Core i7-6700K CPU, and 16GB DDR4 main memory. Ryu SDN controller [138] is selected as the main control plane mechanism due to its support for recent versions of OpenFlow and flexible northbound API in Python. The northbound application is implemented through this API and designed in compliance with the OpenFlow v1.3 specification body [140]. In the Mininet environment, Open vSwitch (OVS) [141] is used as the data plane elements.

In Figure 7.7, the network topology implemented on Mininet is depicted. There are three different locations, each of which has a different number of users positioned to consume the fall risk assessment service. There are seven different cases utilized for assessing the scalability of the proposed systems in terms of the supported number of users at the edge: 1, 5, 10, 20, 30, 40 and 50. The number of users per location for each scenario is presented in Table 7.4.

The fall risk assessment pipeline (depicted as the edge tier in Figure 7.6) is installed on each edge server. The pipeline includes the gait analysis module described in Chapter 5 and the fall risk inference methods presented in Section 7.2. The Mininet

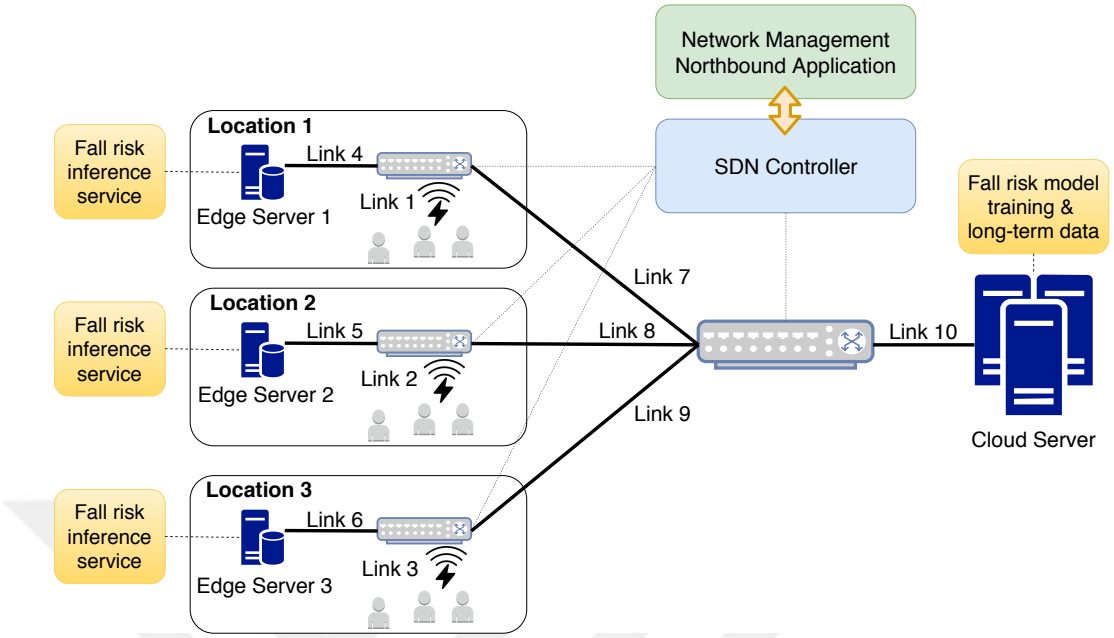


Figure 7.7. Emulation topology of multi-tier architecture.

environment is configured to have one server at each location. On top of the edge tier, a cloud server is positioned to execute the fall risk model training routines when requested. All of the servers in the Mininet environment are created and deployed as CPU limited hosts implemented by the Mininet API. The main parameters of a host are defined as the fraction of the overall system CPU and the number of cores that the created host utilizes. The cloud server is deployed as a processing unit with nearly unlimited power by letting it use the whole processing capacity of the physical machine. The edge servers are less capable in terms of processing power, and so the CPU fraction of each edge server is set to 20% of the physical machine.

In addition to the capacities of the computation resources, the individual properties of the network links are also configurable by Mininet. Similar to the host configurations, the network link parameters are adjusted in accordance with real networking conditions. For instance, the bandwidth is high and the propagation delay is small at the edge of the network. On the other hand, access to the cloud tier is restricted in terms of bandwidth and the propagation delay is higher. The links 1, 2 and 3 emulate typical 802.11n wireless connections and according to the calculation of the average throughput in a typical indoor environment, the bandwidth of these links is configured

Table 7.4. Number of users in emulation scenario locations.

Total Number of Users	**Location 1**	**Location 2**	**Location 3**
1 user	1 user	-	-
5 users	3 users	1 user	1 user
10 users	5 users	3 users	2 users
20 users	8 users	7 users	5 users
30 users	12 users	10 users	8 users
40 users	17 users	13 users	10 users
50 users	25 users	10 users	15 users

to support 200 Mbps data rate. The links 4-9 are operating within the LAN and they are configured to emulate Gigabit Ethernet (1 Gbps). The typical propagation delays across the LAN are almost negligible, hence the propagation delay for these links is set to a low value of 5 ms. Along with these characteristics, link 10 is configured to emulate the real WAN access to communicate with the cloud data centers. Since the Internet is congested and the data rate through the WAN is much lower than the edge of the network, the bandwidth is set to a lower rate (100 Mbps) and the propagation delay between the end-users and the remote cloud servers is set to 250 ms.

The real sensor data selected from our dataset are replayed in Mininet hosts to emulate traffic generation and service request patterns. The sensor sampling frequency is 100 Hz for each sensor, which corresponds to 200 Hz data generation by each user, considering two sensors (one per foot). Each user bundles and transmits one-second-long sensor data in a single message, i.e. each user generates one message per second. In the emulation scenario, the traffic generation of each user lasts for a random duration, according to a uniform distribution between 1-3 minutes, where each user starts 20 seconds after the preceding user, emulating varying loads throughout the scenario.

After receiving the data from the users, a server executes the fall risk assessment routines, by extracting the sensor data bundled in the messages. Since the sequence of the sensor data is important in terms of the fall risk analysis accuracy and the service

is intolerant to any packet loss, TCP is selected as the main transport layer protocol.

In order to evaluate the performance of the multi-tier architecture with SDN as the main orchestration mechanism, the following operation modes are compared: (1) multi-tier with load balancing, (2) multi-tier without load balancing, and (3) only cloud. The multi-tier with load balancing approach exploits the functionality provided by the SDN-based northbound application implementation presented in the previous section. The northbound application tries to minimize the overall service delay by distributing the load among the edge servers. The second approach disables the load balancing algorithm, minimizes the involvement of the SDN control plane and allocates the computation resource that is closest to the end-user. In other words, the requests of the end-users are directly forwarded to the edge servers in the vicinity without any SDN controller functionality except the forwarding and routing logic. Lastly, the more traditional only cloud approach is evaluated to determine the performance when all of the requests are offloaded to the powerful cloud server through a congested network.

Each scenario is repeated 10 times. A single execution takes 15 minutes on the average, including the start-up delay for traffic generation and the standby period to ensure the completion of requests in case of packet retransmissions.

7.4.2.2. Performance Evaluation Results. In Figure 7.8, the proposed multi-tier architecture with load balancing is analyzed in terms of the overall service delay, with varying number of end-users and requests. This scenario illustrates the intermittent monitoring of the patients where each user generates a varying number of requests during the experiments. The multi-tier architecture with load balancing provides the best performance among all. While the only cloud approach provides the same quality of service independent from the traffic load, the multi-tier architecture without load balancing performs the worst in terms of service delay. It should be noted that the y-axis of the figure is in logarithmic scale because the average service delay of multi-tier structure without load balancing with 50 clients is more than 11 seconds. In order to enhance the resolution of the results and demonstrate the differences between each

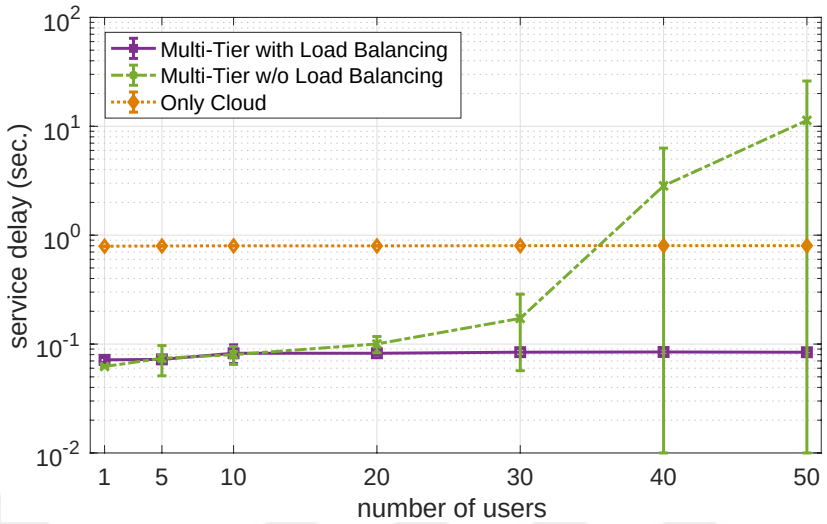


Figure 7.8. Performance comparison of multi-tier approaches.

approach clearly, the service delay is shown in the logarithmic scale.

The main causes of this result is analyzed in Figure 7.9, in the form of delay breakdowns. The contributors of the overall service delay are shown separately for evaluating the performance indicators. The execution delay for the approach where the requests are always offloaded to the cloud tier is almost negligible compared to the network delay, hence the execution delay of the only cloud approach is omitted in Figure 7.9. This is due to the superior computational capabilities of the cloud server. Almost all of the delay is caused by the network delay due to WAN access. On the other hand, when the multi-tier architecture with load balancing approach is inspected, it is apparent that the dominant factor for the overall service delay is again the network delay. Since the load among the computation resources is distributed fairly, the execution delay does not vary much with the changing number of end-users. For the scenario where the load balancing is inactive, as the number of users and the fall risk service requests increase, both the execution and network delay also increase. It can be deduced that both the computation and network resources become congested when the requests are directly assigned to the closest edge server.

In general, it can be argued that edge computing has a potential for providing latency-intolerant services with higher performance. However, considering the scala-

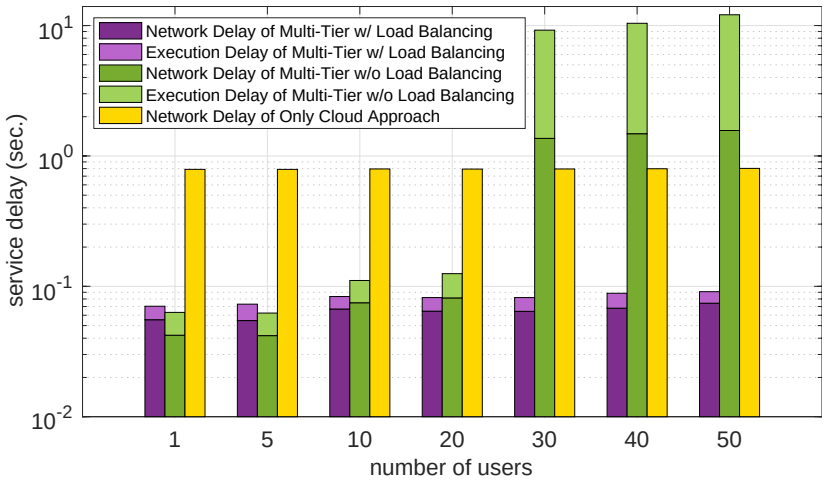


Figure 7.9. Contribution of network and execution conditions in overall delay.

bility issues, it becomes insufficient by itself to meet the requirements of the end-users and healthcare applications without an effective network management entity and a load balancing approach. According to the results depicted in Figure 7.8, the edge tier is capable of assuring the low latency requirement of the fall risk assessment service for a range of different settings. However, once the number of offloaded tasks reaches a certain point, the limited processing capability of the edge servers can no longer accommodate the incoming tasks as desired. Compared to the powerful resources of the cloud tier, the increasing number of service requests results in a scalability problem at the edge, which directly degrades the overall performance of the system. The proposed load balancing approach distributes the offloaded tasks fairly and increases the scalability, as demonstrated by the results.

7.5. Conclusion

In this chapter, we explored the applicability of deep learning to achieve an automated fall risk assessment system. As opposed to the common deep learning approach that favors using the raw data directly as input, we transformed the spatio-temporal gait parameters extracted by our gait analysis system into sequences that can be fed into an LSTM classifier, thus preserving the domain knowledge inherent in the gait parameters. The classification results are encouraging, with an AUC value of 0.943 achieved for our dataset of 60 neurological disorder patients. It should be noted that,

all of the subjects used for this study have some form of gait abnormalities, hence sifting out the pathological gait factors that specifically lead to increased risk of falls is quite challenging. The superior performance of LSTM compared to the more traditional classifiers also show that deep learning methods do indeed have great potential for the problem of fall risk assessment.

We also proposed a computing and communication architecture that can efficiently facilitate pervasive healthcare applications like fall risk assessment. The edge computing paradigm helps to bring the healthcare service routines closer to the users that actually consume them, while the SDN-based load balancing algorithm further helps to reduce service delays. The performance of the architecture is evaluated in an emulation environment with the proposed fall risk assessment system as the use case. Further details of the proposed system and extended performance evaluation results with various other emulation scenarios are published in [112].

The automated fall risk assessment system and its demonstration as a pervasive healthcare service running on an efficient computing architecture exhibit how wearable sensor technologies can be used in real life settings for challenging healthcare problems. The fall risk assessment service also showcases the importance of gait analysis for remote patient monitoring, which is a key objective of this thesis.

8. CONCLUSION

In this thesis, we concentrated on wearable inertial sensors to facilitate a pervasive gait analysis solution. We also demonstrated how the output of such a system can be used for a high level inference objective, namely automated fall risk assessment. This thesis is a step towards achieving a highly-accessible and pervasive gait analysis-based healthcare application usable in non-hospital settings.

One of the primary contributions of this thesis is the gait dataset collected from more than 60 neurological disorder patients. Data collection is always challenging, as finding patients that meet the inclusion criteria is difficult, and unforeseen technical complications may invalidate the already collected data. Converging on the correct data collection procedure requires spending substantial time on the field to assess the real conditions and may also require subsequent changes as modifications and improvements are made to the analysis methods. Even if the perfect procedure is achieved, it may rarely be executed perfectly, leading to sensor placement errors, timing and synchronization problems, and insufficient data to facilitate meaningful analyses. Our own data collection experiences influenced the gait analysis methods proposed in this thesis, as we attempted to formulate approaches adaptive to such errors.

The data collection challenges motivated us to create a robust inertial sensor-based gait analysis system, which is the most important contribution of this thesis. We built upon the Kalman filtering and zero-velocity phase detection techniques of the state-of-the-art, by instilling additional methods such as particle filter-based foot orientation estimation, to establish a sensor misplacement-resilient gait analysis solution. The proposed solution is capable of extracting a rich set of standard gait parameters in the spatial and temporal domains, including higher level derived features that can capture left-right asymmetries and temporal variations in gait. Another strength of our proposal is its applicability for pathological gait conditions, which have the potential to render many other existing gait analysis solutions invalid.

The majority of the existing work, especially the proposals coming from the computer science domain, usually neglect to highlight the usability of their solutions in a clinical context. The clinicians are after all the main stakeholders of a gait analysis system, as the quantification of gait problems can guide their diagnoses and treatment strategies. Therefore, in this thesis, we also provided real examples for the clinical interpretation of the results and conducted a predictor importance assessment study specifically targeted towards gait pathologies in neurological disorders. The findings validate the success of our gait analysis system and demonstrate how its output can be used for clinical purposes.

The proposed gait analysis system can identify many gait abnormalities and nuances that can be difficult to detect by sole observation. Most importantly, it can quantify these abnormalities, making objective assessments possible. Outpatient visits are usually short, giving clinicians barely enough time to recall the patient histories and perform informed assessments. Our system grants the clinicians the ability to objectively assess and track a patient's state between clinic visits, or better yet, to monitor their patients remotely thanks to the wearable sensor technology.

Even though the output of the gait analysis system may be directly used to make abnormality assessments, they can also be utilized as input features for a higher level inference problem such as fall risk assessment. In this thesis, we explored various machine learning approaches to facilitate automated fall risk inference using the spatio-temporal gait parameters as input. We obtained good results with the LSTM network classifier, outperforming the state-of-the-art accuracies. This thesis is one of the earliest works to apply deep learning methods for the problem of fall risk assessment.

Contrary to the approach of feeding raw data directly into a deep learning model, which is frequently encountered in other domains [126], we transformed the gait parameters extracted from the raw data into sequences that are suitable as input for the LSTM classifier. The domain knowledge infused in the gait parameters indeed proved to be beneficial, resulting in a significant boost in the classification accuracy. Con-

sidering the challenging nature of the problem (inferring fall risk among neurological disorder subjects, all having gait abnormalities), the results are indeed promising.

The experiments and evaluations conducted in a laboratory environment lay the groundwork for a pervasive healthcare application and establish a proof of concept, but they do not necessarily show how it will operate in a real world scenario. The most straightforward way to realize a healthcare application in the field is to execute the algorithms on the wearable devices themselves, but the limited battery and computational capabilities rarely allow it. An alternative is to use smartphones that can directly interface with the wearable sensors, however they also have similar restrictions and are not dedicated to the healthcare applications as other personal applications may be running on the device. The alternative at the other extreme is to use cloud servers, which certainly have sufficient computational resources, but the wide area network access may introduce intolerable delays. Besides, establishing the communication between the wearable devices and the cloud servers is not trivial.

To solve these problems and to demonstrate the applicability of the proposed fall risk assessment solution as a realistic pervasive healthcare service, we designed and implemented a computing and communication architecture that employs edge servers to bring the computational resources closer to the users. The different tiers in the proposed architecture are managed with the help of software-defined networking, which provides load balancing among the edge tier to further decrease service delays. The performance evaluation findings indicate that such an architecture can indeed provide a seamless execution environment for delay-sensitive wearable sensor-based healthcare services such as fall risk assessment. Even though this research direction may seem distant to the clinical scope of this thesis, we believe that it presents a good demonstration of how our contributions can be utilized in a real world setting, weaving them closer to the concept of pervasive healthcare.

Gait analysis is the gateway to many clinical applications, such as the identification of gait dysfunctions in neurological disorders and automated fall risk assessment.

This thesis has shown that wearable inertial sensors are viable candidates to facilitate gait analysis and fall risk assessment in a pervasive manner. The aging population has become a worldwide issue, rendering these healthcare problems more critical than ever. We are confident that our contributions stand out as novel solutions to these crucial problems, and we hope that they form a strong basis for future applications to come.

REFERENCES

1. Pirker, W. and R. Katzenschlager, "Gait Disorders in Adults and the Rlderly", *Wiener Klinische Wochenschrift*, Vol. 129, No. 3-4, pp. 81–95, 2017.

2. Tao, W., T. Liu, R. Zheng and H. Feng, "Gait Analysis Using Wearable Sensors", *Sensors*, Vol. 12, No. 2, pp. 2255–2283, 2012.

3. Snijders, A. H., B. P. Van De Warrenburg, N. Giladi and B. R. Bloem, "Neurological Gait Disorders in Elderly People: Clinical Approach and Classification", *The Lancet Neurology*, Vol. 6, No. 1, pp. 63–74, 2007.

4. Whittle, M. W., *Gait Analysis: An Introduction*, Butterworth-Heinemann, 2014.

5. Dadashi, F., B. Mariani, S. Rochat, C. Büla, B. Santos-Eggimann and K. Aminian, "Gait and Foot Clearance Parameters Obtained Using Shoe-Worn Inertial Sensors in a Large-Population Sample of Older Adults", *Sensors*, Vol. 14, No. 1, pp. 443–457, 2014.

6. Stolze, H., J. P. Kuhtz-Buschbeck, H. Drücke, K. Jöhnk, M. Illert and G. Deuschl, "Comparative Analysis of the Gait Disorder of Normal Pressure Hydrocephalus and Parkinson's Disease", *Journal of Neurology, Neurosurgery & Psychiatry*, Vol. 70, No. 3, pp. 289–297, 2001.

7. McIntosh, G. C., S. H. Brown, R. R. Rice and M. H. Thaut, "Rhythmic Auditory-Motor Facilitation of Gait Patterns in Patients with Parkinson's Disease.", *Journal of Neurology, Neurosurgery & Psychiatry*, Vol. 62, No. 1, pp. 22–26, 1997.

8. Nallegowda, M., U. Singh, G. Handa, M. Khanna, S. Wadhwa, S. L. Yadav, G. Kumar and M. Behari, "Role of Sensory Input and Muscle Strength in Maintenance of Balance, Gait, and Posture in Parkinson's Disease: A Pilot Study", *American Journal of Physical Medicine & Rehabilitation*, Vol. 83, No. 12, pp.

898–908, 2004.

9. Hung, T. N. and Y. S. Suh, "Inertial Sensor-Based Two Feet Motion Tracking for Gait Analysis", *Sensors*, Vol. 13, No. 5, pp. 5614–5629, 2013.

10. Ferrari, A., P. Ginis, M. Hardegger, F. Casamassima, L. Rocchi and L. Chiari, "A Mobile Kalman-Filter Based Solution for the Real-Time Estimation of Spatio-Temporal Gait Parameters", *IEEE Transactions on Neural Systems and Rehabilitation Engineering*, Vol. 24, No. 7, pp. 764–773, 2016.

11. Ghasemzadeh, H., P. Panuccio, S. Trovato, G. Fortino and R. Jafari, "Power-Aware Activity Monitoring Using Distributed Wearable Sensors", *IEEE Transactions on Human-Machine Systems*, Vol. 44, No. 4, pp. 537–544, 2014.

12. Jasiewicz, J. M., J. H. Allum, J. W. Middleton, A. Barriskill, P. Condie, B. Purcell and R. C. T. Li, "Gait Event Detection Using Linear Accelerometers or Angular Velocity Transducers in Able-Bodied and Spinal-Cord Injured Individuals", *Gait & Posture*, Vol. 24, No. 4, pp. 502–509, 2006.

13. Wang, Z. and R. Ji, "Estimate Spatial-Temporal Parameters of Human Gait Using Inertial Sensors", *IEEE International Conference on Cyber Technology in Automation, Control, and Intelligent Systems*, pp. 1883–1888, IEEE, 2015.

14. Hsu, Y.-L., P.-C. Chung, W.-H. Wang, M.-C. Pai, C.-Y. Wang, C.-W. Lin, H.-L. Wu and J.-S. Wang, "Gait and Balance Analysis for Patients with Alzheimer's Disease Using an Inertial-Sensor-Based Wearable Instrument", *IEEE Journal of Biomedical and Health Informatics*, Vol. 18, No. 6, pp. 1822–1830, 2014.

15. Salarian, A., H. Russmann, F. J. Vingerhoets, C. Dehollain, Y. Blanc, P. R. Burkhard and K. Aminian, "Gait Assessment in Parkinson's Disease: Toward an Ambulatory System for Long-Term Monitoring", *IEEE Transactions on Biomedical Engineering*, Vol. 51, No. 8, pp. 1434–1443, 2004.

16. Ferster, M. L., S. Mazilu and G. Tröster, "Gait Parameters Change Prior to Freezing in Parkinson's Disease: A Data-Driven Study with Wearable Inertial Units", *Proceedings of the 10th EAI International Conference on Body Area Networks*, BodyNets '15, pp. 159–166, ICST, Brussels, Belgium, 2015.

17. Raveendranathan, N., S. Galzarano, V. Loseu, R. Gravina, R. Giannantonio, M. Sgroi, R. Jafari and G. Fortino, "From Modeling to Implementation of Virtual Sensors in Body Sensor Networks", *IEEE Sensors Journal*, Vol. 12, No. 3, pp. 583–593, 2012.

18. Del Din, S., A. Godfrey and L. Rochester, "Validation of an Accelerometer to Quantify a Comprehensive Battery of Gait Characteristics in Healthy Older Adults and Parkinson's Disease: Toward Clinical and at Home Use", *IEEE Journal of Biomedical and Health Informatics*, Vol. 20, No. 3, pp. 838–847, 2016.

19. Panebianco, G. P., M. C. Bisi, R. Stagni and S. Fantozzi, "Analysis of the Performance of 17 Algorithms from a Systematic Review: Influence of Sensor Position, Analysed Variable and Computational Approach in Gait Timing Estimation from IMU Measurements", *Gait & Posture*, Vol. 66, pp. 76–82, 2018.

20. Bamberg, S. J. M., A. Y. Benbasat, D. M. Scarborough, D. E. Krebs and J. A. Paradiso, "Gait Analysis Using a Shoe-Integrated Wireless Sensor System", *IEEE Transactions on Information Technology in Biomedicine*, Vol. 12, No. 4, pp. 413–423, 2008.

21. González, I., J. Fontecha, R. Hervás and J. Bravo, "An Ambulatory System for Gait Monitoring Based on Wireless Sensorized Insoles", *Sensors*, Vol. 15, No. 7, pp. 16589–16613, 2015.

22. Takeda, R., G. Lisco, T. Fujisawa, L. Gastaldi, H. Tohyama and S. Tadano, "Drift Removal for Improving the Accuracy of Gait Parameters Using Wearable Sensor Systems", *Sensors*, Vol. 14, No. 12, pp. 23230–23247, 2014.

23. Hundza, S. R., W. R. Hook, C. R. Harris, S. V. Mahajan, P. A. Leslie, C. A. Spani, L. G. Spalteholz, B. J. Birch, D. T. Commandeur and N. J. Livingston, "Accurate and Reliable Gait Cycle Detection in Parkinson's Disease", *IEEE Transactions on Neural Systems and Rehabilitation Engineering*, Vol. 22, No. 1, pp. 127–137, 2014.

24. Salarian, A., P. R. Burkhard, F. J. Vingerhoets, B. M. Jolles and K. Aminian, "A Novel Approach to Reducing Number of Sensing Units for Wearable Gait Analysis Systems", *IEEE Transactions on Biomedical Engineering*, Vol. 60, No. 1, pp. 72–77, 2013.

25. Li, G., T. Liu, L. Gu, Y. Inoue, H. Ning and M. Han, "Wearable Gait Analysis System for Ambulatory Measurement of Kinematics and Kinetics", *IEEE SENSORS*, pp. 1316–1319, IEEE, 2014.

26. Chen, Y., W. Hu, Y. Yang, J. Hou and Z. Wang, "A Method to Calibrate Installation Orientation Errors of Inertial Sensors for Gait Analysis", *IEEE International Conference on Information and Automation (ICIA)*, pp. 598–603, IEEE, 2014.

27. Park, S. K. and Y. S. Suh, "A Zero Velocity Detection Algorithm Using Inertial Sensors for Pedestrian Navigation Systems", *Sensors*, Vol. 10, No. 10, pp. 9163–9178, 2010.

28. Song, M. and J. Kim, "An Ambulatory Gait Monitoring System with Activity Classification and Gait Parameter Calculation Based on a Single Foot Inertial Sensor", *IEEE Transactions on Biomedical Engineering*, Vol. 65, No. 4, pp. 885–893, 2018.

29. Anwary, A. R., H. Yu and M. Vassallo, "An Automatic Gait Feature Extraction Method for Identifying Gait Asymmetry Using Wearable Sensors", *Sensors*, Vol. 18, No. 2, p. 676, 2018.

30. Mariani, B., S. Rochat, C. J. Büla and K. Aminian, "Heel and Toe Clearance

Estimation for Gait Analysis Using Wireless Inertial Sensors", *IEEE Transactions on Biomedical Engineering*, Vol. 59, No. 11, pp. 3162–3168, 2012.

31. Kanzler, C. M., J. Barth, A. Rampp, H. Schlarb, F. Rott, J. Klucken and B. M. Eskofier, "Inertial Sensor Based and Shoe Size Independent Gait Analysis Including Heel and Toe Clearance Estimation", *37th International Conference of the IEEE Engineering in Medicine and Biology Society*, pp. 5424–5427, IEEE, 2015.

32. Yang, M., H. Zheng, H. Wang, S. McClean and D. Newell, "IGAIT: An Interactive Accelerometer Based Gait Analysis System", *Computer Methods and Programs in Biomedicine*, Vol. 108, No. 2, pp. 715–723, 2012.

33. Demonceau, M., A.-F. Donneau, J.-L. Croisier, E. Skawiniak, M. Boutaayamou, D. Maquet and G. Garraux, "Contribution of a Trunk Accelerometer System to the Characterization of Gait in Patients with Mild-To-Moderate Parkinson's Disease", *IEEE Journal of Biomedical and Health Informatics*, Vol. 19, No. 6, pp. 1803–1808, 2015.

34. Hsu, C.-Y., Y.-S. Tsai, C.-S. Yau, H.-H. Shie and C.-M. Wu, "Test-Retest Reliability of an Automated Infrared-Assisted Trunk Accelerometer-Based Gait Analysis System", *Sensors*, Vol. 16, No. 8, p. 1156, 2016.

35. Ossig, C., A. Antonini, C. Buhmann, J. Classen, I. Csoti, B. Falkenburger, M. Schwarz, J. Winkler and A. Storch, "Wearable Sensor-Based Objective Assessment of Motor Symptoms in Parkinson's Disease", *Journal of Neural Transmission*, Vol. 123, No. 1, pp. 57–64, 2016.

36. Caldas, R., M. Mundt, W. Potthast, F. B. de Lima Neto and B. Markert, "A Systematic Review of Gait Analysis Methods Based on Inertial Sensors and Adaptive Algorithms", *Gait & Posture*, Vol. 57, pp. 204–210, 2017.

37. Jarchi, D., J. Pope, T. K. M. Lee, L. Tamjidi, A. Mirzaei and S. Sanei, "A Review on Accelerometry-Based Gait Analysis and Emerging Clinical Applications",

IEEE Reviews in Biomedical Engineering, Vol. 11, pp. 177–194, 2018.

38. van Schooten, K. S., M. Pijnappels, S. M. Rispens, P. J. Elders, P. Lips and J. H. van Dieën, "Ambulatory Fall-Risk Assessment: Amount and Quality of Daily-Life Gait Predict Falls in Older Adults", *The Journals of Gerontology Series A: Biological Sciences and Medical Sciences*, Vol. 70, No. 5, pp. 608–615, 2015.

39. Paterson, K., K. Hill and N. Lythgo, "Stride Dynamics, Gait Variability and Prospective Falls Risk in Active Community Dwelling Older Women", *Gait & Posture*, Vol. 33, No. 2, pp. 251–255, 2011.

40. Gietzelt, M., F. Feldwieser, M. Gövercin, E. Steinhagen-Thiessen and M. Marschollek, "A Prospective Field Study for Sensor-Based Identification of Fall Risk in Older People with Dementia", *Informatics for Health and Social Care*, Vol. 39, No. 3-4, pp. 249–261, 2014.

41. Marschollek, M., A. Rehwald, K. Wolf, M. Gietzelt, G. Nemitz, H. Meyer Zu Schwabedissen and R. Haux, "Sensor-Based Fall Risk Assessment–an Expert to Go", *Methods of Information in Medicine*, Vol. 50, No. 5, p. 420, 2011.

42. Schwesig, R., D. Fischer, A. Lauenroth, S. Becker and S. Leuchte, "Can Falls Be Predicted with Gait Analytical and Posturographic Measurement Systems? a Prospective Follow-up Study in a Nursing Home Population", *Clinical Rehabilitation*, Vol. 27, No. 2, pp. 183–190, 2013.

43. Doi, T., S. Hirata, R. Ono, K. Tsutsumimoto, S. Misu and H. Ando, "The Harmonic Ratio of Trunk Acceleration Predicts Falling Among Older People: Results of a 1-Year Prospective Study", *Journal of Neuroengineering and Rehabilitation*, Vol. 10, No. 1, p. 7, 2013.

44. Howcroft, J., E. D. Lemaire and J. Kofman, "Prospective Elderly Fall Prediction by Older-Adult Fall-Risk Modeling with Feature Selection", *Biomedical Signal Processing and Control*, Vol. 43, pp. 320–328, 2018.

45. Riva, F., M. Toebes, M. Pijnappels, R. Stagni and J. van Dieën, "Estimating Fall Risk with Inertial Sensors Using Gait Stability Measures That Do Not Require Step Detection", *Gait & Posture*, Vol. 38, No. 2, pp. 170–174, 2013.

46. Ihlen, E. A., A. Weiss, Y. Beck, J. L. Helbostad and J. M. Hausdorff, "A Comparison Study of Local Dynamic Stability Measures of Daily Life Walking in Older Adult Community-Dwelling Fallers and Non-Fallers", *Journal of Biomechanics*, Vol. 49, No. 9, pp. 1498–1503, 2016.

47. Montesinos, L., R. Castaldo and L. Pecchia, "Wearable Inertial Sensors for Fall Risk Assessment and Prediction in Older Adults: A Systematic Review and Meta-Analysis", *IEEE Transactions on Neural Systems and Rehabilitation Engineering*, Vol. 26, No. 3, pp. 573–582, 2018.

48. Bautmans, I., B. Jansen, B. Van Keymolen and T. Mets, "Reliability and Clinical Correlates of 3D-Accelerometry Based Gait Analysis Outcomes According to Age and Fall-Risk", *Gait & Posture*, Vol. 33, No. 3, pp. 366–372, 2011.

49. Greene, B. R., A. O'Donovan, R. Romero-Ortuno, L. Cogan, C. N. Scanaill and R. A. Kenny, "Quantitative Falls Risk Assessment Using the Timed up and Go Test", *IEEE Transactions on Biomedical Engineering*, Vol. 57, No. 12, pp. 2918–2926, 2010.

50. Silva, J. and I. Sousa, "Instrumented Timed up and Go: Fall Risk Assessment Based on Inertial Wearable Sensors", *IEEE International Symposium on Medical Measurements and Applications (MeMeA)*, pp. 1–6, 2016.

51. Weiss, A., T. Herman, N. Giladi and J. M. Hausdorff, "Objective Assessment of Fall Risk in Parkinson's Disease Using a Body-Fixed Sensor Worn for 3 Days", *PloS One*, Vol. 9, No. 5, pp. 1–10, 2014.

52. Auvinet, B., G. Berrut, C. Touzard, L. Moutel, N. Collet, D. Chaleil and E. Barrey, "Gait Abnormalities in Elderly Fallers", *Journal of Aging and Physical Ac-*

tivity, Vol. 11, No. 1, pp. 40–52, 2003.

53. Silva, J., J. Madureira, C. Tonelo, D. Baltazar, C. Silva, A. Martins, C. Alcobia and I. Sousa, "Comparing Machine Learning Approaches for Fall Risk Assessment", *10th International Joint Conference on Biomedical Engineering Systems and Technologies (BIOSTEC)*, pp. 223–230, 2017.

54. Caby, B., S. Kieffer, M. de Saint Hubert, G. Cremer and B. Macq, "Feature Extraction and Selection for Objective Gait Analysis and Fall Risk Assessment by Accelerometry", *Biomedical Engineering Online*, Vol. 10, No. 1, 2011.

55. Giansanti, D., V. Macellari and G. Maccioni, "New Neural Network Classifier of Fall-Risk Based on the Mahalanobis Distance and Kinematic Parameters Assessed by a Wearable Device", *Physiological Measurement*, Vol. 29, No. 3, p. N11, 2008.

56. Greene, B. R., S. J. Redmond and B. Caulfield, "Fall Risk Assessment Through Automatic Combination of Clinical Fall Risk Factors and Body-Worn Sensor Data", *IEEE Journal of Biomedical and Health Informatics*, Vol. 21, No. 3, pp. 725–731, 2017.

57. Nait Aicha, A., G. Englebienne, K. van Schooten, M. Pijnappels and B. Kröse, "Deep Learning to Predict Falls in Older Adults Based on Daily-Life Trunk Accelerometry", *Sensors*, Vol. 18, No. 5, p. 1654, 2018.

58. Greene, B. R., D. McGrath, L. Walsh, E. P. Doheny, D. McKeown, C. Garattini, C. Cunningham, L. Crosby, B. Caulfield and R. A. Kenny, "Quantitative Falls Risk Estimation Through Multi-Sensor Assessment of Standing Balance", *Physiological Measurement*, Vol. 33, No. 12, p. 2049, 2012.

59. Hsieh, K. L., K. L. Roach, D. A. Wajda and J. J. Sosnoff, "Smartphone Technology Can Measure Postural Stability and Discriminate Fall Risk in Older Adults", *Gait & Posture*, Vol. 67, pp. 160–165, 2019.

60. Liu, Y., S. J. Redmond, M. R. Narayanan and N. H. Lovell, "Classification Between Non-Multiple Fallers and Multiple Fallers Using a Triaxial Accelerometry-Based System", *IEEE Annual International Conference of the Engineering in Medicine and Biology Society, EMBC*, pp. 1499–1502, IEEE, 2011.

61. Senden, R., H. Savelberg, B. Grimm, I. Heyligers and K. Meijer, "Accelerometry-Based Gait Analysis, an Additional Objective Approach to Screen Subjects at Risk for Falling", *Gait & Posture*, Vol. 36, No. 2, pp. 296–300, 2012.

62. Weiss, A., S. Sharifi, M. Plotnik, J. P. P. van Vugt, N. Giladi and J. M. Hausdorff, "Toward Automated, At-Home Assessment of Mobility Among Patients with Parkinson Disease, Using a Body-Worn Accelerometer", *Neurorehabilitation and Neural Repair*, Vol. 25, No. 9, pp. 810–818, 2011.

63. Hua, A., Z. Quicksall, C. Di, R. Motl, A. Z. LaCroix, B. Schatz and D. M. Buchner, "Accelerometer-Based Predictive Models of Fall Risk in Older Women: A Pilot Study", *npj Digital Medicine*, Vol. 1, No. 1, p. 25, 2018.

64. Howcroft, J., J. Kofman and E. D. Lemaire, "Review of Fall Risk Assessment in Geriatric Populations Using Inertial Sensors", *Journal of Neuroengineering and Rehabilitation*, Vol. 10, No. 1, p. 91, 2013.

65. Rajagopalan, R., I. Litvan and T.-P. Jung, "Fall Prediction and Prevention Systems: Recent Trends, Challenges, and Future Research Directions", *Sensors*, Vol. 17, No. 11, p. 2509, 2017.

66. EXEL, *EXEL ExLs3*, 2018, `http://www.exelmicroel.com`, accessed at December 2018.

67. Tunca, C., N. Pehlivan, N. Ak, B. Arnrich, G. Salur and C. Ersoy, "Inertial Sensor-Based Robust Gait Analysis in Non-Hospital Settings for Neurological Disorders", *Sensors*, Vol. 17, No. 4, p. 825, 2017.

68. Muro-De-La-Herran, A., B. Garcia-Zapirain and A. Mendez-Zorrilla, "Gait Analysis Methods: An Overview of Wearable and Non-Wearable Systems, Highlighting Clinical Applications", *Sensors*, Vol. 14, No. 2, pp. 3362–3394, 2014.

69. Trojaniello, D., A. Cereatti, E. Pelosin, L. Avanzino, A. Mirelman, J. M. Hausdorff and U. Della Croce, "Estimation of Step-By-Step Spatio-Temporal Parameters of Normal and Impaired Gait Using Shank-Mounted Magneto-Inertial Sensors: Application to Elderly, Hemiparetic, Parkinsonian and Choreic Gait", *Journal of Neuroengineering and Rehabilitation*, Vol. 11, No. 1, p. 152, 2014.

70. Santhiranayagam, B. K., D. T. Lai, W. Sparrow and R. K. Begg, "a Machine Learning Approach to Estimate Minimum Toe Clearance Using Inertial Measurement Units", *Journal of Biomechanics*, Vol. 48, No. 16, pp. 4309 – 4316, 2015.

71. Bötzel, K., A. Olivares, J. P. Cunha, J. M. G. Sáez, R. Weiss and A. Plate, "Quantification of Gait Parameters with Inertial Sensors and Inverse Kinematics", *Journal of Biomechanics*, Vol. 72, pp. 207–214, 2018.

72. Mariani, B., H. Rouhani, X. Crevoisier and K. Aminian, "Quantitative Estimation of Foot-Flat and Stance Phase of Gait Using Foot-Worn Inertial Sensors", *Gait & Posture*, Vol. 37, No. 2, pp. 229–234, 2013.

73. Skog, I., J.-O. Nilsson and P. Händel, "Evaluation of Zero-Velocity Detectors for Foot-Mounted Inertial Navigation Systems", *International Conference on Indoor Positioning and Indoor Navigation (IPIN)*, pp. 1–6, IEEE, 2010.

74. Panchpor, A. A., S. Shue and J. M. Conrad, "A Survey of Methods for Mobile Robot Localization and Mapping in Dynamic Indoor Environments", *Conference on Signal Processing and Communication Engineering Systems (SPACES)*, pp. 138–144, IEEE, 2018.

75. The MathWorks Inc., *MATLAB R2018a*, 2018, `https://www.mathworks.com/products/matlab`, accessed at December 2018.

76. Microsoft, *Microsoft Kinect v2*, 2014, `https://msdn.microsoft.com/en-us/library/dn758675.aspx`, accessed at December 2018.

77. Baldewijns, G., G. Verheyden, B. Vanrumste and T. Croonenborghs, "Validation of the Kinect for Gait Analysis Using the GAITRite Walkway", *36th Annual International Conference of the IEEE Engineering in Medicine and Biology Society*, pp. 5920–5923, IEEE, 2014.

78. Gabel, M., R. Gilad-Bachrach, E. Renshaw and A. Schuster, "Full Body Gait Analysis with Kinect", *Annual International Conference of the IEEE Engineering in Medicine and Biology Society*, pp. 1964–1967, IEEE, 2012.

79. González, I., I. H. López-Nava, J. Fontecha, A. Muñoz-Meléndez, A. I. Pérez-SanPablo and I. Quiñones-Urióstegui, "Comparison Between Passive Vision-Based System and a Wearable Inertial-Based System for Estimating Temporal Gait Parameters Related to the GAITRite Electronic Walkway", *Journal of Biomedical Informatics*, Vol. 62, pp. 210–223, 2016.

80. Stone, E. E. and M. Skubic, "Unobtrusive, Continuous, In-Home Gait Measurement Using the Microsoft Kinect", *IEEE Transactions on Biomedical Engineering*, Vol. 60, No. 10, pp. 2925–2932, 2013.

81. Ťupa, O., A. Procházka, O. Vyšata, M. Schätz, J. Mareš, M. Vališ and V. Mařík, "Motion Tracking and Gait Feature Estimation for Recognising Parkinson's Disease Using MS Kinect", *Biomedical Engineering Online*, Vol. 14, No. 1, p. 97, 2015.

82. Rocha, A. P., H. Choupina, J. M. Fernandes, M. J. Rosas, R. Vaz and J. P. S. Cunha, "Parkinson's Disease Assessment Based on Gait Analysis Using an Innovative RGB-D Camera System", *36th Annual International Conference of the Engineering in Medicine and Biology Society*, pp. 3126–3129, IEEE, 2014.

83. Procházka, A., O. Vyšata, M. Vališ, O. Ťupa, M. Schätz and V. Mařík, "Use of

the Image and Depth Sensors of the Microsoft Kinect for the Detection of Gait Disorders", *Neural Computing and Applications*, Vol. 26, No. 7, pp. 1621–1629, 2015.

84. Pehlivan, N., C. Tunca, G. Salur and C. Ersoy, "Gait Analysis Using Kinect: Towards In-Home Gait Analysis", *25th Signal Processing and Communications Applications Conference (SIU)*, pp. 1–4, May 2017.

85. Bland, J. M. and D. G. Altman, "Measuring Agreement in Method Comparison Studies", *Statistical Methods in Medical Research*, Vol. 8, No. 2, pp. 135–160, 1999.

86. Watson, P. and A. Petrie, "Method Agreement Analysis: A Review of Correct Methodology", *Theriogenology*, Vol. 73, No. 9, pp. 1167 – 1179, 2010.

87. Axer, H., M. Axer, H. Sauer, O. W. Witte and G. Hagemann, "Falls and Gait Disorders in Geriatric Neurology", *Clinical Neurology and Neurosurgery*, Vol. 112, No. 4, pp. 265–274, 2010.

88. Pradhan, C., M. Wuehr, F. Akrami, M. Neuhaeusser, S. Huth, T. Brandt, K. Jahn and R. Schniepp, "Automated Classification of Neurological Disorders of Gait Using Spatio-Temporal Gait Parameters", *Journal of Electromyography and Kinesiology*, Vol. 25, No. 2, pp. 413–422, 2015.

89. Verghese, J., A. F. Ambrose, R. B. Lipton and C. Wang, "Neurological Gait Abnormalities and Risk of Falls in Older Adults", *Journal of Neurology*, Vol. 257, No. 3, pp. 392–398, 2010.

90. Nonnekes, J., R. J. Goselink, E. Ružička, A. Fasano, J. G. Nutt and B. R. Bloem, "Neurological Disorders of Gait, Balance and Posture: A Sign-Based Approach", *Nature Reviews Neurology*, Vol. 14, No. 3, p. 183, 2018.

91. Alafeef, M. and M. Fraiwan, "On the Diagnosis of Idiopathic Parkinson's Dis-

ease Using Continuous Wavelet Transform Complex Plot", *Journal of Ambient Intelligence and Humanized Computing*, pp. 1–11, 2018.

92. Bourgeois, A. B., B. Mariani, K. Aminian, P. Zambelli and C. Newman, "Spatio-Temporal Gait Analysis in Children with Cerebral Palsy Using, Foot-Worn Inertial Sensors", *Gait & Posture*, Vol. 39, No. 1, pp. 436–442, 2014.

93. Gietzelt, M., K. Wolf, M. Kohlmann, M. Marschollek, R. Haux *et al.*, "Measurement of Accelerometry-Based Gait Parameters in People with and Without Dementia in the Field", *Methods of Information in Medicine*, Vol. 52, No. 4, pp. 319–325, 2013.

94. Greene, B. R., S. Rutledge, I. McGurgan, C. McGuigan, K. O'Connell, B. Caulfield and N. Tubridy, "Assessment and Classification of Early-Stage Multiple Sclerosis with Inertial Sensors: Comparison Against Clinical Measures of Disease State", *IEEE Journal of Biomedical and Health Informatics*, Vol. 19, No. 4, pp. 1356–1361, 2015.

95. Blazkiewicz, M., I. Wiszomirska and A. Wit, "Comparison of Four Methods of Calculating the Symmetry of Spatial-Temporal Parameters of Gait", *Acta of Bioengineering and Biomechanics*, Vol. 16, No. 1, pp. 29–35, 2014.

96. Lord, S., T. Howe, J. Greenland, L. Simpson and L. Rochester, "Gait Variability in Older Adults: A Structured Review of Testing Protocol and Clinimetric Properties", *Gait & Posture*, Vol. 34, No. 4, pp. 443–450, 2011.

97. Tibshirani, R., "Regression Shrinkage and Selection Via the Lasso", *Journal of the Royal Statistical Society. Series B (Methodological)*, pp. 267–288, 1996.

98. Breiman, L., "Random Forests", *Machine Learning*, Vol. 45, No. 1, pp. 5–32, 2001.

99. Reynard, F. and P. Terrier, "Determinants of Gait Stability While Walking on

a Treadmill: A Machine Learning Approach", *Journal of Biomechanics*, Vol. 65, pp. 212 – 215, 2017.

100. Cortes, C. and V. Vapnik, "Support-Vector Networks", *Machine Learning*, Vol. 20, No. 3, pp. 273–297, 1995.

101. Hollman, J. H., E. M. McDade and R. C. Petersen, "Normative Spatiotemporal Gait Parameters in Older Adults", *Gait & Posture*, Vol. 34, No. 1, pp. 111–118, 2011.

102. Iosa, M., A. Fusco, F. Marchetti, G. Morone, C. Caltagirone, S. Paolucci and A. Peppe, "The Golden Ratio of Gait Harmony: Repetitive Proportions of Repetitive Gait Phases", *BioMed Research International*, Vol. 2013, 2013.

103. Nelson, A. J., D. Zwick, S. Brody, C. Doran, L. Pulver, G. Rooz, M. Sadownick, R. Nelson and J. Rothman, "The Validity of the GaitRite and the Functional Ambulation Performance Scoring System in the Analysis of Parkinson Gait", *NeuroRehabilitation*, Vol. 17, No. 3, pp. 255–262, 2002.

104. Moon, Y., J. Sung, R. An, M. E. Hernandez and J. J. Sosnoff, "Gait Variability in People with Neurological Disorders: A Systematic Review and Meta-Analysis", *Human Movement Science*, Vol. 47, pp. 197–208, 2016.

105. Hausdorff, J. M., "Gait Variability: Methods, Modeling and Meaning", *Journal of Neuroengineering and Rehabilitation*, Vol. 2, No. 1, p. 19, 2005.

106. Rennie, L., E. Dietrichs, R. Moe-Nilssen, A. Opheim and E. Franzén, "The Validity of the Gait Variability Index for Individuals with Mild to Moderate Parkinson's Disease", *Gait & Posture*, Vol. 54, pp. 311–317, 2017.

107. Hausdorff, J. M., M. E. Cudkowicz, R. Firtion, J. Y. Wei and A. L. Goldberger, "Gait Variability and Basal Ganglia Disorders: Stride-To-Stride Variations of Gait Cycle Timing in Parkinson's Disease and Huntington's Disease", *Movement*

Disorders, Vol. 13, No. 3, pp. 428–437, 1998.

108. Erro, R., G. Santangelo, M. Picillo, C. Vitale, M. Amboni, K. Longo, F. Giordano, M. Moccia, P. Barone and M. T. Pellecchia, "Side of Onset Does Not Influence Cognition in Newly Diagnosed Untreated Parkinson's Disease Patients", *Parkinsonism & Related Disorders*, Vol. 19, No. 2, pp. 256–259, 2013.

109. Mootanah, R., H. Hillstrom, K. Gross, J. Niu, M. Nevitt, C. Lewis, J. Torner, J. Hietpas and D. Felson, "Stance and Single Support Time Asymmetry Identify Unilateral Knee Oa and the Involved Limb: The Multicenter Osteoarthritis Study", *Osteoarthritis and Cartilage*, Vol. 21, pp. S246–S247, 2013.

110. Frenkel-Toledo, S., N. Giladi, C. Peretz, T. Herman, L. Gruendlinger and J. M. Hausdorff, "Effect of Gait Speed on Gait Rhythmicity in Parkinson's Disease: Variability of Stride Time and Swing Time Respond Differently", *Journal of Neuroengineering and Rehabilitation*, Vol. 2, No. 1, p. 23, 2005.

111. Del Din, S., A. Godfrey, B. Galna, S. Lord and L. Rochester, "Free-Living Gait Characteristics in Ageing and Parkinson's Disease: Impact of Environment and Ambulatory Bout Length", *Journal of Neuroengineering and Rehabilitation*, Vol. 13, No. 1, p. 46, 2016.

112. Baktir, A. C., C. Tunca, A. Ozgovde, G. Salur and C. Ersoy, "SDN-Based Multi-Tier Computing and Communication Architecture for Pervasive Healthcare", *IEEE Access*, Vol. 6, pp. 56765–56781, 2018.

113. Tinetti, M. E. and C. S. Williams, "Falls, Injuries Due to Falls, and the Risk of Admission to a Nursing Home", *New England Journal of Medicine*, Vol. 337, No. 18, pp. 1279–1284, 1997.

114. Stevens, J. A., P. S. Corso, E. A. Finkelstein and T. R. Miller, "The Costs of Fatal and Non-Fatal Falls Among Older Adults", *Injury Prevention*, Vol. 12, No. 5, pp. 290–295, 2006.

115. LeCun, Y., Y. Bengio and G. Hinton, "Deep Learning", *Nature*, Vol. 521, No. 7553, p. 436, 2015.

116. Roman de Mettelinge, T. and D. Cambier, "Understanding the Relationship Between Walking Aids and Falls in Older Adults: A Prospective Cohort Study", *Journal of Geriatric Physical Therapy*, Vol. 38, No. 3, pp. 127–132, 2015.

117. Vinyals, O., C. Blundell, T. Lillicrap, D. Wierstra *et al.*, "Matching Networks for One Shot Learning", *Advances in Neural Information Processing Systems*, pp. 3630–3638, 2016.

118. Steven Eyobu, O. and D. Han, "Feature Representation and Data Augmentation for Human Activity Classification Based on Wearable IMU Sensor Data Using a Deep LSTM Neural Network", *Sensors*, Vol. 18, No. 9, p. 2892, 2018.

119. Xu, G., J. Z. Huang *et al.*, "Asymptotic Optimality and Efficient Computation of the Leave-Subject-out Cross-Validation", *The Annals of Statistics*, Vol. 40, No. 6, pp. 3003–3030, 2012.

120. Graves, A. and J. Schmidhuber, "Framewise Phoneme Classification with Bidirectional LSTM and Other Neural Network Architectures", *Neural Networks*, Vol. 18, No. 5-6, pp. 602–610, 2005.

121. Greff, K., R. K. Srivastava, J. Koutník, B. R. Steunebrink and J. Schmidhuber, "LSTM: A Search Space Odyssey", *IEEE Transactions on Neural Networks and Learning Systems*, Vol. 28, No. 10, pp. 2222–2232, 2017.

122. Sundermeyer, M., H. Ney and R. Schlüter, "From Feedforward to Recurrent LSTM Neural Networks for Language Modeling", *IEEE Transactions on Audio, Speech, and Language Processing*, Vol. 23, No. 3, pp. 517–529, 2015.

123. Zeyer, A., P. Doetsch, P. Voigtlaender, R. Schlüter and H. Ney, "A Comprehensive Study of Deep Bidirectional LSTM RNNs for Acoustic Modeling in Speech

Recognition", *IEEE International Conference on Acoustics, Speech and Signal Processing (ICASSP)*, pp. 2462–2466, 2017.

124. Feng, Y., Y. Li and J. Luo, "Learning Effective Gait Features Using LSTM", *23rd International Conference on Pattern Recognition (ICPR)*, pp. 325–330, IEEE, 2016.

125. Herath, S., M. Harandi and F. Porikli, "Going Deeper into Action Recognition: A Survey", *Image and Vision Computing*, Vol. 60, pp. 4–21, 2017.

126. Ordóñez, F. J. and D. Roggen, "Deep Convolutional and Lstm Recurrent Neural Networks for Multimodal Wearable Activity Recognition", *Sensors*, Vol. 16, No. 1, p. 115, 2016.

127. Kingma, D. P. and J. L. Ba, "Adam: A Method for Stochastic Optimization", *3rd International Conference for Learning Representations (ICLR)*, 2014.

128. Murphy, K. *et al.*, "The Bayes Net Toolbox for Matlab", *Computing Science and Statistics*, Vol. 33, No. 2, pp. 1024–1034, 2001.

129. Demšar, J., "Statistical Comparisons of Classifiers over Multiple Data Sets", *Journal of Machine Learning Research*, Vol. 7, No. Jan, pp. 1–30, 2006.

130. Satyanarayanan, M., "The Emergence of Edge Computing", *Computer*, Vol. 50, No. 1, pp. 30–39, 2017.

131. Verbelen, T., P. Simoens, F. De Turck and B. Dhoedt, "Cloudlets: Bringing the Cloud to the Mobile User", *3rd ACM Workshop on Mobile Cloud Computing and Services*, pp. 29–36, 2012.

132. Rahmani, A. M., T. N. Gia, B. Negash, A. Anzanpour, I. Azimi, M. Jiang and P. Liljeberg, "Exploiting Smart E-Health Gateways at the Edge of Healthcare Internet-Of-Things: A Fog Computing Approach", *Future Generation Computer*

Systems, Vol. 78, pp. 641–658, 2018.

133. Cao, Y., P. Hou, D. Brown, J. Wang and S. Chen, "Distributed Analytics and Edge Intelligence: Pervasive Health Monitoring at the Era of Fog Computing", *Proceedings of the 2015 Workshop on Mobile Big Data*, pp. 43–48, ACM, 2015.

134. Uddin, M. Z., "A Wearable Sensor-Based Activity Prediction System to Facilitate Edge Computing in Smart Healthcare System", *Journal of Parallel and Distributed Computing*, Vol. 123, pp. 46–53, 2019.

135. Nguyen, B., N. Choi, M. Thottan and J. Van der Merwe, "SIMECA: SDN-Based IoT Mobile Edge Cloud Architecture", *IFIP/IEEE Symposium on Integrated Network and Service Management (IM)*, pp. 503–509, 2017.

136. Sun, X. and N. Ansari, "EdgeIoT: Mobile Edge Computing for the Internet of Things", *IEEE Communications Magazine*, Vol. 54, No. 12, pp. 22–29, 2016.

137. McKeown, N., T. Anderson, H. Balakrishnan, G. Parulkar, L. Peterson, J. Rexford, S. Shenker and J. Turner, "OpenFlow: Enabling Innovation in Campus Networks", *ACM SIGCOMM Computer Communication Review*, Vol. 38, No. 2, pp. 69–74, 2008.

138. *Ryu*, 2018, `http://osrg.github.io/ryu/`, accessed at December 2018.

139. *Mininet*, 2018, `http://mininet.org`, accessed at December 2018.

140. Open Networking Foundation, *OpenFlow*, 2016, `https://www.opennetworking.org/sdn-resources/openflow`, accessed at December 2018.

141. Pfaff, B., J. Pettit, T. Koponen, E. J. Jackson, A. Zhou, J. Rajahalme, J. Gross, A. Wang, J. Stringer, P. Shelar *et al.*, "The Design and Implementation of Open VSwitch.", *Symposium on Networked Systems Design and Implementation*, pp. 117–130, 2015.